FPCB MAGNETIC MICROMIRROR FOR LASER MARKING/ENGRAVING SYSTEM

By

Karlmarx Golanthan Karuppaih Periyasamy

Bachelor of Engineering, Aeronautical Engineering, Anna University, Chennai, India,2010.

A thesis

presented to Ryerson University

in partial fulfillment of the

requirements for the degree of

Master of Applied Science

in the Program of

Mechanical and Industrial Engineering

Toronto, Ontario, Canada, 2017

AUTHOR'S DECLARATION FOR ELECTRONIC SUBMISSION OF A THESIS

I hereby declare that I am the sole author of this thesis. This is a true copy of the thesis, including any required final revisions, as accepted by my examiners.

I authorize Ryerson University to lend this thesis to other institutions or individuals for the purpose of scholarly research.

I further authorize Ryerson University to reproduce this thesis by photocopying or by other means, in total or in part, at the request of other institutions or individuals for the purpose of scholarly research.

I understand that my thesis may be made electronically available to the public.

Abstract

FPCB magnetic micromirror for laser marking/engraving systems

Karlmarx Golanthan Karuppaih Periyasamy

Master of Applied Science, Mechanical Engineering, Ryerson University, 2017

The thesis presents the design and development of a novel, rotational micro mirror using Flexible Printed Circuit Boards (FPCB) for the applications in laser marking/engraving system. The use of the new material helps in reducing the overall cost of the laser scanning system when compared to other MEMS based scanners but with higher mirror surface quality. The device mainly caters to applications that require low powered laser (<1watt), small working area (< 20x20mm) and slow scanning speed (2 mm/sec). The scanner consists of two orthogonally positioned quasi static micromirrors which are driven by magnetic lorentz force. Based on the developed laser scanner, a complete laser marking/engraving system was developed which is capable of engraving materials such as leather, TPU smartphone cases, etc. Further, the thesis also addresses a new problem (drifting) associated with the polyimide material used as the substrate for FPCB actuators and a modified vector scanning methodology is proposed to overcome it.

Acknowledgements:

First and foremost, I express my sincere gratitude to my supervisor Dr. Siyuan He for giving me the opportunity to pursue my Master of Applied Science program, for his consistent motivation, guidance and encouragement, which were the driving factors to complete my research successfully.

Besides my advisor, I would like to thank Bella Yang (Fastline circuits), Mateusz Szymański (OPT lasers technology) and CMC Microsystems for their technical help and support regarding the FPCB circuits and Lasers systems.

I thank my fellow lab mates Yuan Xue, Hui Zho and Devanshu for being good friends and bringing me to pace regarding the MEMS research concepts.

I also thank my friends Abdul, Ajith, Ashish, Manikandan and Shri Shankari for their support.

Finally, I dedicate this thesis to my father (K.K.Periyasamy), mother (M.Thavamani Devi) and my girlfriend (R.Ashwini) as it would not have been possible without their support and sacrifices.

Table of Contents

List of figures

List of Tables

Chapter 1. Introduction

1.1 What is Laser engraving/marking?

The laser engraving/marking systems utilize laser beam to either vaporize or alter the surface properties of the materials upon contact, based on the application required. Unlike the visible white light which has numerous wavelength the laser beams are monochromatic. Hence, they can be focused over a long distance with minimal divergence to a small spot. Owing to the very small spot size, majority of the light energy is converted into heat energy which is responsible for the surface modifications on the target [1]. Based on the type of target material used the same machine can be used for marking, engraving and cutting operations [2]. The following Table 1. provides the common differences between Laser marking and engraving system [3] [4].

Table 1. Difference between Laser marking and engraving.

S.no:	Laser marking	Laser engraving
1)	Surface discoloration of the target material due to oxidation.	Noticeable removal of materials (up to 3.175mm)
2)	Four common types: Annealing, foaming, carbon migration and coloration	Three common types: Etching, deep laser engraving and laser ablation.
3)	Slower operation with lower power than the material irradiance limit.	Faster operation and very high laser power necessary for material vaporization. May require multiple pass.

The recent government regulations and industrial standards have made it mandatory for all the critical parts to have clear and legible UDI (Unique Device Identification) numbers, labels, logos and barcodes for easier product traceability in various industries ranging from automobile, medicine, textile, electronics and semiconductor products [5] [6]. Moreover, there is a growing

interest among the public to create unique and customized personal products. Thus, the marking/engraving industry has gained its momentum in recent years. The following Figure 1. shows the application of laser engraving/marking in various fields [7] [8].

Figure 1. Sample images of laser engraving/marking on the various materials a) surgical knife b) steel name plates c) automotive parts d) smartphones e) accessories- watches f) leather pouches [7] [8].

Compared to other marking techniques such as the electro chemical etching, dot peening and inkjet, laser marking offers major benefits such as high-quality surface finish, non-contact approach- no/minimal use of additional inks, the capability of marking materials difficult for other techniques and durability of the marking/engraving [9] [10] [11]. A laser marking/engraving system consists of two main parts, a laser source and the laser scanning mechanism.

1.2 Laser Source

Based on the material type to be engraved, the laser source units are selected. Some of the commonly used laser source for engraving/marking are diode laser, fiber laser, crystal laser and CO_2 laser. Among them, diode laser is more suitable for applications that require low power (<5 watt) as they are more cost efficient at those power levels [12] [13]. Further, the selection of wavelength also play a major role in focussed spot size and material absorption. The following Figure 2. shows different laser source and its corresponding wavelengths that can be used for marking [14].

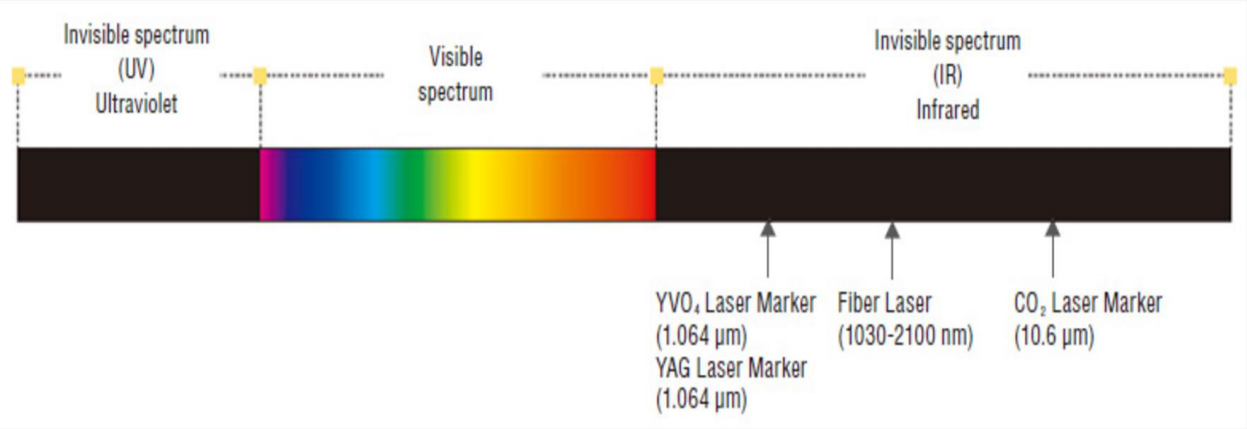

Figure 2. Wavelength spectrum that can be used for laser marking/engraving [14].

1.3 Laser scanning mechanism

As the name suggests, they steer the focused laser beam to the desired location on the material surface for marking/engraving. Generally, there are two conventional laser scanning mechanisms, namely,

1) X-Y plotter table
2) Galvano laser scanner

1.3.1 X-Y plotter table

In this arrangement, the laser head is fixed to a plotter table setup and travels along the rails to engrave the area using high speed stepper motors connected by V-belts. Hence, the working area is dependent on the size of the plotter table rails. Usually these laser scanners can cover a work area as large as few feet with relatively slower scanning speed (100s mm/sec) as the laser source must travel to cover the complete work area. Being large, they are not suitable for applications that require smaller working area [15] [16]. The Figure 3. shows a plotter table type engraver from Darkly labs (a start up company specializing on laser plotters) with dimension and maximum work area of 490 X440 mm and 305 X 210mm respectively [17].

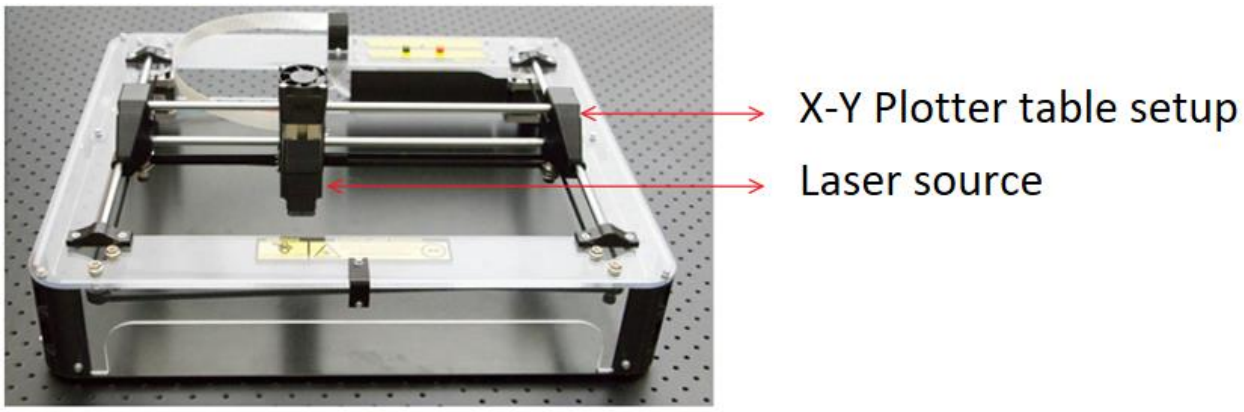

Figure 3. Emblaser 1-plotter type engraving/marking machine from Darkly Labs [17].

1.3.2 Galvano laser scanner

Unlike the plotter table setup, the laser source remains fixed and the laser beam is steered on the surface of the target materials. This is achieved with the help of Galvano scanners. These are nothing but high reflective mirror plates attached to motors (galvanometer). Each mirror is capable of unidirectional actuation and together they are aligned orthogonally to provide the necessary bidirectional actuation. This scanning mechanism requires a closed loop control system with a feedback position detector to ensure the position of the mirror precisely and perform necessary

minor corrections if necessary [18] [19]. Generally, focussing a laser beam over a very long distance with the same intensity is very difficult. Thus, these models have a smaller work areas (< 1 foot on each side) but the scanning speeds are much faster than a typical plotter table usually in range of (1000s mm/sec). Moreover, they have a size of about 61x34x43mm excluding the driving unit which are bulkier than the scanners itself. A driving unit for single mirror measures around 77.5x65.9x45.5mm and a Galvano scanner requires two of these units therefore, making the entire system bulky [20]. Moreover, these scanners are very expensive than their typical plotter table counterpart, as the cost of each scanner ranges from 100s ~ 1000s dollars depending on the following factors [20] [21] [22]:

1) Area - Larger working area requires expensive focussing optics such as F-theta lens.
2) Accuracy- The accuracy of a Galvano scanner mainly depends on the complexity of the driving unit and feedback position detector.
3) Speed- The galvanometers are much faster than a typical stepper motor. Hence, the design and property of the mirrors used should be capable of withstanding larger acceleration acting on the rotating shaft.

The Figure 4. shows an image of a small beam dual axis Galvano scanners (GVS112) along with its driving units from Thorlabs [20].

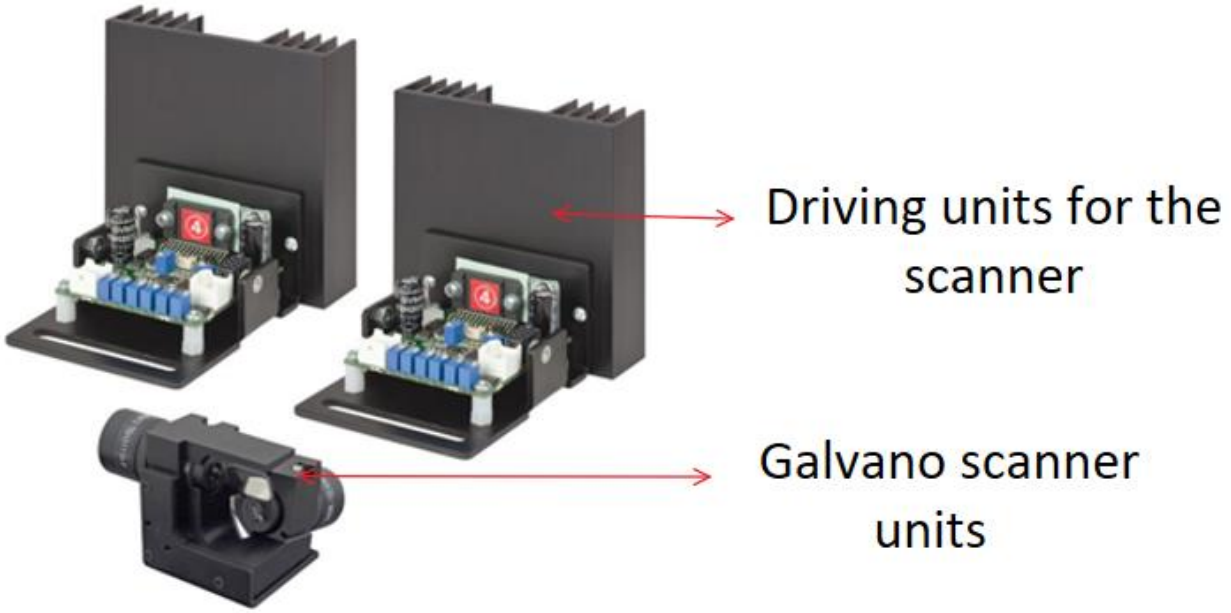

Figure 4. Small beam dual axis Galvano scanners (GVS112) along with its driving units from thorlabs [20].

Both the scanning mechanisms consist of multiple moving parts such as motors, encoders, servo circuit, etc. which adversely affects the reliability and increases the maintenance. Moreover, these systems consume more power. Hence, they are not suitable for point and shoot operations

Recently, there is an increasing interest in the laser marking/engraving of consumer goods such as jewelry, name plate, creating personalized signature on wallets/belts, cell phone cases, clothing, etc. These applications require small laser working area (1~2 inch on each side), low laser power (<1 watt ~ a few watts) and low scanning speed (< 5mm/s) [23] [24]. However, these applications require low cost and compact form factor. One of the major cost factor of the engraving system is the laser source. Generally, the semiconductor diode laser source is often chosen for the above-mentioned requirements mainly due to their cost-efficient nature for corresponding laser power, usually in a range of (e.g., tens to a few hundred dollars). Also, due to its small size, usually in the range of few tens of inches, (~ 60 $inch^3$) thus making them easy to handle [25] [26]. Therefore, the

corresponding laser scanning mechanism will be of low cost (e.g., 10s ~ a few dollars dollars), small size (e.g., ~ 5 $inch^3$) along with simple structure and minimal maintenance thus making the whole system suitable for laser marking/engraving of consumer goods. But neither of the conventional laser scanning mechanisms can meet the above characteristics. The lack of low cost and small size laser scanners in this sector is the main reason for the absence of portable machines for laser marking/engraving of consumer goods.

1.4 MEMS micromirrors

In the past few years, MEMS micromirrors were sought to build low cost and compact scanners for laser marking/engraving system. Micromirrors are small actuators which can provide necessary mechanical actuation for the corresponding input energy. These micromirrors have already been successfully developed and used in various other applications such as display, communication, biomedical devices, etc. [27] [28] [29] [30] [31] [32] and they have already demonstrated their small size and low-cost potential. However most of the existing micromirrors are not suitable for laser marking/engraving applications due to their low aperture flatness, e.g., ROC (Radius of Curvature) ranging from centimeters ~ less than 1 meter, while high mirror plate flatness (ROC >10 meters) is required for laser marking/engraving application in order to completely reflect the incident radiation without any loss as heat [33] [34]. But the poor qualities in these fabricated micromirrors are mostly attributed to the fabrication process such as SOIMUMPS, bulk micro machining [35]. Generally, a micromirror consist of actuators and mirror plates which are fabricated in a single process in the conventional fabrication process. Hence, the quality of the mirror plates is hard to control due to the limitation of the fabrication process such as requirement of release holes. To overcome this, a new set of micromirrors known as bonded micromirrors were developed in which both actuators and mirror plates were fabricated separately and bonded in the

later process. Due to this the mirror plate dimensions, shape and quality are independent of the actuator [36]. Such micromirrors were already developed by two companies namely Mirrorcle technologies Inc. and Worldstar tech (Toronto, Canada). Both the companies already have their working products in the market based on their mirrors. Some of the commercially available MEMS mirror based marking/engraving systems are explained below.

1.5 Nextgen Laser Marker by Worldstar technologies

The device uses a 5-8watt fiber laser which has an wavelength of 1064 nm. It uses one 2 Directional quasi static MEMS mirror for scanning the laser beam spot. The mirror has a speed of 20mm/degree and a maximum rotational angle of ± 5° (mechanical). Hence, it can engrave a maximum area of 50 X50 mm on materials such as stainless steel, gold, carbide aluminium etc. It has an overall dimension of 150 X 100 X 25 mm (LxBxH) and weighs around 1kg making it one of the most compact laser marker of such category. But the information regarding its pricing and availability are limited [37]. It is expected to be at least >1000 USD as the scanning mirrors of such category costs around 400 to 650 USD [38]. The Figure 5. shows the image of the Nextgen laser marker [37].

Figure 5. Nextgen laser marker/engraver by Worldstar Tech. Inc [37].

1.6 NLL 10 label laser by NanoSec Technology GmbH

The device uses a 1-watt diode laser operating at 405 nm and a MEMS scanning system based on the micromirrors developed by Mirrorcle technologies. It has an engraving speed of 0.2 cm^2/s and 100 mm/s for raster and vector scanning methods respectively with a print resolution greater than 500 dpi. The entire device is a cube (a= 200 mm) weighing about 5 Kg and has a maximum working area of 45 X 45mm. The system was predominantly designed to be a simple and low-cost laser label marker capable of marking foil, leather, plastics etc [39]. The following Figure 6. shows the image of the NLL 10 label laser by NanoSec Technology GmbH [39].

Figure 6. NLL 10 Label laser module by NanoSec Technonolgy GmbH [39].

1.7 Micromirrors by Mirrorcle

Though, companies such as Sercalo Microtechnology, Texas Instruments, INNOCLE, STMicroelectronics etc. have been developing MEMS mirror, Mirrorcle was one of the very few company which mainly focused on developing bonded micromirrors specific for laser engraving/marking. As mentioned in the previous section, the NLL10 label laser machines uses a two-axis scanning gimbal-less micromirror manufactured using ARI-MEMS fabrication

technology by Mirrorcle [39] [40]. The mirrors use a bias differential voltage electro static technique to achieve the necessary actuation. Further, the mirrors are made from single crystal silicon and have a maximum scanning of ± 6° (mechanical) and ± 7° (mechanical) for quasi static operation and resonant modes respectively. The aperture size ranges from 2mm to 9mm and offers some major benefits such as [41],

- Capable of both resonant and quasi static scanning modes.
- Capable of achieving analog tilt angles for point to point scanning.
- Very high surface quality. (ROC: >5 m, Roughness: <10 nm)
- Can withstand up to 3-watt laser of any wavelength on a mirror size greater than 2mm.
- High repeatability at room temperature (0.0005°)

Figure 7. shows the image of a packaged bonded micromirror of varying aperture size by Mirrorcle technologies [41].

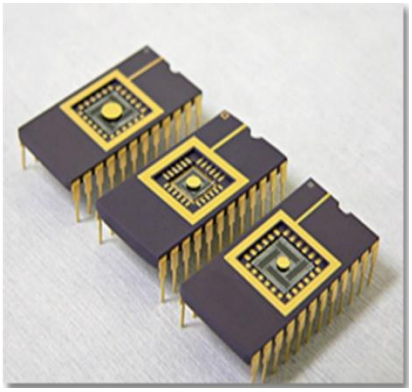

Figure 7. Bonded micromirror of varying aperture size by Mirrorcle Technologies Inc [41].

The following Table 2. provides information about the various MEMS micromirrors by Mirrorcle and their specifications [38] [42].

Table 2. Specifications of various bonded MEMS micromirrors by Mirrorcle Technologies Inc [38] [42].

Actuator name	Die size (mm)	Mechanical tilt angle ± (°)	Available mirror size (mm)	Cost (USD)
A7B1.1	5.20X5.20	7	1.6-3.6	648-738
A7B2.1	5.20X5.20	5.5	2.4-3.6	648-738
A8L1.1	7.25X7.25	5.5	2.4-4.2	667-877
A4SR8.X	8X8	5	1.6-2.4,4.2,5	836-1046
A1B1.5	4.23X4.23	4.75	1.6-3.6	529-699
A1B2.2	4.23X4.23	4.5	0.8-3.6	529-699
A1B1.4	4.23X4.23	4	1.6-3.6	609-699
A1B2.4	4.23X4.23	4	0.8-3.6	529-699
A4QQ8.3	8X8	3.75	1.6-5	836-1046
13Z2.1	7.26X7.26	2.5	1.6-5	NA
A5L2.1	7.25X7.25	0.8	1.6-5	707-877

Though the micromirrors could be a viable alternative to the Galvano scanner, they are still expensive [38]. Based on their aperture size their price ranges from USD 529 ~ USD 1046 making them unsuitable for the low cost portable laser marking/engraving machines for consumer goods. The high cost of the mirrors is mainly attributed to the complex and expensive microfabrication process of the actuators [43]. Therefore, a low-cost MEMS mirror (few dollars) made from a cost-effective fabrication process will satisfy all the above-mentioned requirements. Flexible Printed Circuit Board (FPCB) is one such technology which uses a mature, low-cost process and is suitable for making MEMS micromirrors [43].

1.8 Flexible Printed Circuit Board

Flexible Printed Circuit Board are circuit designs printed using lithography techniques on flexible a substrate. These are similar to the PCB boards but instead of rigid base structure, flexible materials such as polyimide, polyester, Teflon and glassmat are used as the substrate. Among all the materials, Polyimide is most widely preferred due to its good mechanical, electrical properties and also provide better adhesion with copper layers. The copper used as the conductive layer is a rolled annealed copper instead of the regular copper (electro deposited copper) to have a sustainable electrical connection while enhancing the flexibility of actuator [44] [45] [46]. FPCBs are being used since the late 1970 in various applications such as connector in electronic device, sensors (electrocardiography sensor, tactile sensor skin, temperature sensor) and support actuators in some inflatable structures [43] [47] [48] [49] [50]. Since the technology has been long around it has become very matured and easily adaptive to mass manufacturing. Moreover, they are less complex when compared to other micro manufacturing process such as Polymumps, Metalmumps and CMOS.

Based on the number of conductive layers of circuits printed on the substrate, they are categorized as single layer, double layer and multilayer FPCB. The conductive layer may either be laminated on one side or sandwiched between the two polyimide substrates depending on the type of FPCB. In case of multilayer FPCB there is an insulation layer between the conductive layers to prevent short circuiting. Based on how the circuit pattern is generated on the substrate the FPCB fabrication is classified into two processes 1) Additive process 2) Subtractive process. Among the two, subtractive process is most widely adopted as it is more economical, cost efficient and comparatively robust [44] [51].

1.9 Fabrication of FPCB through subtractive process

In this method, the laminate containing insulation and conductive layers are pre-cleaned chemically to eliminate contaminants and ensure better bonding. The laminate can be chosen based on the type of FPCB required (Single layered or double layered). The exposed copper layers are coated with photo resist film (dry film or ink) and the corresponding alignment holes are drilled. The preprocessed laminates are then overlayed and aligned with masks containing desired circuit pattern with the help of alignment holes. The entire setup is exposed to UV radiation to transfer the desired circuit patterns on the laminates. Only the exposed area cures and after curing it is subjected to subsequent etching process where the uncured area of the copper layer is removed. Both the UV exposure and the etching process may be carried out on both sides depending on the requirement. Then the etched laminates are laminated with coverlayer using high heat and pressure to protect the circuit patterns from environmental factors [52] [46]. Figure 8. shows the steps involved in fabrication of double sided FPCB [46].

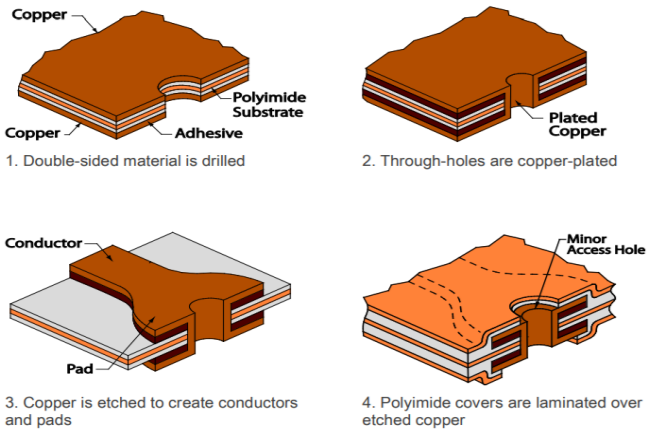

Figure 8. Steps involved in fabricating a double sided FPCB [46].

Whereas, in case of multilayer FPCB, the middle laminates (single or double layered) are prepared separately and laminated together to form multi layered FPCB and the electrical connection between different conductive layers can be established with the help of copper platted through

holes. Therefore, the multilayered FPCB are not suitable to be used as actuators due to their reduced flexibility associated with its lamination process [51].

Hence, by using the FPCB fabrication technology to fabricate micro mirrors, it is possible to fabricate a micro-actuator with all the advantages of a typical MEMS mirror while maintaining low costs even for the customized models. Based on the literature review, the FPCB based rotational actuators for laser engraving/marking would be the first of its kind. Hence, the following thesis would not only focus on the development of micromirror and would also address the problems encountered with such actuators.

1.10 Thesis Objective

1) Develop a novel, magnetic MEMS micromirror using a new material known as Flexible Printed Circuit Boards (FPCB) which was previously used as connector, sacrificial layer, sensors etc. By doing so, it is possible to develop a micromirror with high surface quality and large aperture but at low cost than the conventional micromirrors.

2) Develop a laser scanning system using the designed micromirror by placing two of unidirectional actuators orthogonal to each other. Which are capable of operating at both quasi static and resonant modes.

3) Develop a complete laser engraving/marking system which includes both hardware assembly such as low powered laser and the novel laser scanning system developed in this research and the corresponding software code, for the applications that require compact and low-cost marking/engraving system.

4) Identification of a new problem (drifting) associated with the FPCB based micro actuators and provide possible solutions to minimize or eliminate the problem.

The organization of thesis is as follows:

- Chapter 2 deals with the design and principle of the FPCB micromirror, as well as the scanner and the laser marking/engraving system based on it.
- Chapter 3 presents the modeling of the complete system and the simulation of the micromirror.
- Chapter 4 deals with the prototyping and experimental tests of the micromirror and the scanner. Further, this section also deals with identification of a new problem associated with FPCB micromirror-Drifting.
- Chapter 5 deals with implementation of a new scanning methodology to overcome drifting problem discussed in chapter 4 and the experimental results obtained using our newly developed FPCB micromirror based laser marking/engraving.
- Chapter 6 presents the summarization of Conclusion.

Chapter 2. Design of the FPCB micromirror and the engraving/marking system

The micromirrors are a combination of an actuator and a reflective top surface. Which reflects the incident laser beam based on the actuator rotation. In this section, we will discuss in detail about their design.

2.1 Micro actuator

Microactuators are small devices which can convert the input energy into mechanical motion. Based on the type of input energy used, they are classified into four major categories such as [53]:

1) Electrostatic actuators

2) Piezo electric actuators

3) Thermal actuators

4) Magnetic actuators

2.1.1 Electrostatic actuators

These actuators use columbic force of attraction or repulsion between the two charged bodies, due to the applied voltage and can be easily fabricated by both typical MEMS fabrication process or FPCB technology (only the simple designs) [54] [55] [56] [43]. Generally, these are one of the most commonly preferred method for actuation as they provide simple integration into the system and have very fast response time (<0.1ms) along with minimal power consumption. But these actuators generally provide small actuation for the applied voltage when compared to other major

actuators and there is pull in effect which seriously affects the actuator performance. There are two types of electrostatic actuators, 1) parallel plate actuators and 2) comb drives actuators. The latter was newly developed to overcome the above-mentioned disadvantages [57]. Only the parallel plate actuators have been previously developed with FPCB technology [43]. Comb drive actuators are mostly preferred for the torsional actuation as they can reach large rotational angle. But, it will make the fabrication process complicated, thus increasing the cost. The following Figure 9. shows an electrostatic FPCB based resonant micromirror developed for laser pattern generation [43].

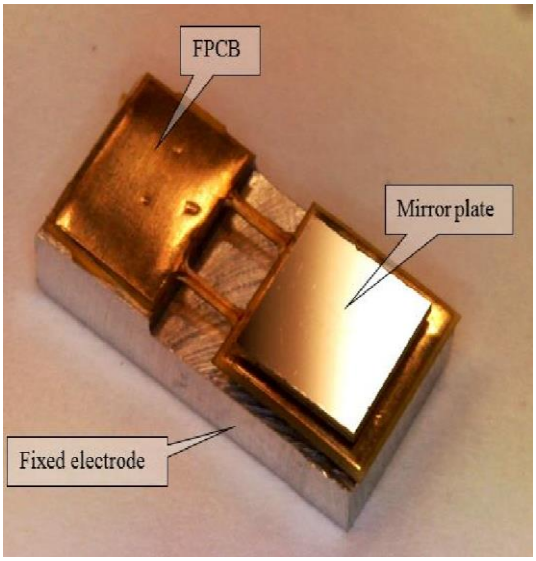

Figure 9. FPCB based resonant electrostatic micromirror for laser pattern generation [43].

2.1.2 Piezoelectric actuators

As the name suggests these actuators use piezoelectric effect of the materials to achieve the desired actuation. When the piezoelectric material experiences input energy (Alternating Current) they provide corresponding deformation, which can be used for the actuation. These actuators are linear (voltage-rotation angle relation) and have various advantages such as faster response, low power consumption and high force density. But the major factors which makes it unsuitable for the current

application is complicated fabrication process and smaller angular displacement range for the applied input voltage [58] [59].

2.1.3 Thermal actuators

These actuators use input heat energy given in the form of applied current, to generate the thermal expansion, thereby providing the corresponding mechanical actuation. Such actuators are also known as electrothermal actuators (heat actuators). They are generally made of two dissimilar metals which expand at different rates due to the application of heat. These actuators are relatively simple to fabricate but they have higher power consumption and slow response time. Further the presence of thermal fatigue due to repeated heat cycles affects the performance of the actuators. There is a special type of thermal actuator known as Shape Memory Actuators (SMA), which are made of material like copper-aluminium-nickel alloy and nickel-titanium alloy (NiTi). These alloys have peculiar characteristics of remembering the original shape (shape before the deformation) and returning to it upon the application of heat [60] [61] [59].

2.1.4 Magnetic actuators

The magnetic actuators can be based on either one of the principles: 1) Magnetic Lorentz force 2) Magnetic force of attraction/repulsion 3) variable reluctance. The main advantages of these actuators are 1) large displacement for the applied current than any other categories of actuator 2) ease of bidirectional actuation 3) more suitable for harsh environments 4) linear relationship between the applied current and rotation angle 5) low voltage operation. But there are some disadvantages which prevents them from being used widely, such as the high-power consumption and complicated fabrication process (regular MEMS fabrication) [62] [63] [59]. The following

Figure 10. shows a) cantilever type Lorentz force actuator capable of three axis actuations [62] b) magnetic force of attraction/repulsion actuator with a solenoid and nickel film [63].

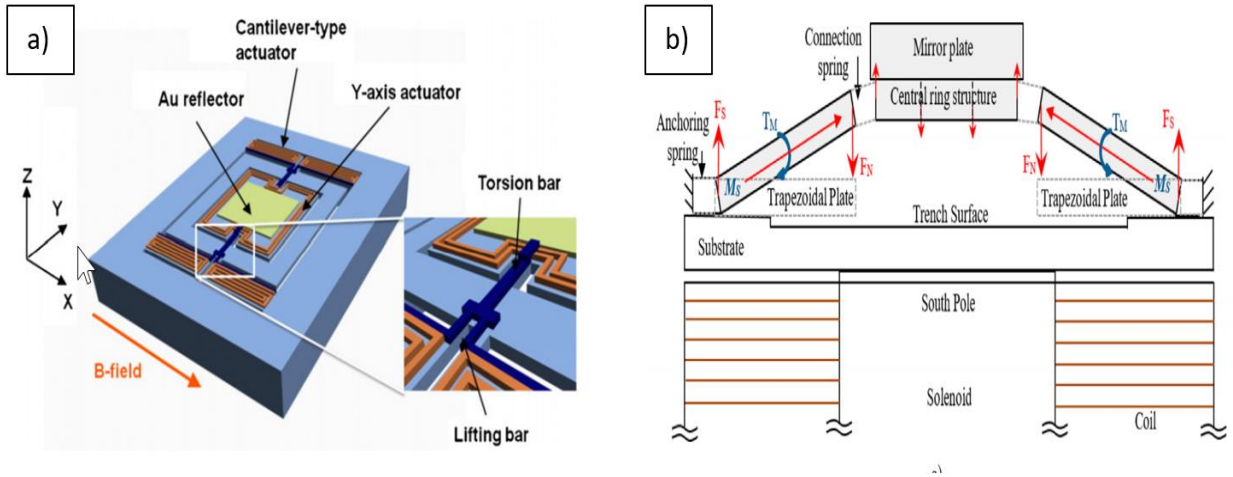

Figure 10. a) cantilever type Lorentz force actuator capable of three axis actuations [62] b) magnetic force of attraction/repulsion actuator with a solenoid and nickel film [63].

Table 3. Compares the various advantages and disadvantages with different types of actuation mechanism [59].

Description	Thermal	Electrostatic	Piezoelectric	Magnetic
Power consumption	☒	☑	☑	☒
Response time	~	☑	☑	~
Displacement	☑	☒	☑	☑
Low voltage	☑	☒	~	☑
Robustness	~	☑	☑	☑
Adaptiveness to FPCB fabrication technology	☒	~	☒	☑

The Table 3. compares the various advantages and disadvantages associated with different types of actuation mechanism where ☑- represents good performance, ☒- represents poor performance and ~ - represents decent performance under each category [59].

Though all the above-mentioned actuation mechanism has their own advantages and disadvantages, selection is made based on the following requirements:

1) It should be easy to fabricate mainly using FPCB technology to keep the overall costs low.

2) It should have linear relationship between the applied current and rotation angle to have a better control over the mirror.

3) It should have large displacement for the applied current to achieve a larger engraving area.

4) It should have decent mirror response time. Though the response time will determine the speed of the engraving/marking machine, it also depends on the irradiance caused by the laser spot on the target material. Hence, it is not considered to be a major determining factor.

5) It should be robust to work in harsh environment, such as the intense heat caused by the laser beam, without causing failure.

Based on all these requirements, the magnetic actuation system is suitable for the application. The next major consideration is the power consumption. Generally, the magnetic actuators consume more power to produce large deflection. In order to keep it low (<0.1 watt) we have opted for the Lorenz force based actuator instead of the magnetic attraction/repulsion based actuators.

Therefore, the novel actuator proposed is a Flexible Printed Circuit Board (FPCB) based magnetic Lorentz force actuator capable of operating at quasi static modes. The design of the individual actuator and the scanning system will be explained in the forth coming sections.

2.2 Design of the FPCB based rotational actuator

As the name suggests the Lorentz force actuators uses the principle of magnetic Lorentz force to provide the necessary actuation which can be given by the following equation [64]:

$$F = BIL \sin(\theta) \quad (1)$$

Where,

F= Actuation force (N)

B= Magnetic flux density (T)

I = Current through the conductor (A)

L= Length of the conductor (m)

θ = The angle between the direction of the current and magnetic field. The force is maximum when the $\theta = 90°$ (perpendicular) and zero when $\theta = 0°$ (parallel).

It is known that the actuation force is directionally proportional to the applied flux density, current and the length of the current carrying conductor. Hence, by increasing these factors we can increase the overall actuation force, and thereby increase the engraving area. Each actuator assembly consist of FPCB based actuator film printed with the desired driving circuits, placed between the poles of two strong neodymium cube magnets.

2.2.1 Design of the actuator film

Each actuator film consists of a central plate connected to the two supporting pads by torsion beams. Hence, when the current is applied through the circuit in the FPCB film an actuation force is produced. Based on the direction of the current passed through it, the direction of the actuation

force varies (Flemings left hand rule or motor rule) and thus providing the desired unidirectional rotation. Further, the width of the torsion beam and the thickness of the actuator also contributes to the rotational angle. Wider the torsion beam, the system will be more stable, but at the expense of rotational angle. The design of the printed circuit must be in such a way that it helps in increasing the actuation force. Hence, a dual copper layer concentric coil design on the central plate would increase the overall length of the conductor and thereby increase the total actuation force**.** Once the actuator design is made, the next step would be the design of the mirror plates with high surface quality, large aperture capable enough to withstand the laser beam. It is then bonded with actuator to form the complete micromirror. Similarly, other parameters such as, the selection of the permanent magnets and the applied current may also contribute to increase the rotational angle. But there are physical limitations, to the magnet size and the applied current, that should be used to keep the overall size, cost and power consumption low.

2.2.2 Selection of the magnets

As mentioned above, to keep the dimensions of the magnet small, while retaining its magnetic strength, N52 grade Neodymium (NdFeB) cube magnets are chosen. Based on the magnetic materials used to fabricate them, the neodymium magnets are graded. The grades of the magnets would determine the strength of the magnets, typically ranging from N35 to N52. Cube magnets are chosen as they can retain their magnetic field strength over longer distance and easy to integrate into the design when compared to the other shapes.

2.2.3 Design of the laser scanning system

Finally, the micro actuator mechanism consists of two unidirectional FPCB based rotational actuator assembly, placed together orthogonally in such a way that each actuator scans along X or

Y axis. The selection of the X and Y axis can be determined by fixing the actuator horizontally or vertically. Further details about the dimensions would be discussed in the chapter 3. The Figure 11. shows the basic design sketch of the individual X axis actuator and the magnet arrangement fixed vertically from top view.

Figure 11. Design sketch of the individual X axis actuator and the magnet arrangement fixed vertically from top view.

2.3 Design of the micromirror based laser engraving system

Apart from the laser scanning system, the other major parts of the engraving system are the laser source and the corresponding optics.

2.3.1 Selection of laser source

As mentioned in the chapter 1 (introduction- section laser source), the selection of the laser source and its wavelength depends on the type materials that will be used for engravings. Since the current applications are mostly limited to smartphone cases and leather products, the visible diode lasers are opted due to their cost efficiency in this category than the fiber or CO_2 laser. It is known that wavelength is directly proportional to the minimum spot size achievable [65]. Hence by choosing

the smallest wavelength in the visible spectrum, either 405 nm (violet) or 445nm (blue), it is possible to a achieve the smaller spot size and moreover it would also work well with planned target materials. However, the 405 nm lasers are expensive than their 445nm counterpart while they don't provide a major upgrade in terms of beam properties. Hence, the 445 nm, 2.5 diode laser was opted. Since the entire engraving/marking system was made modular, the laser source can be replaced with a different model based on the requirement.

2.3.2 Selection of optics

Selection of optics plays a major role in determining the working area of machine especially in machines where the laser source is fixed and only the beam scans the area. In such cases, optics can either be placed before or after the scanner. The latter method uses the F- theta lens which helps in increasing the working area, enhances the engraving precision and minimize laser power loss due to divergence. But usage of such lens would tremendously increase the product cost, as typical F-theta lens itself might cost around few hundred USD. Moreover, these lenses are available only at selected wavelengths (mostly in IR range) [66] [67]. Since the engraving area for the proposed model is small (< 25 mm), the optics can be placed before the laser scanner and the conventional focusing lens available with the laser source can be used.

There are two types of optics system in this category: 1) Three element lens 2) G series lens. Each lens system has its own advantages and disadvantages [68].

1) Three element lenses – As the name suggests, it has three individual lenses held together in a single enclosure. It provides better beam characteristics but there is a power loss due to the multiple lens interface.

2) G series lens – These are single element lens and generally classified as G1, G2, G3, G4, G5, G6 or G7. It offers higher laser power output as the power loss due to the number of lens is reduced and at the same time it also affects the beam characteristics.

Since, most of the target materials to be used requires only low power (<1 watt), three element lenses are an apt choice as they prioritize on the laser beam characteristics such as better spot size with minimal divergence and thus contributes to better engraving quality.

2.3.3 Design of the engraving/marking machine

Laser source and scanning assembly are placed in a tandem arrangement as the focused beam from the three-element lens enters the scanning assembly placed at 45° to incident beam, which scans the laser spot across all the four quadrants. Selection of the scanning modes would also determine the scanning speed and programming complexity. Though the developed laser scanning system can operate at both raster and vector scanning modes. Initial programming limits their usage only to the vector scanning mode to engrave the image. However, there are certain changes to be made in the programming software code to achieve both the functions in the same machine.

2.3.3.1 Raster scanning mode

In this mode, the entire working area is converted into individual pixels and the laser beam scans the entire working area back and forth rapidly. The laser beam is modulated in only specific pixels to be engraved. Though the current raster scans are much faster than the vector scanning mode it is mostly suitable only for dense patterns. When patterns are separated from each other. The scanner speed is low as it scans the empty sections of the working area as well. The raster scans are mainly used for engraving logos. Images and text [69] [70].

2.3.3.2 Vector scanning mode

Unlike the raster scanning, the laser beam scans only areas with patterns. Instead of pixelated images (bitmap) vector images are used which provide the X and Y movement for the scanning system and the laser is kept ON during most of the engraving time and modulated only while transition from one vector line to another. The amount of data stored to perform engraving is much higher than the raster mode as the system has to store the coordinates (X, Y) for each data point rather than just the modulation data in the case of raster scan. Hence, its mostly suitable for the engravings patterns which are well spaced from each other and mainly used in industries for engraving image borders, outlines of texts and intricate shapes. The following Figure 12. shows the scanning pattern of a) vector and b) raster modes [69] [70].

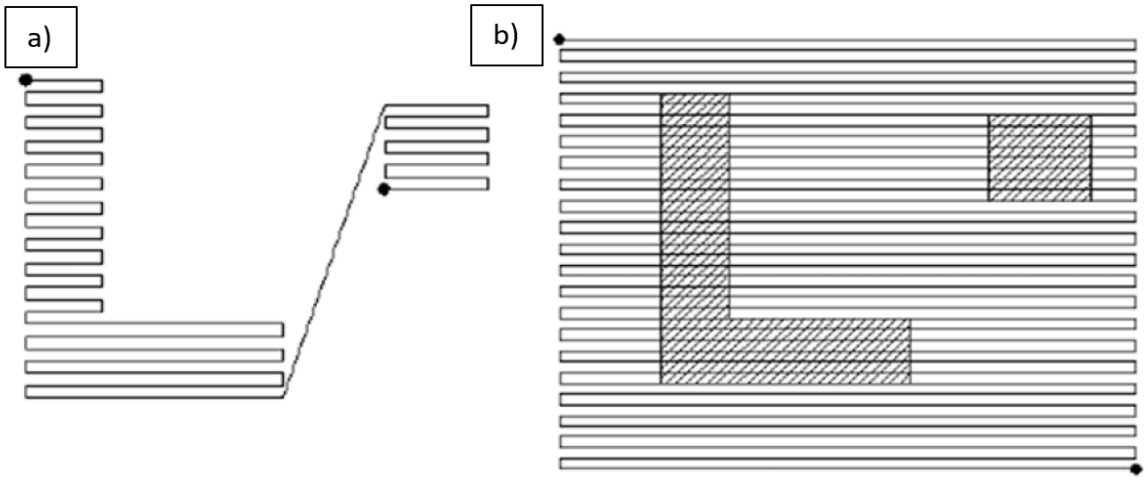

Figure 12. The scanning pattern of a) vector and b) raster modes [69].

Due to the time restrictions and the complexity involved in the creating software codes the current research, offers only the vector scanning operations in detail. Once the design of the actuator system and laser assembly is complete the next step is the modelling the complete system and performance estimation of the micromirrors through simulations which will be discussed in the following chapter 3. The following Figure 13 shows the schematic representation of the complete engraving system.

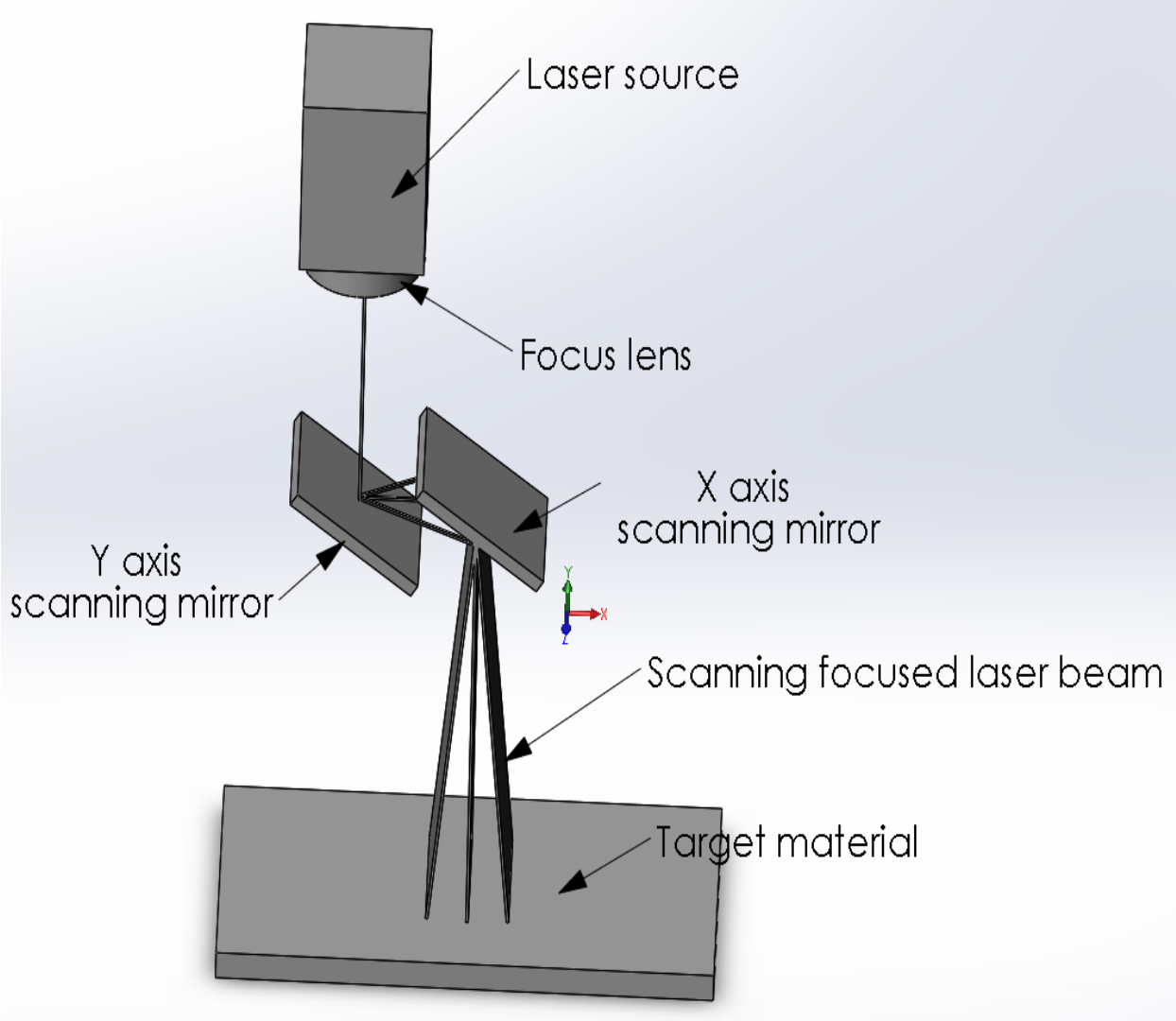

Figure 13. Schematic representation of the proposed laser marking/engraving system.

Chapter 3. Modelling and simulation of the FPCB micromirror and the engraving/ marking system

3.1 Modelling of the FPCB actuator film

Modelling of the FPCB actuator film and its supporting mechanical structures are done using Autocad and Solidworks respectively. The FPCB actuator film consists of a flexible polyimide substrate sandwiched between two copper coils. Both the top and bottom copper coils are connected by a through hole in the central plate. The centre plate houses the concentric coil structure. Since the horizontal copper coils (top and bottom section of the concentric coil) does not contribute to the overall actuation force, the central plate is made rectangular as it provides longer vertical coils (left and right). The central plate houses 8 concentric copper coils on each side of the actuator and each copper coil has a track width and track gap of 0.1mm respectively. Here track width refers to the width of each copper turn and track gap refers to the distance between each turn. Both the top and bottom surface of FPCB film are covered with polyimide based cover layer with cut-outs on one of the supporting pads to house the solder pads. The bonded mirror is a silicon based mirror plate measuring the same width of the central plate. The following Table 4. provides information about the dimensions of FPCB actuator, silicon mirror plate and magnets. It should be noted that all the values mentioned here are in mm.

Table 4. Dimensions of the FPCB actuator film, silicon mirror plate and magnets.

Dimensions of the entire FPCB actuator film								
Mirror plate								
Length of the sides (a)			Thickness (b)					
4			0.12					
FPCB actuator film (overall dimension)								
Length (c)			Width (d)			Thickness (e)		
26			4			0.11 (±0.03)		
FPCB actuator film (individual section)								
Central plate		Torsion beams		Support pads				
Length (f)	Width (g)	Length (h)	Width (i)	Pad A		Pad B		
				Length (j)	Width (k)	Length (l)	Width (m)	
6	4	5	0.5	3	4	7	4	
Dimension of the fillets on the polyimide film and the copper coils								
Polyimide film (n)			Copper coil (o)					
0.5			0.1					
FPCB actuator film (copper coil)								
1) Concentric coil on the Central plate								
Number of coils on each side	Track width (n)	Track gap (o)	Length of the outermost coil (Vertical- section a) (q)	Width of the outermost coil (horizontal-section b) (r)				
8	0.1	0.1	5.7	3.7				
2) Copper layer on the torsion beam								
Beam A		Beam B						
Length (s)	Width (t)	Upper coil	Lower coil					
		Length (u)	Width (v)	Length (w)		Width (x)		
5.5	0.1	5.5	0.1	10.6		0.1		
3) Copper layer on the support pad B (solder pads 1 and 2)								
Length (y)			Width (z)					
2.60			3.40					

Diameter of the connecting through holes in the polyimide substrate.		
Central plate	Support pads (solder pad section)	
0.2	0.2	
Thickness of individual layers of FPCB film (excluding adhesives)		
Layer name	Thickness	
Base substrate (polyimide)	0.025	
Copper layers (both upper and lower)	0.018	
Cover layer (both upper and lower)	0.025	
Magnets		
Grade	Type and material	Size
N52	Neodymium/cube	6.35

The following Figures 14 shows the dimensions of the various sections of the FPCB actuator. 13) FPCB actuator with cover lay and bonded mirror.

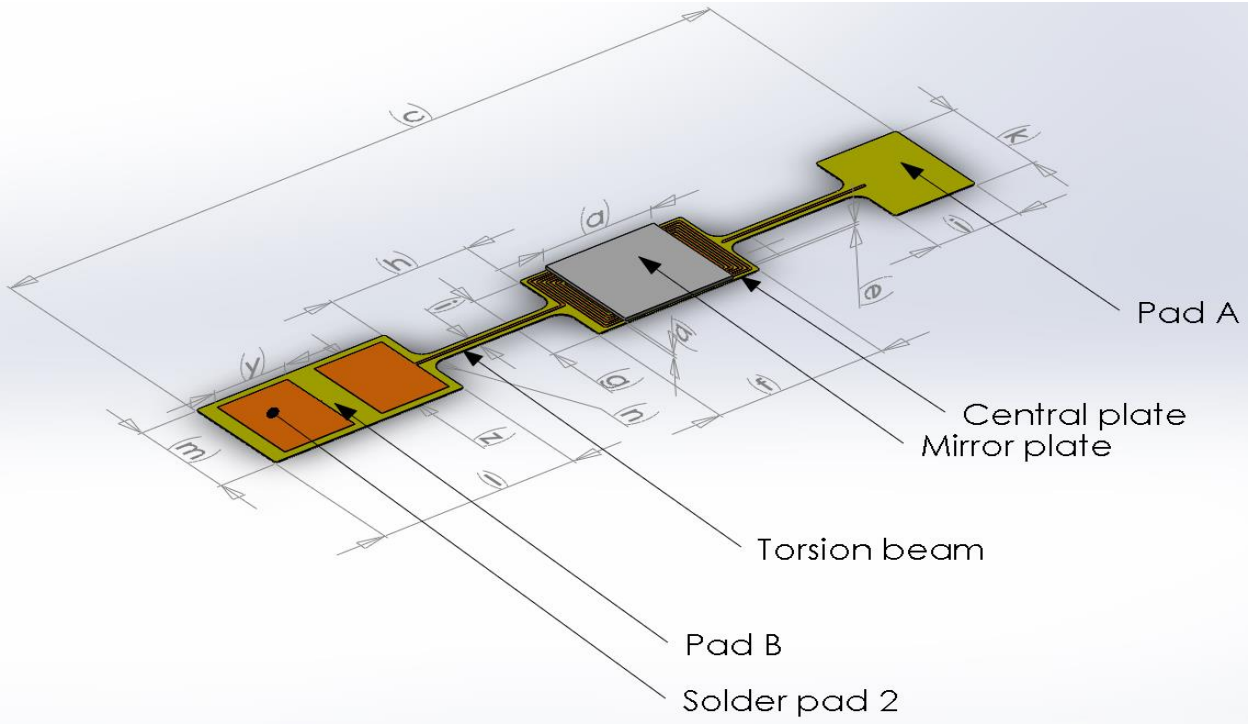

Figure 14. Major dimensions of the FPCB actuator with cover lay and bonded mirror.

To display the inner structure and arrangement of the coils the top cover layer and the bonded mirrors are hidden in the Figure 15. In both the Figures 14 and 15 the dimensions of the parts are marked with alphabets for which the corresponding numerical values can be referred from the Table 4.

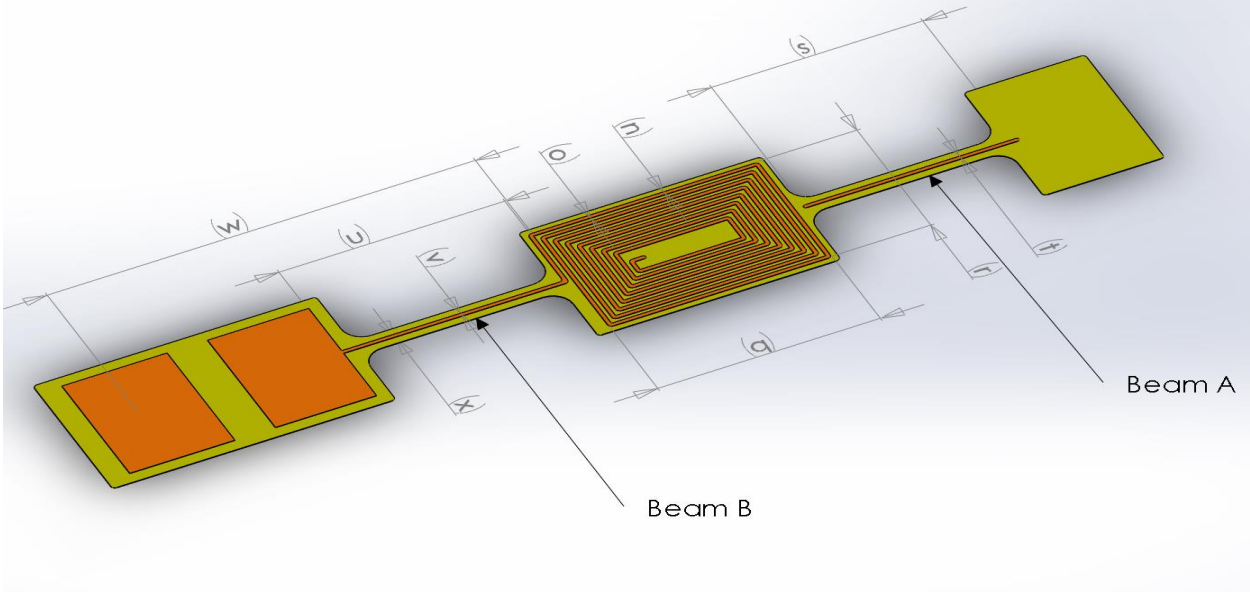

Figure 15. Dimensions of the inner copper coil of the FPCB actuator.

3.2 Modelling of the Individual actuator

Once the dimensions of FPCB actuator and magnets are determined, the corresponding support structures are modelled in solid works. Since each actuator is unidirectional the supporting structures should be designed in such a way that each mirror scans either in X or Y axis. Individual X or Y axis scanners are placed orthogonally to achieve a complete bidirectional scanning. It is known that the magnetic flux density is maximum at the centre of magnet (3.175mm from the magnet base). Hence placing the FPCB film at a height of 3.175 mm from the magnet base would help in increasing the rotational angle of the micromirror and there by increase the overall

engraving area. But placing the actuator at such height would affect the quality of the reflected beam from the first actuator due to the presence of the magnets. Based on the position of the FPCB film between the poles of magnet. There are two major configurations as explained below.

Configuration 1) Distance between the magnet base and FPCB actuator film is 3.175 mm.

Configuration 2) Distance between the magnet base and FPCB actuator film is 6 mm.

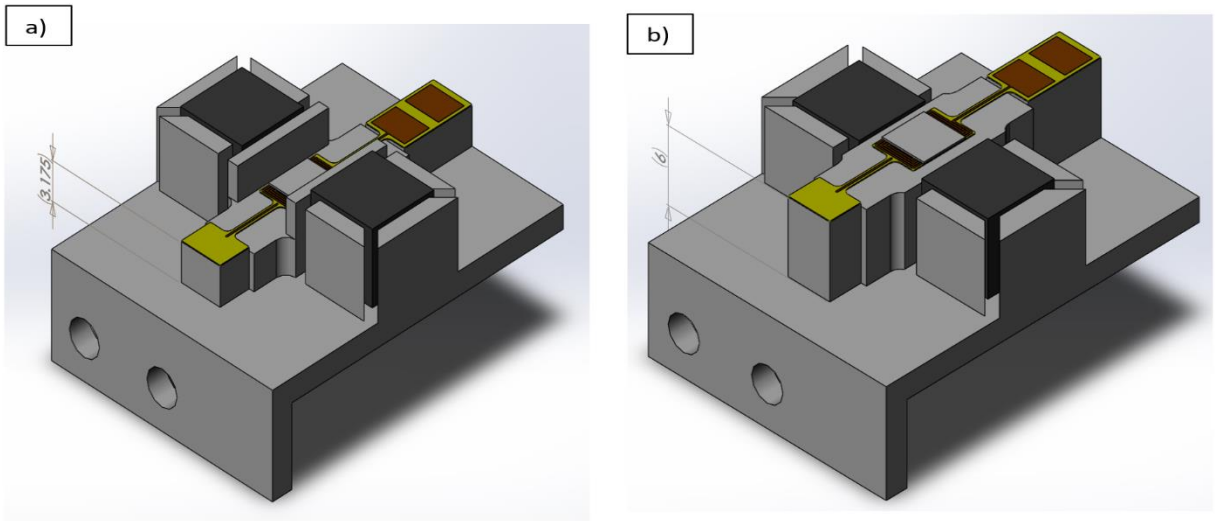

Figure 16. The two configurations of X axis FPCB actuators. a) configuration 1 b) configuration 2.

The Figure 16. shows the two configurations of the X axis scanner based on the height at which FPCB actuators can be placed from the magnet base between the magnetic poles. a) configuration 1 b) configuration 2.

Due to the physical limitations (size of each X and Y axis scanners) both the scanners should be separated at least by 9.5 mm. In that case, among the two configurations the later would provide better quality laser beams spots as the incident radiation is reflected completely without any interference by the magnets and the reflected beam must travel only 9.5 mm to reach the second mirror if the mirrors are placed at 6 mm from the metal base instead of 18.35 mm. In case of

configuration 2 where the mirrors are placed at 3.175mm from the magnet base, it may result in laser over shoot on the second mirror when the first mirror reaches larger rotational angle. Further, a scanning system with combination of both the configuration is also possible where the mirror 1 would be in configuration 1 and mirror 2 would be in configuration 2. The following Table 5. shows the maximum rotational angle (mechanical) achievable without laser overshoot on second mirror for different configurations when incident beam has a diameter of 1.5 mm and the distance between the two actuator is 9.5mm.

Table 5. Maximum rotational angle achievable without Laser overshoot on the second actuator (mirror).

Scanning system Configuration type	Description	Maximum rotational angle achievable without overshoot from the mirror 2. (mechanical angle)
Configuration 1	Mirror 1 and mirror 2 placed at 3.175 from magnet base.	± 2°
Configuration 2	Mirror 1 and mirror 2 at 6 from magnet base	± 3.5°
Combination of Configuration 1 and 2	Mirror 1 at 3.175 and mirror 2 at 6 from magnet base.	± 2.75°

Though individual micromirrors can achieve a larger rotation angle with configuration 1. Due to the laser offshoot on the second scanning mirror, they are rendered useless in the current scanning system. Hence, to ensure a large working area as possible with the configuration 2 and to obtain a high quality reflected beam from the laser scanning system, few changes were made in designing the support structure.

1) The FPCB film is placed between the poles of the permanent magnets which are only 6mm apart and thereby ensuring higher magnetic strength to achieve higher actuation force.

2) Both the X and Y axis scanners are separated only by a minimum distance of 9.5mm.

Based on all the above-mentioned requirements the mechanical supports for the FPCB actuators were designed. The Table 6. provides the major dimensions of both X and Y axis actuator. It should be noted that all the values are in mm:

Table 6. Major dimensions of both X and Y axis actuator.

Actuator 1 (Y axis scanner)							
Length (a)	Width (b)	Thickness (c)	Separation distance between the magnet poles (d)	Magnet holder width (e)	Height of FPCB actuators from magnet base (f)	Vertical Distance from the actuator holder and actuator base (g)	Gap between FPCB actuator and metal base (h)
30	26	15	6	6.35	6	15	0.40
Actuator 2 (X axis scanner)							
Length (i)	Width (j)	Thickness (k)	Separation distance between the magnet poles (l)	Magnet holder width (m)	Height of FPCB actuators from magnet base (n)	Horizontal Distance from the centre of actuator and actuator base (o)	Gap between FPCB actuator and metal base (p)
30	22.8	15	6	6.35	6	9.4	0.40

All the tables and figures carry only the important dimensions. Whereas, the complete design sketch used for fabricating each structure are included in appendix A. The following Figures 16

and 17. shows the complete arrangement of the 17) horizontal actuator (X axis scanner) 18) vertical actuator (Y axis scanner) with various outer dimensions as mentioned in Table 6.

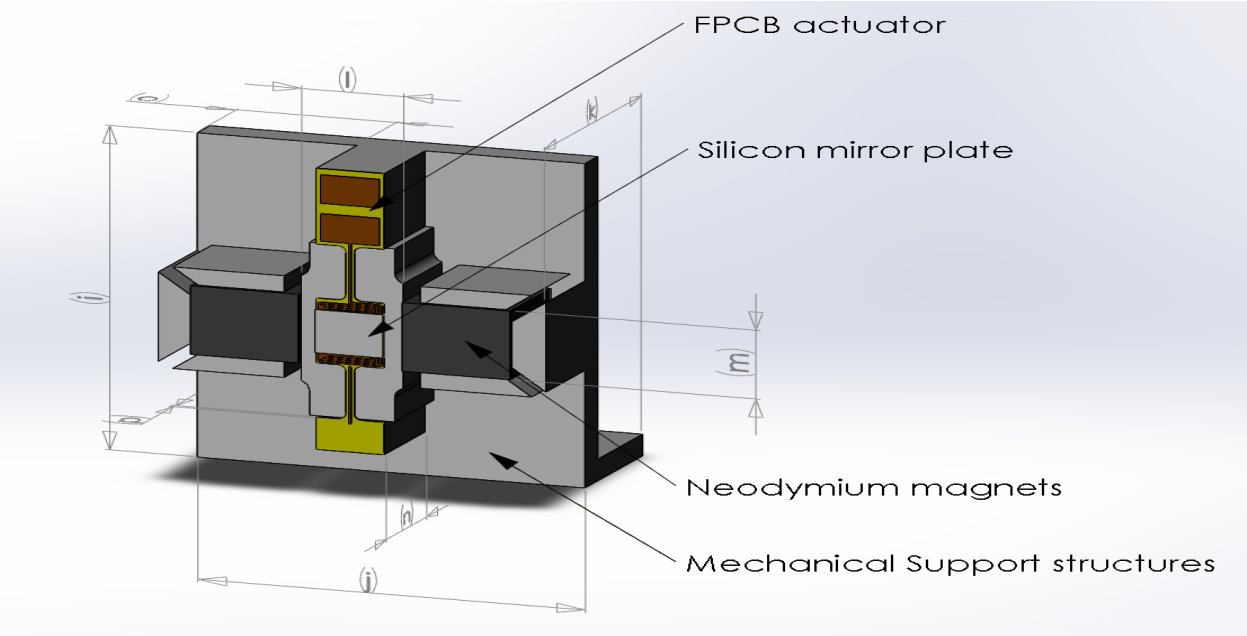

Figure 18. Major dimensions of X axis scanner as mentioned in Table 6.

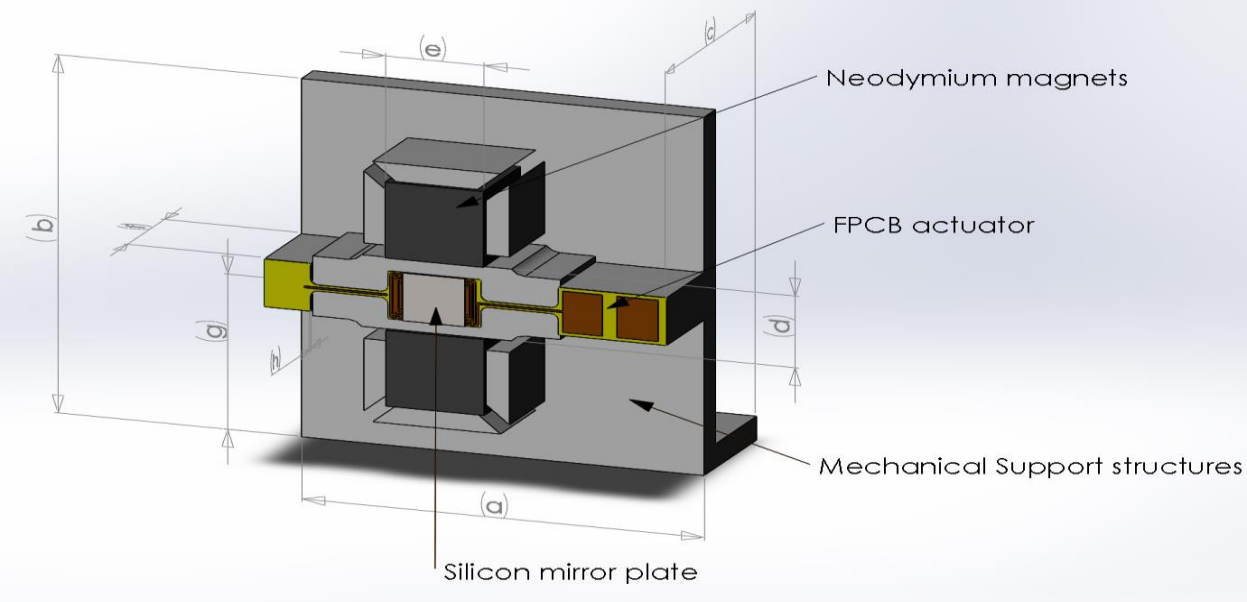

Figure 17. Major dimensions of Y axis scanner as mentioned in Table 6.

3.3 Modelling of the laser scanner base plate

Once the individual actuators are modeled, they are assembled in a common base to form the complete scanning system. The following Figure 19. shows the image of the base plate which holds the individual actuators using two screws:

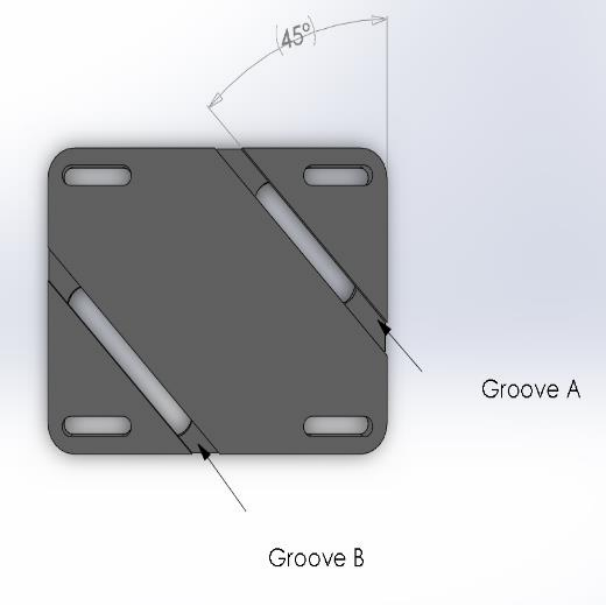

Figure 19. Modelled base plate which holds the X and Y axis scanners.

It is designed in such a way that the individual actuators can be placed orthogonal to laser beam along with provision to change the position and angle of the individual actuators or scanners and the position of the entire scanning system for alignment with laser beam. The grooves A and B are used to align the mirrors while maintaining the angle 90^{o} to incident laser beam. In some cases, when single screws are used (instead of double screws), each mirror can be placed at different angles as per the requirement. The FPCB actuators along with the base plate, completes the novel laser scanning system. The Figure 20. shows the image of the modelled laser scanning system: a) front view b) top view.

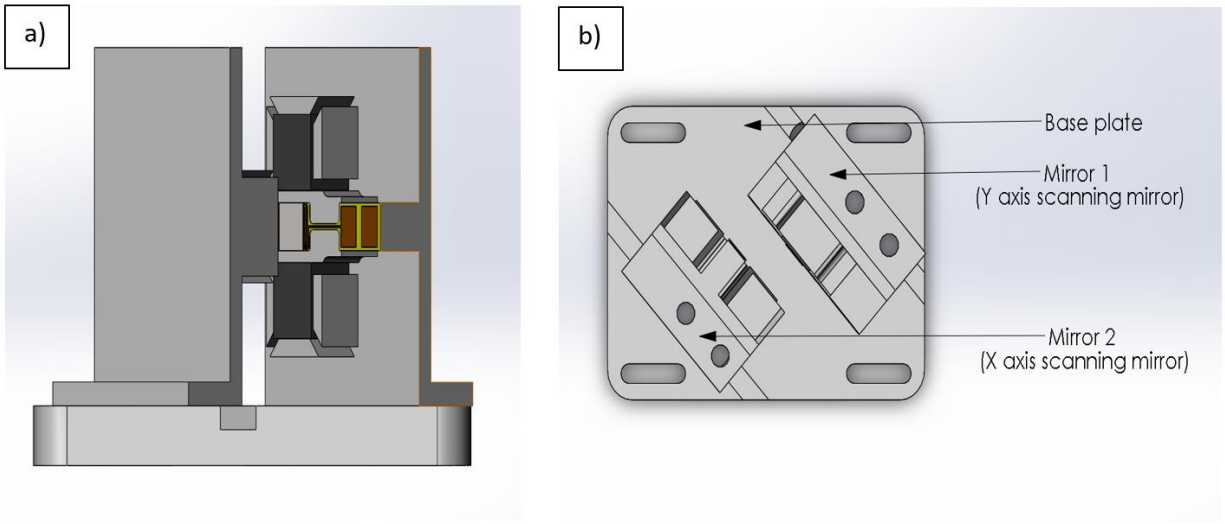

Figure 20. Modelled laser scanning system a) front view b) top view.

3.4 Assembly of the laser marking/engraving system

Once the scanning system is modelled, the laser source and the scanning system are aligned in a tandem arrangement and enclosed inside shell to prevent accidental laser exposure. The system and its supporting structures are designed to operate at two modes, namely, 1) standard mode 2) point and shoot mode.

1) Standard mode:

   The entire system is mounted on base stand and a vertical pole with the help of a holder. This mode is more suitable when the target pieces are small and can be placed within the engraving area. The working height and the engraving area can be controlled by moving the engraving/marking module along the vertical pole in addition to adjusting the focusing lens. The following Figure 21. shows the isometric view of the complete

engraving/marking system in standard mode with base and holding pole as additional addons.

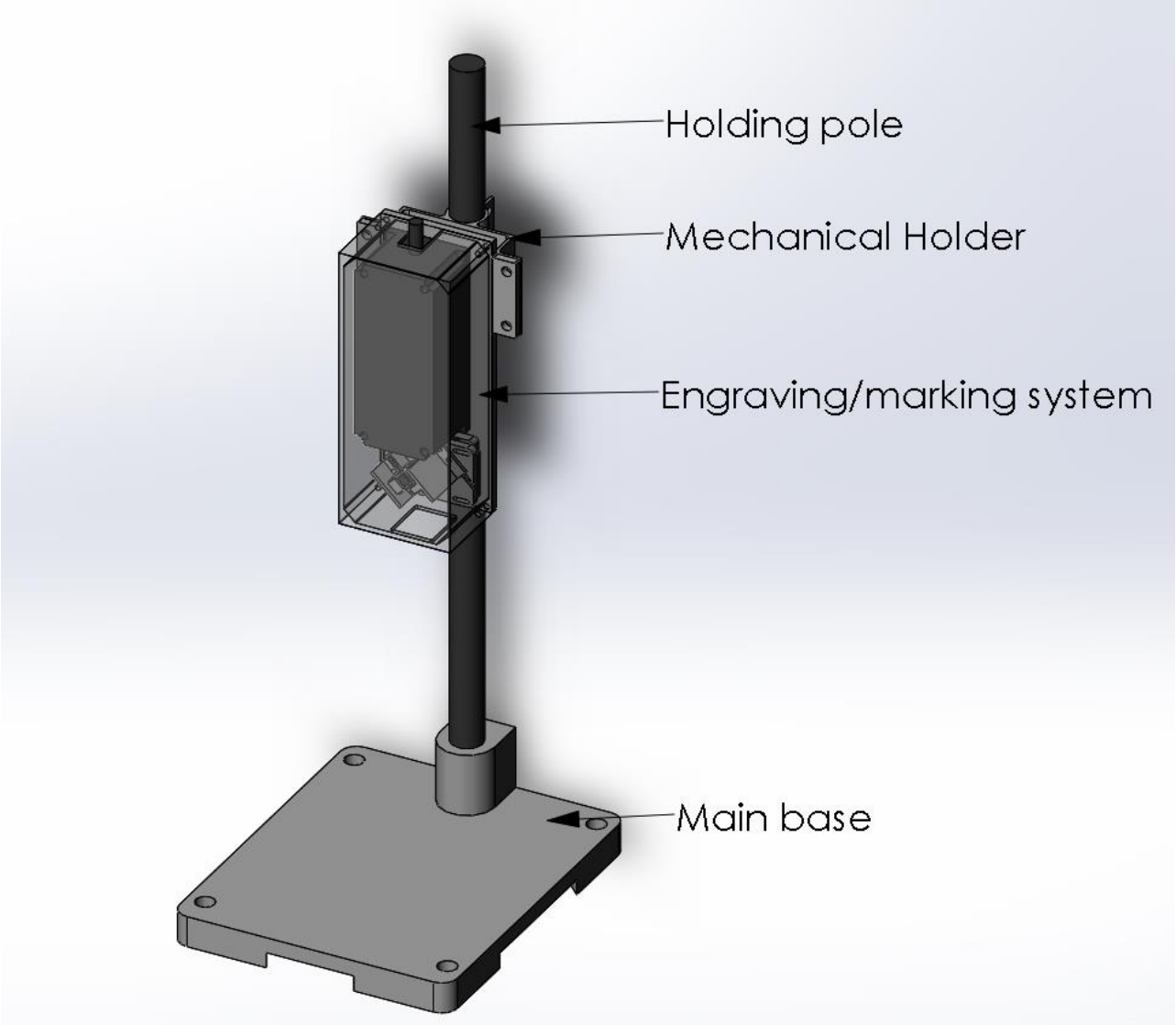

Figure 21. Isometric view of the complete engraving/marking system in standard mode.

2) Point and shoot mode:

This mode is mostly suitable for mobile applications where the target material is larger than the base holder or in case where the engraving/marking to be made on a preassembled part. Since the entire module weighs only less than 1Kg it can be used for point and shoot

operations from a working distance of less than 115 mm for better results. The following Figure 22. shows the complete engraving/marking system in point and shoot mode without drivers a) front view b) top view.

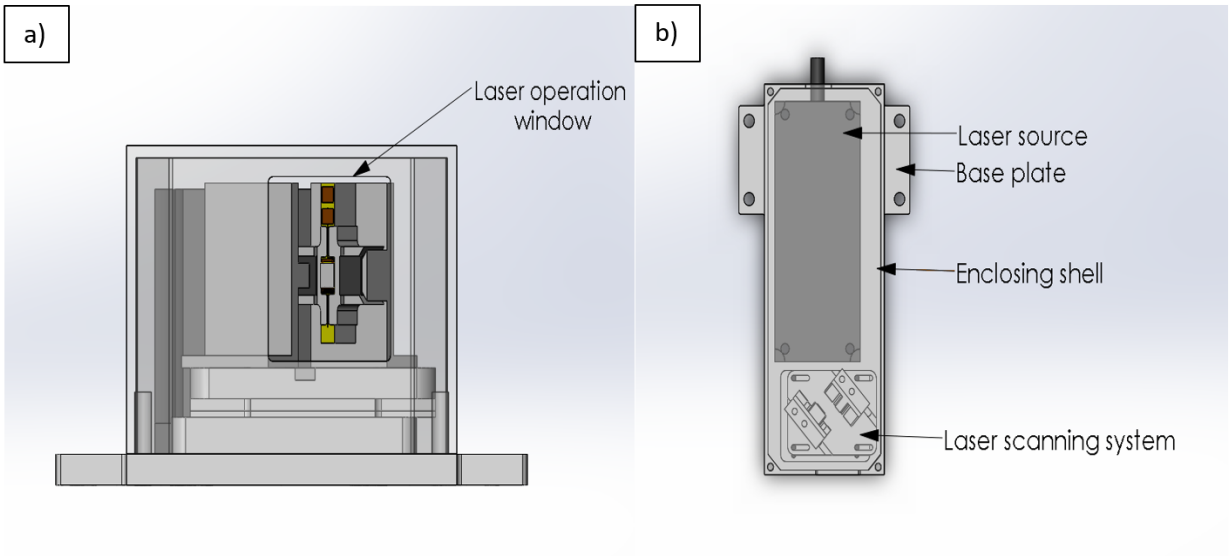

Figure 22.a) Front b) Top view of the laser engraving/marking system in point and shoot mode.

The complete engraving system is designed to operate in such a way that the focused laser beam exiting the optics is scanned along the X and Y axis by controlling the voltage applied to the micromirrors individually to trace the image or text to be engraved.

3.5 Simulation of Micromirror for performance estimation

The simulations for performance estimation of the micromirrors are carried out using Ansys 17.0. To run the simulation efficiently, the mechanical structures are not included in the simulation as it would increase the meshing and execution time. Since material property data for major components such as polyimide film and coil are not available within the Ansys database, the respective data are availed from other sources. The following Table 7. provides information about the material properties used for each component.

Table 7. Material properties of each components used in the simulations.

Part name	Materials used	Availability within Ansys database
Mirror plate	Silicon anisotropic	Yes
Polyimide	Kapton material properties [71]	No
Copper coil	Copper alloy	Yes (under general materials)
Rolled annealed copper	Material data [72]	No

3.5.1 Polyimide

The material data for the polyimide/Kapton (commercial name) is obtained from Dupont chemicals [71] and the following anisotropic material properties were used for the simulation to get better results: Young's modulus of $E_X = 3.1\ Gpa$, $E_Y = 3.0\ Gpa$, $E_Z = 3.1\ Gpa$, Density 1420 kg/m^{-3}, Poisson's ratio $v_{XY} = 0.39$, $v_{YZ} = 0.39$, $v_{XZ} = 0.34$, and Shear modulus $G_{XY} = 1.3\ Gpa$, $G_{YZ} = 1.3\ Gpa$, $G_{XZ} = 1.2\ Gpa$.

3.5.2 Copper coil

For FPCB circuits, generally two types of copper alloys are preferred, 1) Hot rolled annealed copper (RA copper) and 2) Electro Deposited copper (ED copper). The ED copper is less expensive to fabricate but more prone to structural failure, whereas, the RA copper is expensive and suitable for high flexibility operations such as the actuators. Hence, the properties of RA copper (C10400) are chosen instead of the regular copper for better results. It has a Young's modulus of 120 GPa, Density of 8970.3 kg/m^{-3} and Poisson's ratio of 0.34.

3.6 Assumptions for the simulation

The simulations and the results obtained were based on the following assumption (due to limited material data availability for polyimide and rolled annealed copper):

1) The data supplied by the manufacturer for Polyimide or Kapton are based on the consideration that the material is isotropic in nature, but in actuality the material is anisotropic (the properties are different in all three axes). Since the polyimide has always been used only as a sensor or connector and not as an actuator, there is limited information regarding the young's modulus, bulk modulus and Poisson ratio of the anisotropic polyimide film (as both the FPCB manufacturer and supplier were not able to provide those specific data). However, one research work presents the properties for a lab made polyimide film which is transversely isotropic due to the fabrication process (spin coating) [71]. Currently, to my knowledge, there are no data regarding the anisotropic properties of the commercial polyimide films.

2) The FPCB actuator film and the silicon mirror are assumed to be bonded without adhesive, since there are no proper data regarding the thickness and the property of the epoxy based adhesive used in FPCB actuator film fabrication. Hence, the increase in weight of the actuator caused by the adhesive is excluded.

3) For the magnetostatic simulations, entire FPCB film is considered to be made of silicon (anisotropic) and the regular copper alloy, available in the ANSYS database because the magnetostatic simulations require the magnetic properties of both polyimide and RA copper for which the data is very limited.

3.7 Static simulation

Static simulations are used to identify the relation between the applied current and the rotational angle. The following method can be used obtained the current required to rotate the actuator for a specific angle. In Ansys, it is not possible to obtain the relation using single analysis. Hence, the entire process is split into two major sections:

1) Structural section
2) Magnetostatic section

3.7.1 Structural analysis

For structural analysis, the magnets and other supporting structures are suppressed. The complete FPCB film along with the bonded mirror is fixed at the supporting pads. A force couple is applied to the edges of the central plate in the actuator due to which the material rotates. The corresponding mechanical rotational angle can be found using the following equation (trigonometric function).

$$\text{rotational angle} = \sin^{-1}\left(\frac{total\ y\ directional\ deformation\ (minimum\ value+maximum\ value)}{width\ of\ the\ central\ plate\ of\ the\ FPCB\ actuator}\right) \quad (2)$$

$$\text{rotational angle } (\theta) = \sin^{-1}\left(\frac{a}{4}\right) \quad (3)$$

Based on the angle produced the corresponding mechanical torque is calculated. This procedure is repeated for different force input and the corresponding torques values are calculated and stored in excel sheets. The following Figure 23. shows the deformation of the FPCB actuator film produced for applied force of 1.25 mN.

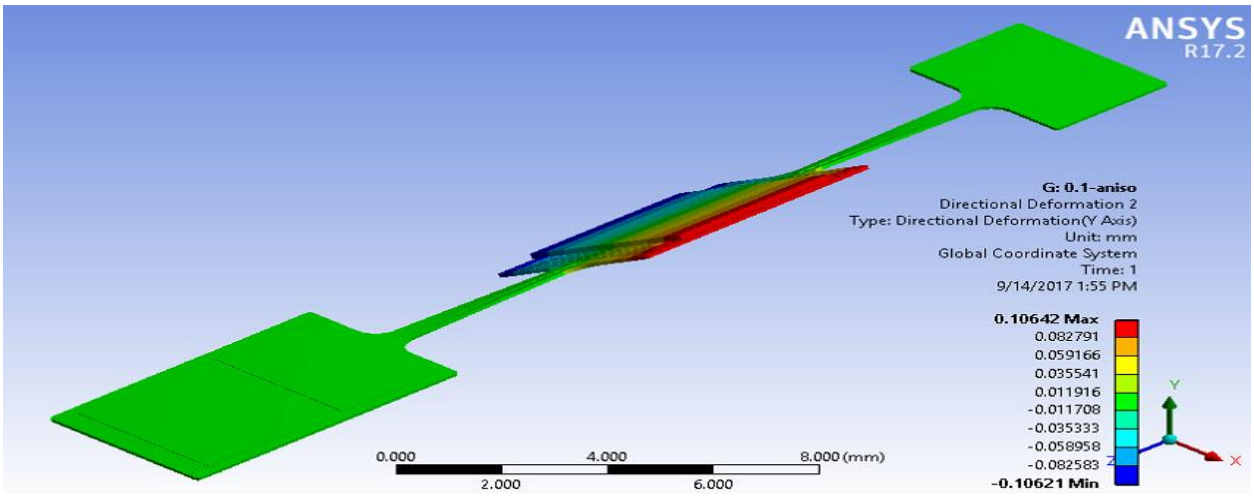

Figure 23.Deformation of the FPCB film for the applied force of 1.25mN.

3.7.2 Magneto static analysis

Once the mechanical torque is calculated the torque generated by the magnetic lorentz force should also be calculated, which is done using the magnetostatic analysis. In this section, the torsion beam of the actuator film is sliced off and only the central plate is used for the analysis. The model is rotated in solidworks for a predefined angle based on the angles subtended by the forces applied in structural section (stored in excel sheets). Then, these pre-rotated models are imported into Ansys under magnetostatic analysis. This section is mainly used to identify the magnetic field produced at each coil in the actuator. Since only the vertical coils contribute to the actuation force (based on magnetic Lorentz force). The X and Y component of magnetic flux density is identified and the corresponding resultant flux density and its orientation (angle) is found at each vertical coil. To increase the accuracy, the entire vertical coil is divided into individual section. And the same is repeated for all the 16 coils on top and bottom surface of the actuator film. The flowing figure 24 shows pre-rotated model used in magneto static simulation.

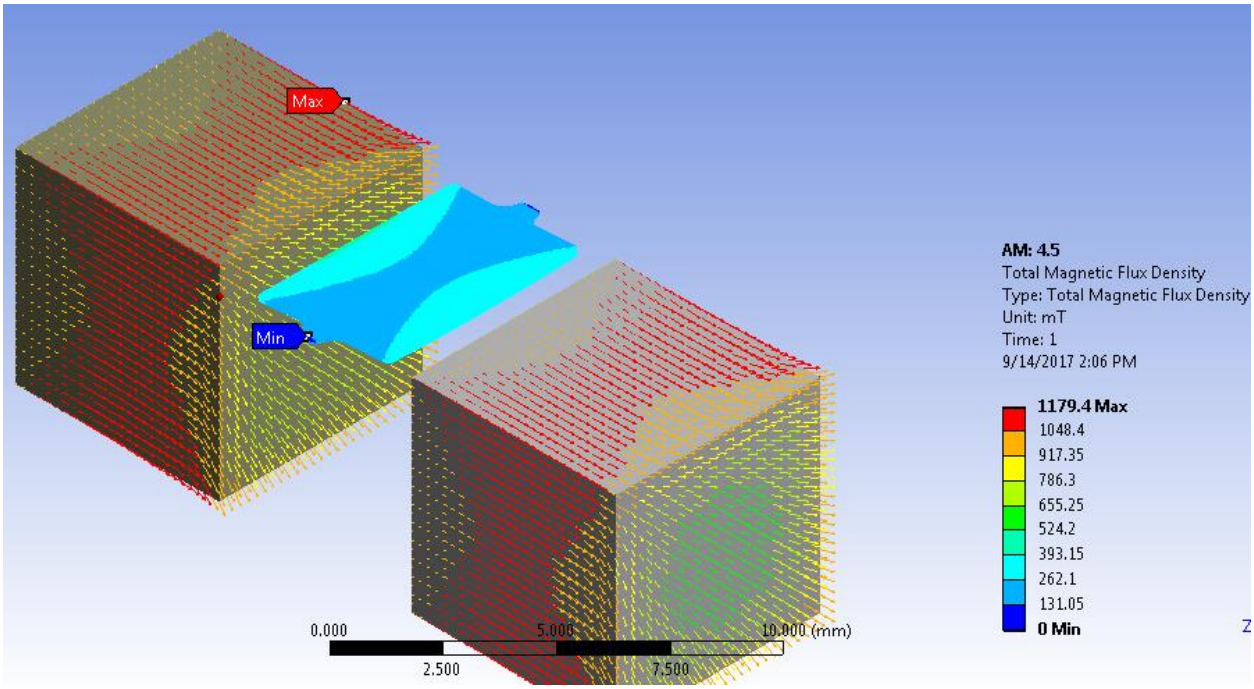

Figure 24. Sliced model used in magneto static simulation to calculate the magnetic flux density on each coil.

Once the flux density data are collected the magneto static force acting on each coil can be calculated using the equation 1 along with its corresponding torque (excluding the current value). Then the torque produced for the all the coils are calculated and summed up. Based on these data the current required to deflect the actuator for each rotational angle can be found by equating the mechanical torque and the summation of the torque produced by the magneto static force produced at each coil (excluding the current applied) for each rotational angle as given in the following equation (8).

$$\sum \text{Torque produced by coil 1} + \ldots. \text{ Torque produced by coil 16} = \text{Mechanical torque.} \quad (4)$$

$$\sum (\text{Magneto static force} \times \text{Distance from the axis of rotation} \times \text{Sine } \theta) = \text{Mechanical force applied} \times \text{distance from the axis of rotation} \times \text{Sine } \theta. \quad (5)$$

$$\sum (F_1 \times D_1 \times \text{Sine } \theta_1) + (F_2 \times D_2 \times \text{ Sine } \theta_2) + \ldots (F_{16} \times D_{16} \times \text{ Sine } \theta_{16}) = F \times D \times \text{Sine } (90°). \quad (6)$$

$\sum$ ((Magnetic field (B_1)×Current through conductor (I)×length of the conductor (L_1) ×Sin θ_1)× Distance from the axis of rotation and coil 1×Sine θ_1 …) = F×D×1. (7)

Since the current applied through each coil is the same, it can be found by equating the rest of the terms,

$$\text{Current (I)} = \frac{\text{F}\times\text{D}}{\sum ((B_1\times L_1\times \text{Sin}\ \theta_1)\times \text{D1}\times \text{Sine}\ \theta_1 \ldots + B_{16}\times L_{16}\times \text{Sin}\ \theta_{16})\times \text{D16}\times \text{Sine}\ \theta_{16})} \quad (8)$$

Similarly, the current can be obtained for various rotational angles and the following Table 8. provides information about the current required to obtain various rotational angles.

Table 8. Current required to produce each rotational angle.

Mechanical Rotational angle (°)	Current required to produce the mechanical rotational angle (mA)
0.38	13.95
0.76	27.21
1.52	54.84
1.90	68.54
2.28	81.89
2.66	95.13
3.05	108.63
4.57	160.39

3.8 Resonant frequency simulations

The resonant frequency can be determined using the modal analysis available at Ansys workbench. Since, the laser scanner can also operate at raster modes. The identification of the natural frequency would help in determining the speed at which the micromirrors can scan (usually less than the

natural frequency). The boundary conditions used for the structural simulation can be used for the modal simulation, but without the addition of load or force. It is found that the natural frequency of the FPCB based actuator at mode 2 (rotational mode) is 405.55 Hz. The following Figure 25. shows the FPCB micromirrors rotating at natural frequency 405.55 Hz.

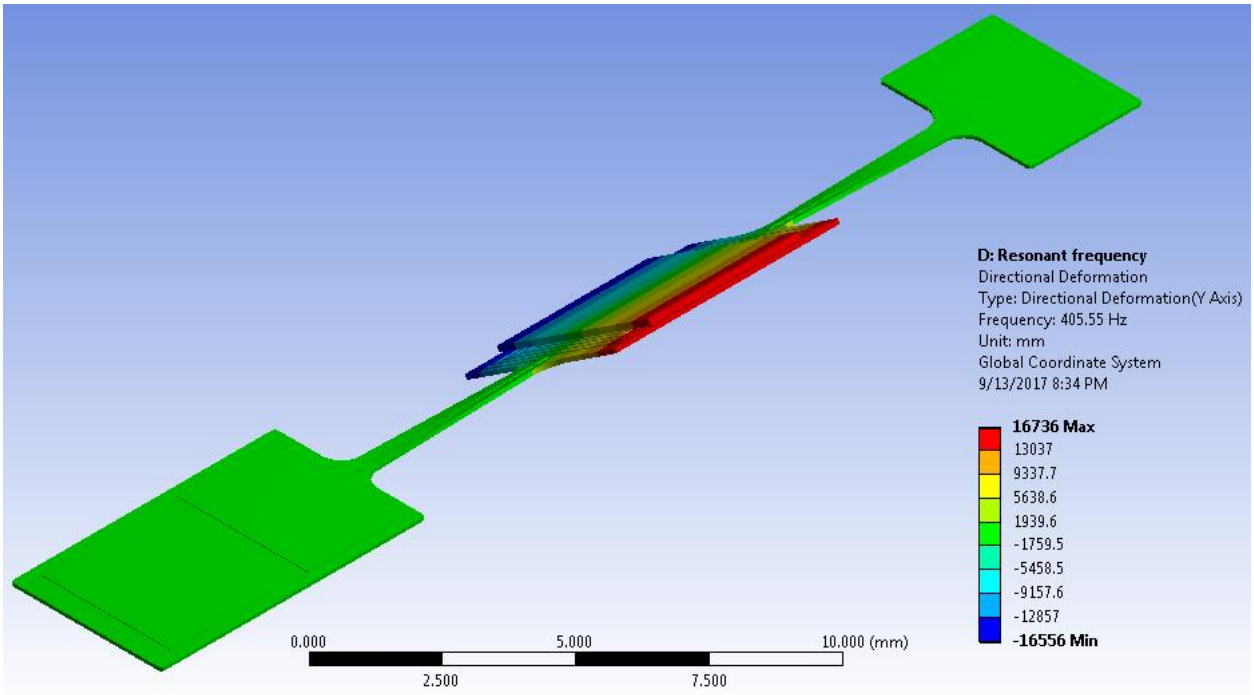

Figure 25. Resonant frequency simulation of the actuator.

3.9 Stress analysis

Though the FPCBs are designed to be flexible, it should be ensured that the stress acting on the polyimide substrate and copper coils are well within the limits to prevent any failure. The major stress prone region is the copper coil, especially in the area where the torsion beam connects with central plate. It should be noted that the yield strength of the copper is 80 MPa [43], hence the stress acting on the material even for high rotational should be less than the yield strength to prevent the failure of the actuator. Since the von misses stress acting on the copper coil for the

applied force of 1.25 mN is only 24.19 Mpa (which is within the range), the actuators are less prone to failures during the nominal operating condition of the mirrors due to stress. The following Figure 26. Shows the equivalent (von misses) stress acting on the copper coil along the torsion beam for an applied force of 1.25mN.

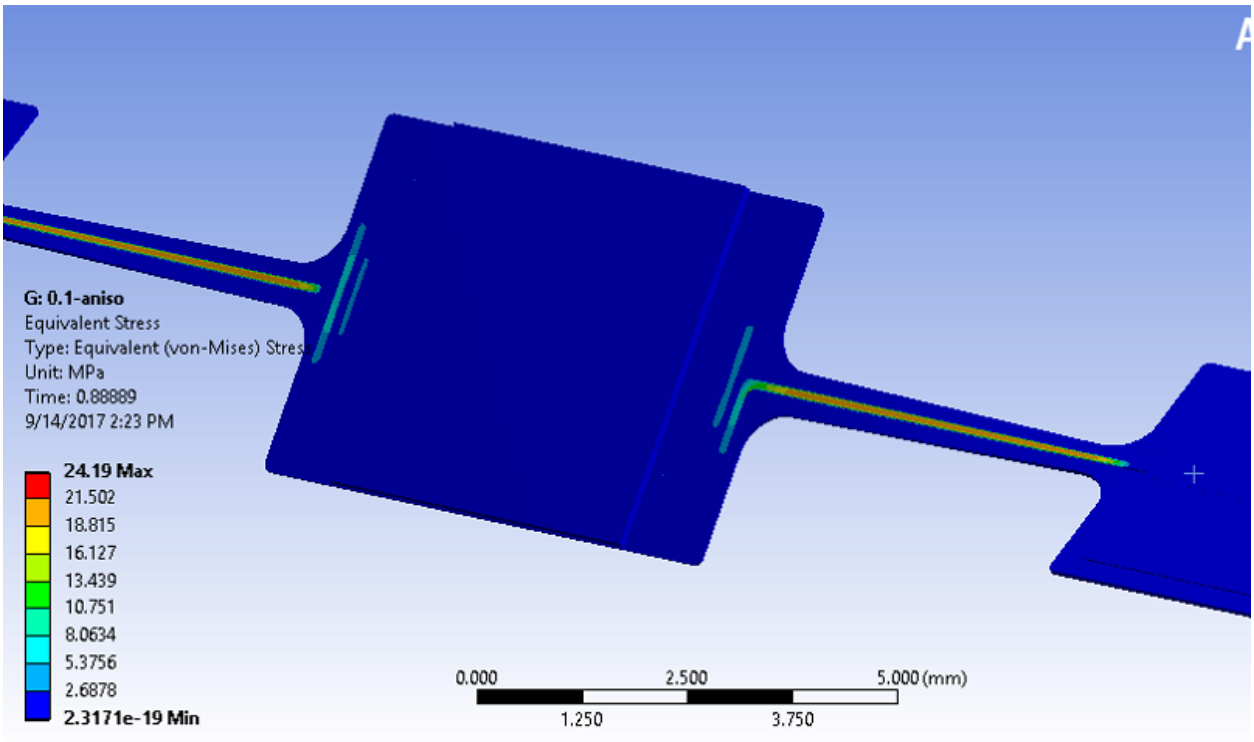

Figure 26. Stress acting on the FPCB actuator for the applied force of 1.25mN.

Chapter 4. Prototyping and performance testing

4.1 Fabrication of the hardware components

4.1.1 FPCB actuator films

Once the modelling and performance simulations are completed with satisfactory results, the parts are sent out for fabrication. The FPCB actuator films are fabricated by Fastline circuits, China. Two designs (Model 1 & Model 2) of the FPCB actuators were fabricated. Both the designs are similar in terms of dimensions except the width of the torsion beams, where the model 1 has a width of 0.5 mm and the model 2 has a width of 1mm. The following Figure 27. shows the image of the fabricated FPCB actuators, both model 1 and model 2.

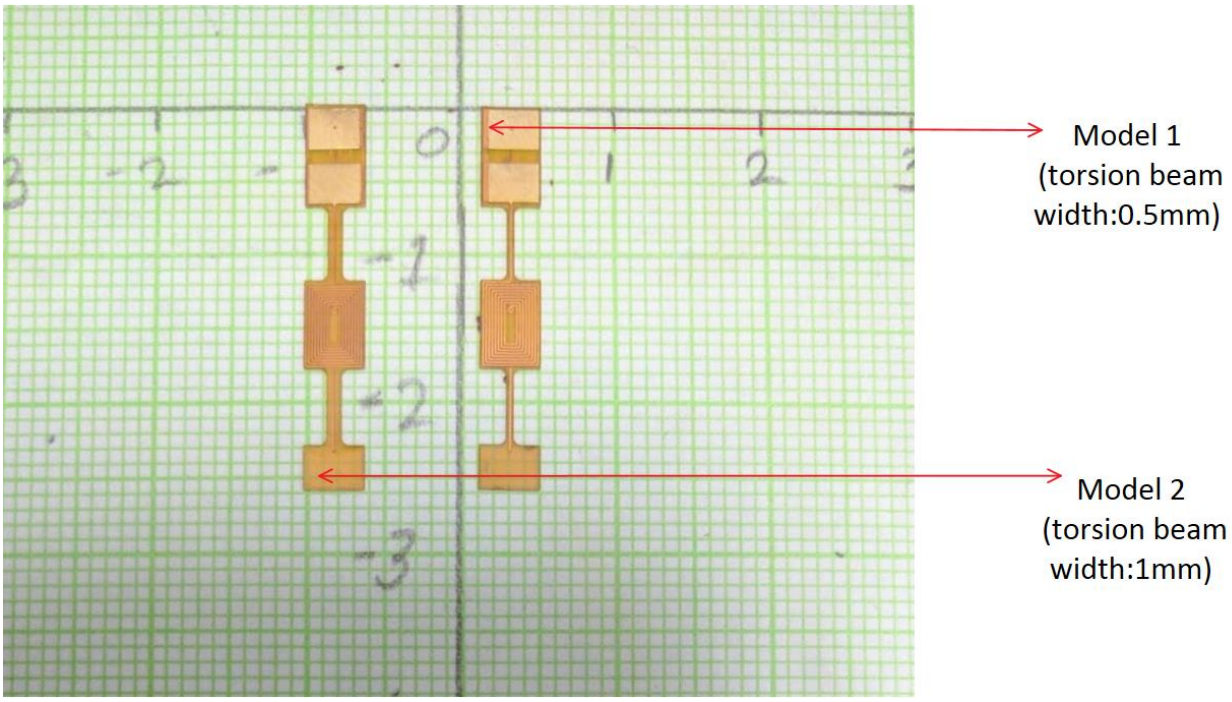

Figure 27. Fabricated FPCB actuators both model 1 and model 2.

Since the FPCB actuators are fabricated on a large laminate using lithography technique, the cost of individual actuators can be reduced with increase in the number of pieces per order. For testing purpose, 40 pieces of model 1 were fabricated at a cost of 100 USD, where each piece costs only 2.5 USD. Similarly, 10 pieces of Model 2 were made at a cost of 10 USD per piece. Moreover, the cost of customization (mask cost) is eliminated when the designs are reordered as the manufacturer stores the mask design for future usage. Hence the price of actuator mainly depends on the fabrication quantity and can be further lowered to few cents in case of mass production.

4.1.2 Silicon mirror plates

The mirror plates used are fabricated by dicing a polished silicon wafer coated with thin metal film into small squares. The selection of the metal film and the dimensions of the silicon mirrors determine the cost of the mirror plate.

4.1.2.1 Selection of metal film

Metals such as gold, silver, aluminium can be used as a thin film coat. Based on the wavelength of the incident radiation, the reflectivity varies [73]. The Figure 28. shows the reflectance of various metals based on the wavelength of the incident radiation.

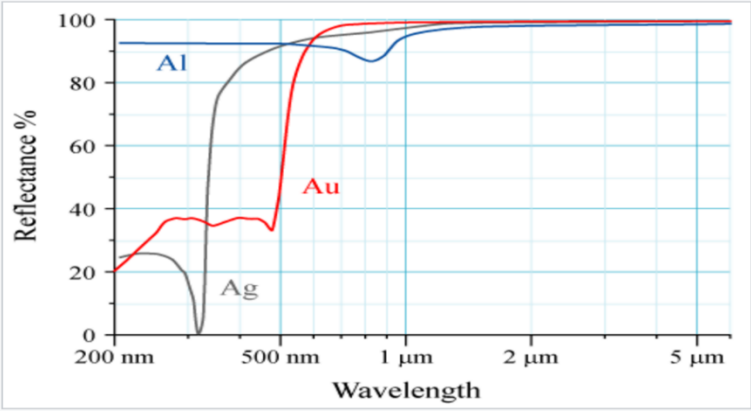

Figure 28. Reflectance of various metals based on the incident wavelength [73].

Among the three, aluminium has better reflection at lower wavelength and has a reflectivity greater than 90 % at a 445nm. Also, the cost of coating aluminium is much cheaper than gold or silver. Hence the mirror plates are coated with thin layer of aluminium.

4.1.2.2 Selection of aperture size

For laser engraving/marking, the mirror aperture size should be large enough to completely reflect the incident laser beam. At the same time, if the aperture is very large, it would drastically affect the speed of the mirrors. Hence a mirror plate of 4 X 4 mm should be apt for performing the above-mentioned task.

The cost of fabricating a single mirror plate (excluding the type of metal coated) can be calculated approximately by using the following method [43].

Cost of a typical 6-inch silicon wafer per piece: 3-5 (USD)

Approximate number of 4x4 mirror plates that can be diced from a single silicon wafer: 1000

Number of silicon wafers that can be coated in a single run using MEMS process: 10

Hourly rate for the coating process: 100 (USD)

Number of hours required to complete the deposition process: 10

Number of individual mirror plates that can be fabricated = number of mirror plates per 6-inch wafer × total number of wafers = (1000 × 10) =10000

Total cost of fabrication = deposition cost + purchase cost for 10 wafers =1000 + (5 × 10) =1050

Cost for single mirror plate= total cost / total number of fabricated mirrors = 1050/10000=0.105 USD.

Hence, the fabricated mirror plates can be as low as 11 cents whereas the typical mems mirrors fabricated along with actuators would cost around 20 USD or higher. The quality of the fabricated mirror is also much better than the mems mirror with a surface roughness in the range of 2-3nm and radius of curvature of about few tens of meters (>15m) [43].

4.1.3 Laser source and focussing optics

As mentioned in chapter 3 (section: selection of laser source), the laser source used is a 2.5-watt diode laser operating at a wavelength of 445 nm. It was purchased from OPT laser (European laser manufacturer) along with the three-element glass lens [74]. Since it is a tunable lens, the focal length can be varied from 30 to 150 mm for better results. The table 9. shows the specification of the laser source used.

Table 9. Specification of the laser source [74].

Specifications	Description
Wavelength	445 nm
Modulation type	Analog/TTL
Modulation frequency	100 Hz
Operating mode	Multimode
Operating current	5 A
Beam divergence (full angle)	2 mrad
Beam diameter at output	5 mm
Beam type	Rectangular
Diode lifetime	5000 hrs

4.1.4 Magnets and support structures

The magnets were purchased from K&J magnetics [75]. As mentioned in chapter 2 (section: selection of magnets), 80 pieces of N52 grade neodymium cube magnets (a=6.35mm) were purchased, at a cost of 82 cents each. The cost of magnets can further be reduced by ordering from a different supplier (from different countries) and in bulk quantities.

The mechanical support structures for the scanning system and the complete engraving system can be fabricated either in metal or plastic (ABS plastic) using 3D printer.

4.1.4.1 3D printed model

Though the cost of a good 3D printer is expensive, it is an one-time investment and can be used to print several models at low cost. They offer high flexibility, quick fabrication and low cost per model, but at the expense of precision and finished quality when compared to metal fabricated parts. Hence the 3D printed models were used to perform the preliminary analysis to finalize the model design which can be used to fabricate the final aluminium scanner assembly. The following figure 29. shows the a) front view and b) top view of the 3D printed scanner assembly using Flash forge creator Pro (3 D printer).

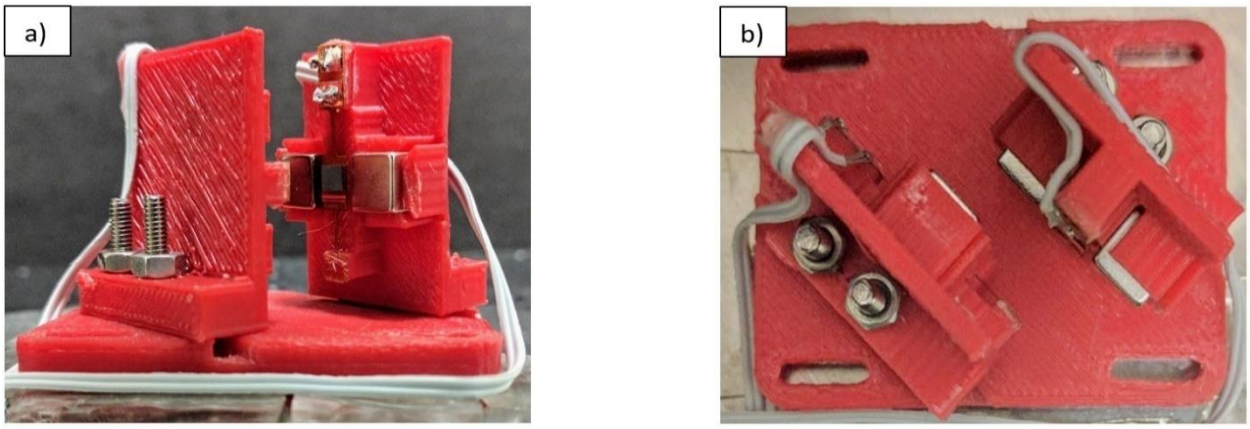

Figure 29.a) Front view b) Top view of the 3D printed scanner assembly.

4.1.4.2 Aluminium based model

The supporting mechanical structure for the laser scanner and the engraving/marking assembly is fabricated either in aluminium or a steel base. Since aluminium is non-magnetic, light weight, it is used for the scanner assembly and engraving/marking module. Due to the structural strength of steel, it is used for the holder, pole and main base. The design sketches used for the fabrication are included in the appendix A.

4.2 Assembly of the engraving/marking system

The silicon mirror plate and FPCB actuator are bonded manually using heat resisting epoxy based adhesive. It has a working temperature of 180° C to prevent the bonding failure due to heat generated by the incident laser beam. The bonding surfaces are visually inspected and precleaned to eliminate any contaminants and ensure better bonding. The magnets are placed in the respective holders in such a way that they attract each other (north and south poles) and are bonded to the base of the mechanical structure. Similarly, the support pads of the FPCB actuator and the metal base are bonded together using the same adhesive. The orientation of the FPCB film on the metal base determines the axis in which mirror scans (X or Y axis). The entire assembly is cured at room temperature for 24 hours to ensure better overall bonding and later the wires are soldered to the corresponding solder pads and fixed or bonded to the side walls of the actuator to prevent any additional stress on the solder. Once the individual X and Y axis actuators are assembled, they are placed orthogonally on the base plate using two M3 screws for each actuator. The total cost of the laser scanner including the customized model is less than 20 USD (3D printed model) making it several folds cheaper than other conventional scanner. The following Figure 30. shows the laser scanner assembly in different views a) Front view b) Top view of the micro mirror scanning system and c) The design of individual micromirror setup.

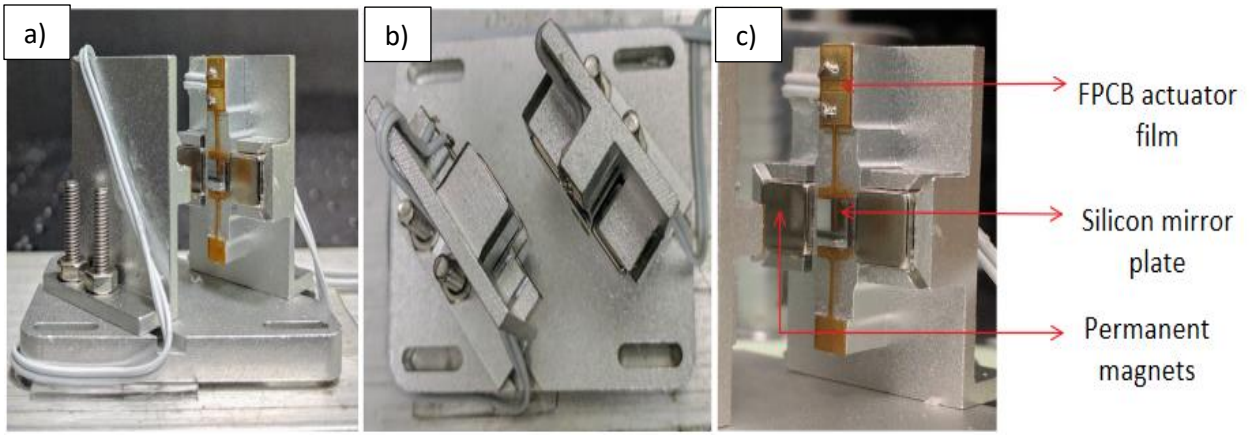

Figure 30.a) Front view b) Top view of the assembled laser scanner c) The design of the individual micromirror setup.

Similarly, the laser source is also fixed on the base plate using four M5 screws. The assembled laser scanners can be aligned to the laser beam and adjusted along all three axes (X and Y using the corresponding grooves present in the scanner assembly and Z axis using the height adjuster plates). The height adjuster plates resemble the scanner base plate and are manufactured with different thickness (1mm and 2mm). Movements on the Z-axis are controlled in steps of 1mm. The complete engraving system measures about 180x70x55 mm in length, breadth and height respectively. The laser scanner assembly and driving unit measures only about 52x39x31mm and 50x35x35mm respectively, which is much smaller than the other scanning mechanisms. Moreover, the laser source uses most of the space in the engraving system as the scanner itself occupies only 10% of the total volume (excluding the drivers, as they are placed outside the system). Hence, by replacing the laser source module or by using a smaller laser module the entire system can be made more compact.

The Figure 31. shows the image of the proposed laser engraving/marking system in standard mode a) Side view without enclosure b) side view with safety enclosure c) front view without enclosure.

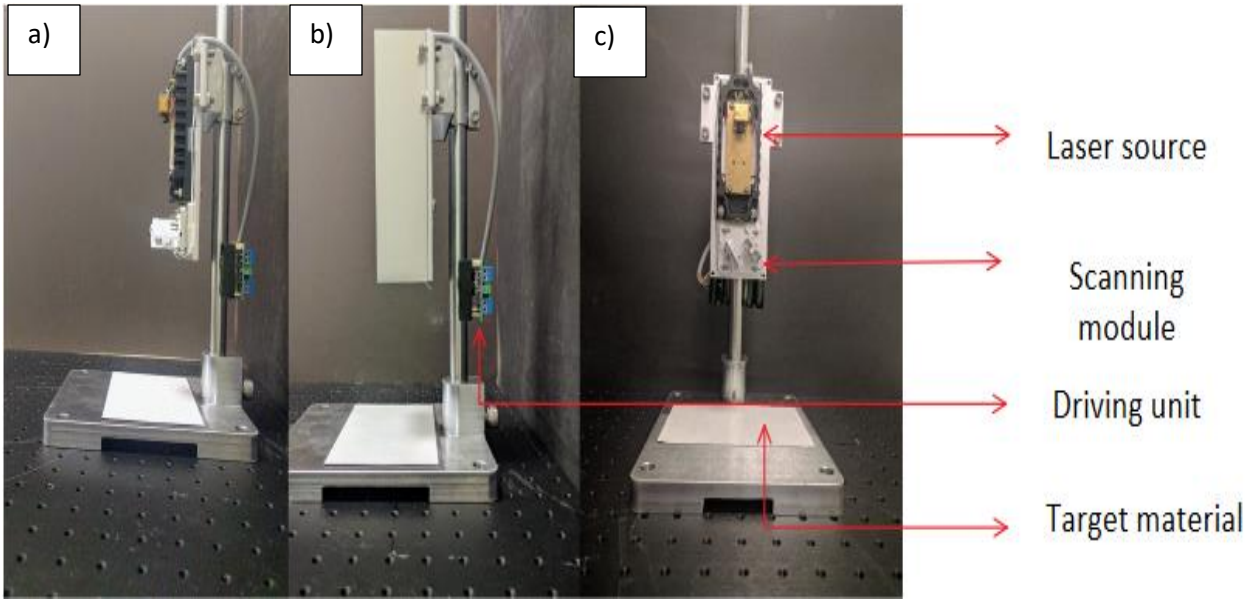

Figure 31. The proposed laser engraving/marking system in standard mode a) Side view without enclosure b) Side view with safety enclosure c) Front view without enclosure.

4.3 Software coding

Once the engraving/marking systems are assembled, the corresponding software to operate the mirrors are developed. It is understood that by controlling the voltage/current applied to micromirrors, the mirrors can be used to trace the desired pattern. In this case, the mirrors guide the laser beam on the target material resembling the input pattern and thereby marking or engraving the surface. Thus, the control software for the mirrors can be developed in LABVIEW (Laboratory Virtual Instrument Engineering Workbench) made by National instruments [76]. It is a graphical programming language (G language) making it easier for the users to understand when compared to C and C++. Several lines of code are readily available in the LabVIEW palette as function blocks for creating a particular function, thus making it easy even for the new users to code

efficiently. Moreover, it has better compatibility with ARM microprocessors, FPGA, DSP and other embedded platforms. Hence, Labview development platform was used for creating control program for the engraving/marking system as it ensures shorter development time.

The major aim of the control program is to transfer a series of input values into analog signal through RIO (Reconfigurable Input/Output) devices to control the micromirror. The following section only briefly describes the program coding and a detailed explanation of the Labview program & FPGA can be found elsewhere [77]. The control program consists of two main sections -1) Host Labview program referred as Real Time (RT) program. 2) FPGA (Field Programmable Gate Arrays) program.

4.3.1 RT program

This section of the program is predominantly used for preprocessing the input values and transfer it to the FPCB part of the program. This can be achieved by using Direct Memory Access First In -First Out (DMA FIFO) flipflops, which transfers the series data based on the order in which they are received by the data structure. It can be used to transfer data between 1) two host programs (RT programs) or 2) two FPGA programs or 3) between a RT and FPGA program. For the current case, the data transfer occurs between the RT and FPGA program. Hence three DMA FIFOs are created which controls the data flow for each mirror and laser modulation. Based on the received data the micromirrors actuate with corresponding laser modulation. The following Table 10. provides information about the FIFOs and the corresponding parts of the engraving/marking system which they control.

Table 10. FIFOs and the part of the engraving/marking system it controls.

FIFO name	Description of data flow	Device for which it controls the Data flow
Host to target 1	Host RT program to FPGA section of the program	Micromirror 1 (Y axis micromirror)
Host to target 2		Micromirror 2 (X axis micromirror)
Modul		Laser modulation control

Though there are three FIFO's, the basic principle and programming are the same. A series of input data values are fed into the program in the form of excel sheets stored as .csv files. This is achieved using a function block called as "read from spreadsheet" function block and the data are passed through a multiplier which acts as an on/off switch and can also be used to either send out data or send only 0's based on the requirement. Since the FPGA design environment accepts only the signed 16-bit integer or I16 format, the data values (double) are stored in excel sheets and must be converted to corresponding I16 value through the following equation.

$$b = \frac{32767 \times a}{10} \tag{9}$$

where,

a= desired value stored in excel sheets

b= corresponding I16 value

32767 maximum value that can be represented by I16 format [78], in our case its 10V which is the maximum output voltage through the system (PXle 1062 Q system). Hence it is accomplished by simply multiplying the incoming data with 3276.7 through a second multiplier (converter 1). The converted values are then passed to the host side of the FIFO. The open reference command is

used to initialize the target FPGA receiver name where the data should be transferred which is followed by the run command to run the FIFO module and finally the reference is closed. Similar pattern is followed for all the three FIFO's controlling each micromirror and laser modulator. Since the laser modulation is either 1 or 0, it can be used in double format instead of I16. The entire code is enclosed within a for loop to run the program code repeatedly for specific iterations. The following Figures 32 and 33 shows 32) RT program for the X and Y axis micromirror. and 33) RT program for the Laser modulation.

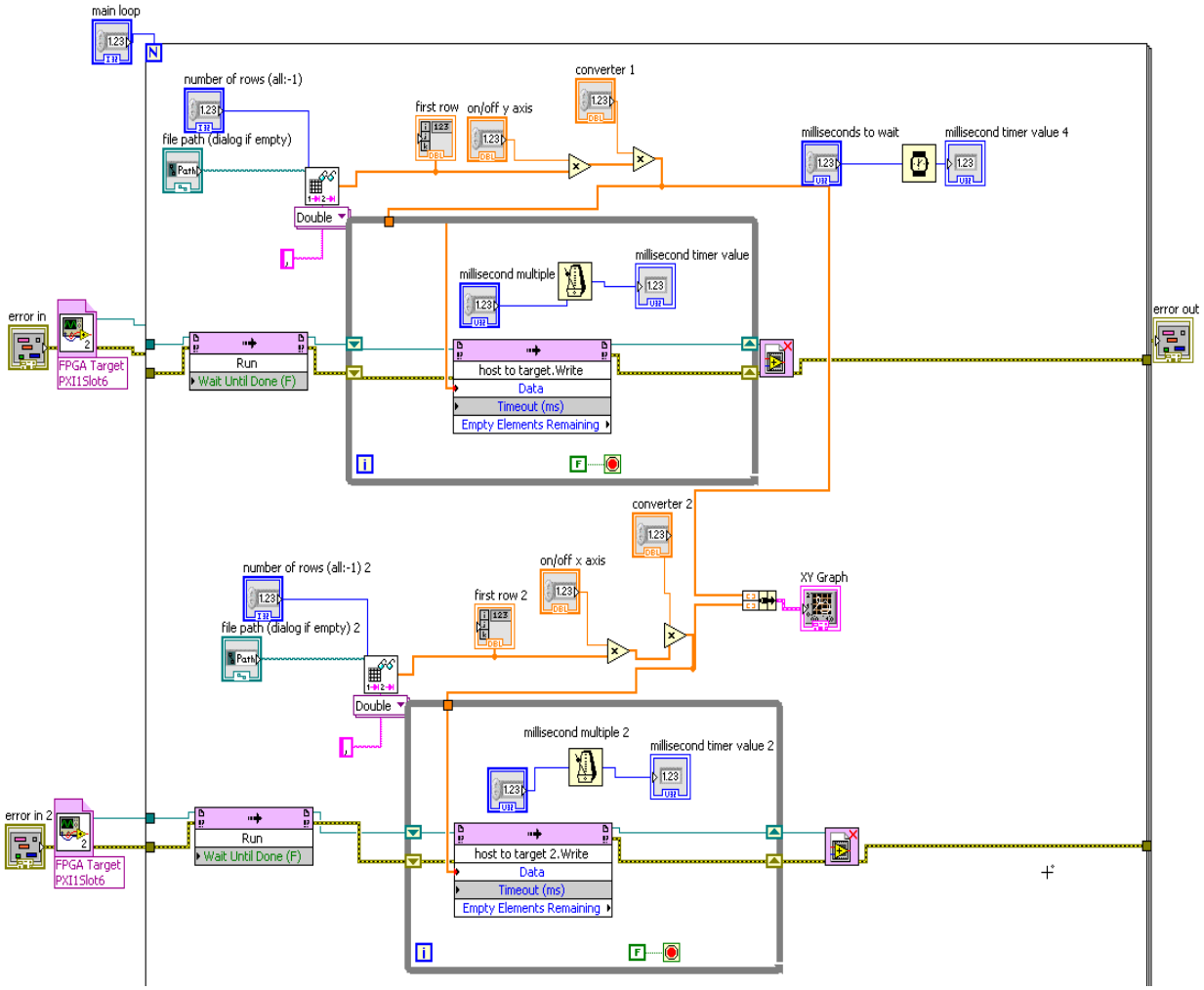

Figure 32. The RT program for X and Y axis micromirror.

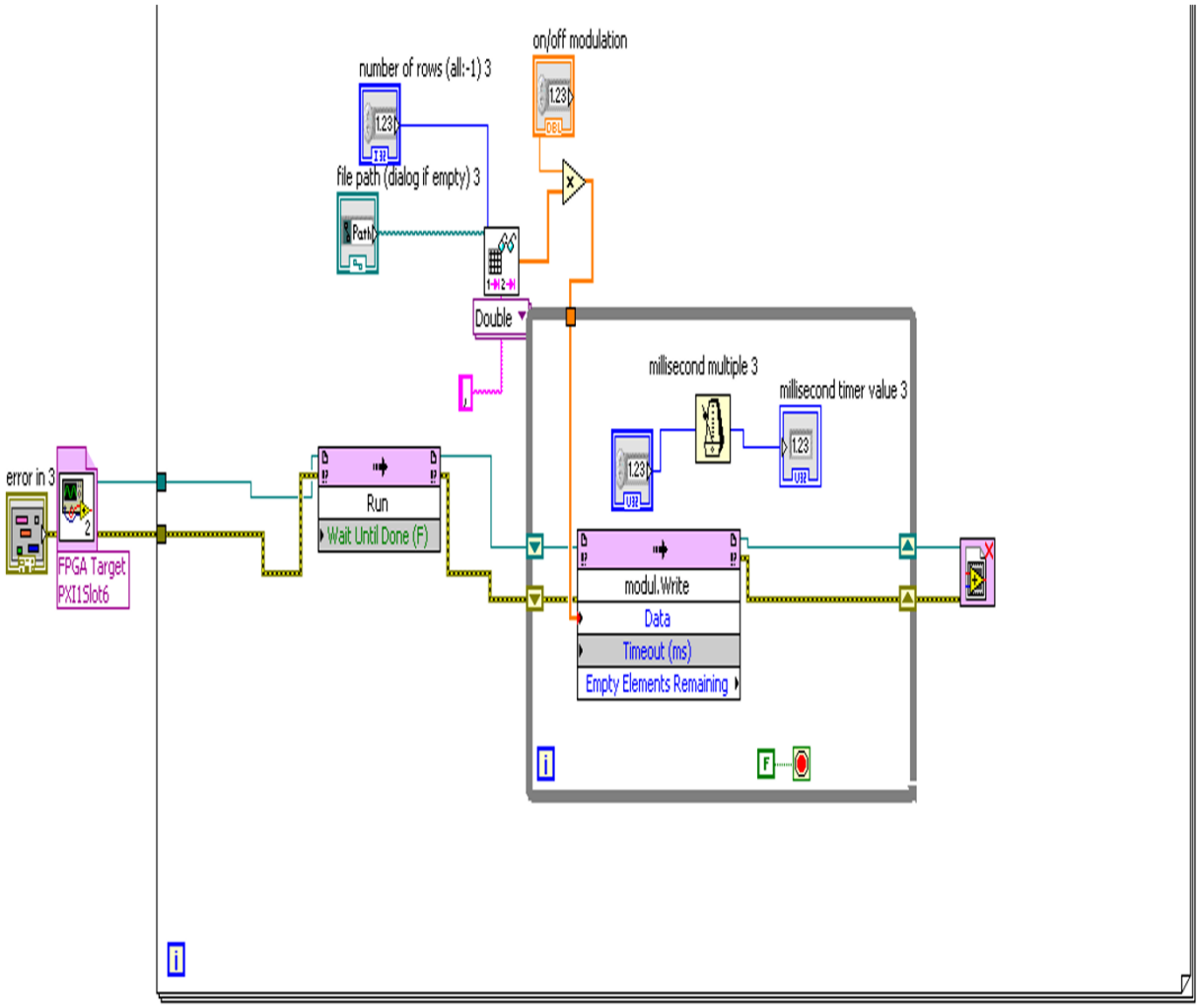

Figure 33. The RT program for the laser modulation.

4.3.2 FPGA program

This section of the program accepts the data in series, one after the other in the order they are sent. It is considered as the execution section of the program where the data is converted into corresponding analog voltages. The program logic for the X and Y axis micromirror is to receive the data and pass it to the FPGA node (Connector 0/AO). A FPGA node is an output port which sends out the signal. The details about the connector and other electrical setups will be explained

in the forthcoming sections. The following Figure 34. shows the complete image of the FPGA code:

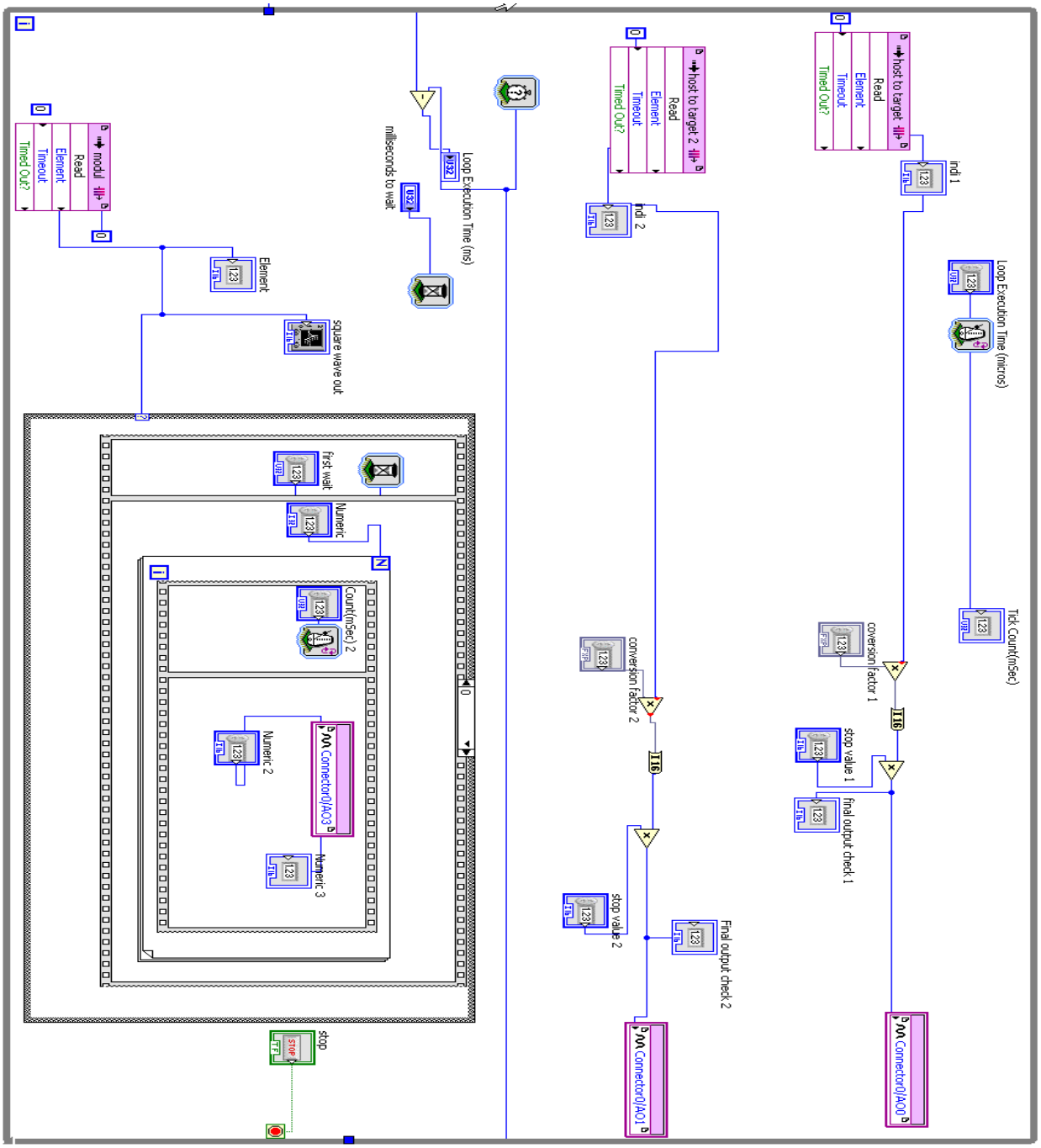

Figure 34.FPGA section of the program.

The entire program is enclosed within a while loop to continuously receive the data from the RT program. The loop execution time is controlled using a loop timer. One of the major advantages of the FPGA unit is the minimum loop time, which is in the range of nano seconds. For the engraving/marking process using a low powered laser, the loop time required is in the range of milliseconds, which can be controlled using the loop timer. The third FIFO (module), which transfers the data related to the laser modulation, goes through additional sequence and case structure before transferring to the FPGA node. The regular case structure has two cases which executes a set of instruction when the input data is 1 and executes a different set of functions for 0. It is used for modulating the laser. When the input data from the RT program is 1 it turns off the laser, whereas, when the input is 0 it activates a secondary sequence structure to turn on the laser only for a specified amount of time. The laser operational time is determined depending on the laser response time and the loop execution time. This helps in removing noise in the laser beam spot caused by mirror actuation. Unlike the RT program, where the changes to the program code can be made in real time, the FPGA section must be coded and compiled. The compilation process burns the code on the FPGA target by altering the connections to the logic gates present in the chip.

4.4 Experimental setup and testing

Once the software section of the engraving/marking machine is completed, it is used to evaluate the performance of the mirror through tests such as the 1) relation between voltage and rotational angle 2) resonant frequency and 3) response time. The results are compared with simulation results to estimate the error associated with the simulations. Based on the test conducted, the experimental setup varies. However, for all the cases the national instruments multifunction I/O (1062 Q) with Reconfigurable Input Output device (RIO)-model 7854 R is used as the control unit to control the

micromirror. The RIO 7854 R can output up to ± 10V but only at 0.1 mA, hence the voltage signals are passed through a current amplifier before the mirror setup. The current amplifier used is an inhouse developed compact unit, designed by a colleague (Hui Zho). It has totally four channels, two input channels connected to the RIO unit and two output channels connected to each of the micromirrors. The following Figure 35. shows the image of the current amplifier and its channels:

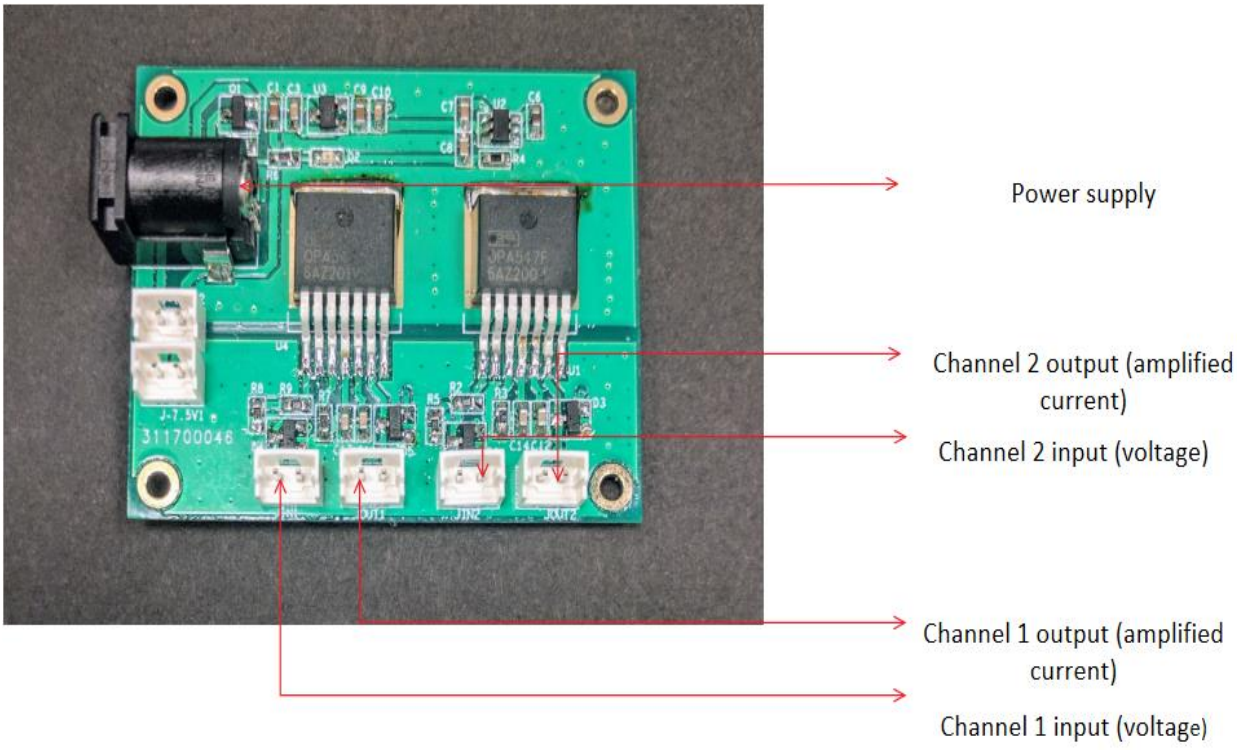

Figure 35. The current amplifier and its I/O channels.

4.4.1 Experimental testing conditions

1) It should be noted that all the tests are carried out on the model 1(torsion beam width =0.5mm) as the model 2 offered only 50% of the rotational angle for the applied current.
2) The following test results are obtained without considering the drifting phenomenon. "Drifting" is a major problem associated with the FPCB based actuators, and its cause, description, possible solution and experimental verification of the problem will be

discussed in the following sections as it requires in depth explanation. The tests are carried out after implementing the solution to the drifting problem.

3) The focused laser beam is modulated to low power (< 5 mw) for safety reasons.
4) For all the tests, the input values are applied as voltages and the corresponding current is calculated using Ohm's law. Resistance of both X and Y micro actuator assemblies are 2.93 Ω.

4.4.2 Static testing

Static testing is the experimental verification of current vs rotational angle simulation. The relationship between the applied current/voltage and the corresponding rotational angle can be found using the laser beam pointed on the mirrors. When the mirror rotates, the laser beam reflected by the mirror also moves. By calculating the distance travelled by the laser spot from the initial position on the screen, the corresponding rotational angle of the micromirror can be calculated using trigonometric function. To determine the distance traveled by the laser spot precisely, a grid paper is attached to the screen which is fixed orthogonally at a predefined distance from the mirror. The reflected laser beam spot is aligned to centre of the gird paper and for each input current the distance traced by the laser spot (after 90ms) is noted and the corresponding rotational angle is calculated using the following formula:

Fixed distance between the mirrors and the screen placed orthogonally: a = 115mm

Distance travelled by the laser spot from the origin on the grid screen after 90ms: b (mm)

Optical rotational angle for the input current: $\tan^{-1}(\frac{b}{a})$ (θ) (10)

Corresponding mechanical rotational angle: $\frac{optical\ rotational\ angle}{2}$ (θ) (11)

Similarly, different current inputs ranging from 0 to 164 mA is applied and the corresponding rotational angles are calculated as shown in Table 11.

Table 11. Voltage vs mechanical rotational angle.

Voltage applied as input (V)	Resistance of both X and Y micromirrors	Corresponding current input (A)	Working distance or 'a' (mm)	Mechanical rotational angle ± (θ)
0	2.93	0	115	0
0.0486	2.93	0.016587031	115	0.420221945
0.0972	2.93	0.033174061	115	0.778781592
0.1451	2.93	0.049522184	115	1.187335214
0.193	2.93	0.065870307	115	1.548465638
0.2411	2.93	0.082286689	115	1.947541842
0.2892	2.93	0.098703072	115	2.305524258
0.3374	2.93	0.115153584	115	2.702789866
0.3857	2.93	0.131638225	115	3.088674533
0.4342	2.93	0.148191126	115	3.482028429
0.4817	2.93	0.16440273	115	3.852297136

The following Figure 36 and 37. shows the graphical representation of the input current vs mechanical angle of the micromirror for the experimental and simulated results (up to 3 degrees) and the corresponding experimental setup used to obtain them. Foe better understanding both the images are presented in the following page.

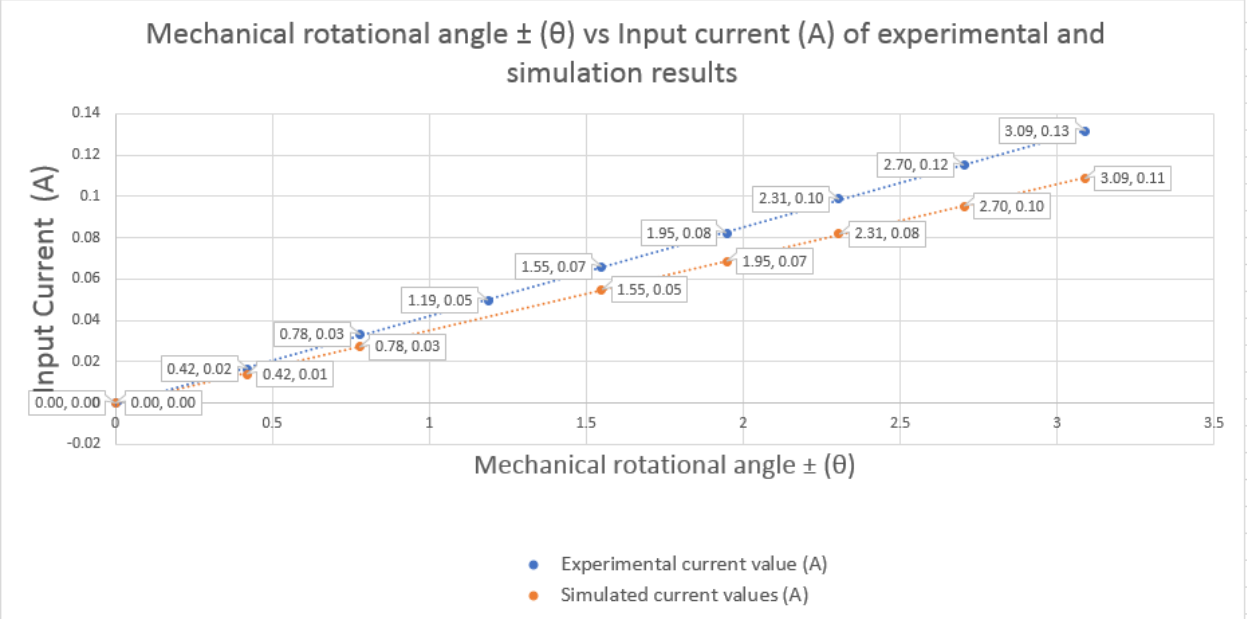

Figure 36. Input Current (A) vs Mechanical rotational angle ± (°) of experimental and simulation results.

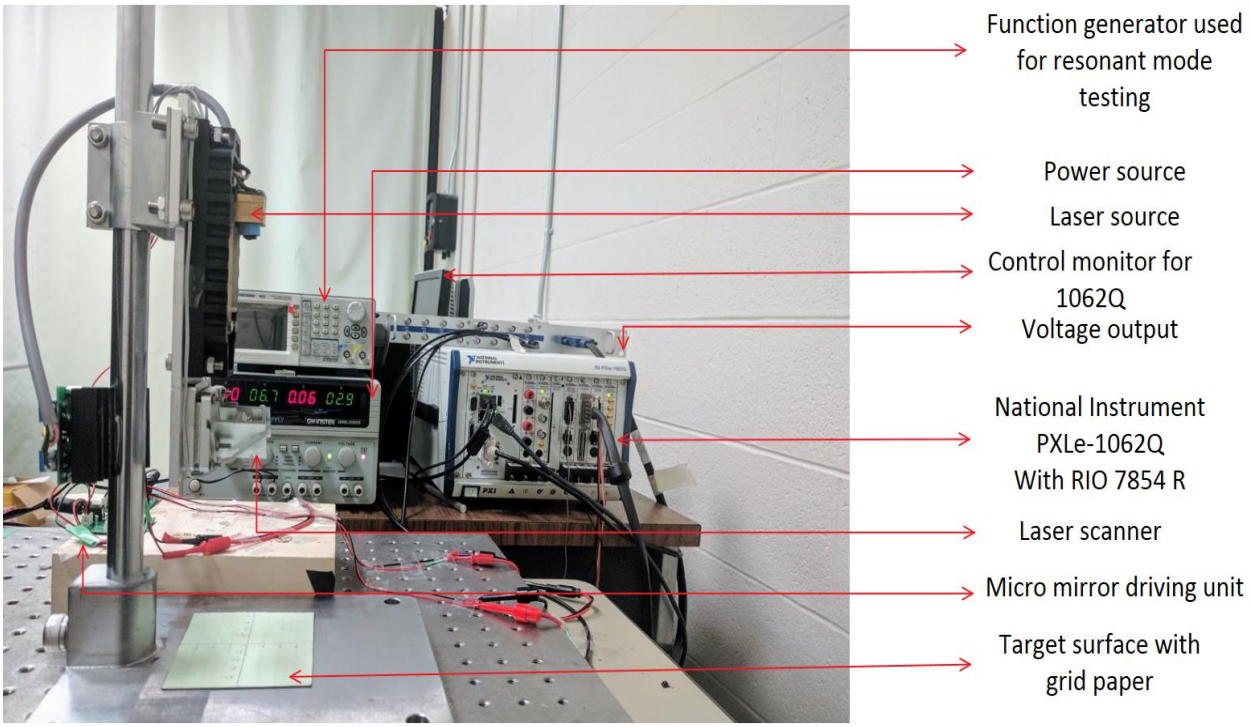

Figure 37. Experimental setup for the static test.

4.4.3 Resonant frequency testing

The resonant frequency testing is conducted using the same experimental set up with a minor modification that the RIO 7854 R is replaced with a function generator as the input voltage source to the current amplifier for easy operation. During the preliminary testing with different prototypes, the mirrors are found capable of reaching up to ± 50° (optical) at an input current of 133mA. For the current prototype, the gap between the actuator and metal base is 0.40 mm which can withstand a maximum rotational angle of < ± 5.5° (Mechanical). Hence the resonant frequency tests are conducted at low current (16.59 and 33.16 mA). Since the natural frequency is expected to be at 405.55Hz based on the simulation results, the frequency is increased in steps of 25/50 Hz up to 300 Hz and further step value is reduced based on the requirement and corresponding rotational angle is noted using the same method as used in voltage vs rotational angle testing. The test is continued beyond the resonant frequency till the rotational angle reaches close to 0°. The actuators reach its natural frequency at 414/415 Hz for an applied current of 16.58 and 33.16mA respectively. Even for low current input (33.16 mA) the mirrors are capable reaching up to 5.35° (mechanical). Thus, the resonant performance of the mirrors is much higher which makes the scanners suitable for other devices such as laser line generators, LIDAR etc. The following Figure 38. shows the graph plotted between rotational angle and frequency at 16.58 and 33.16mA:

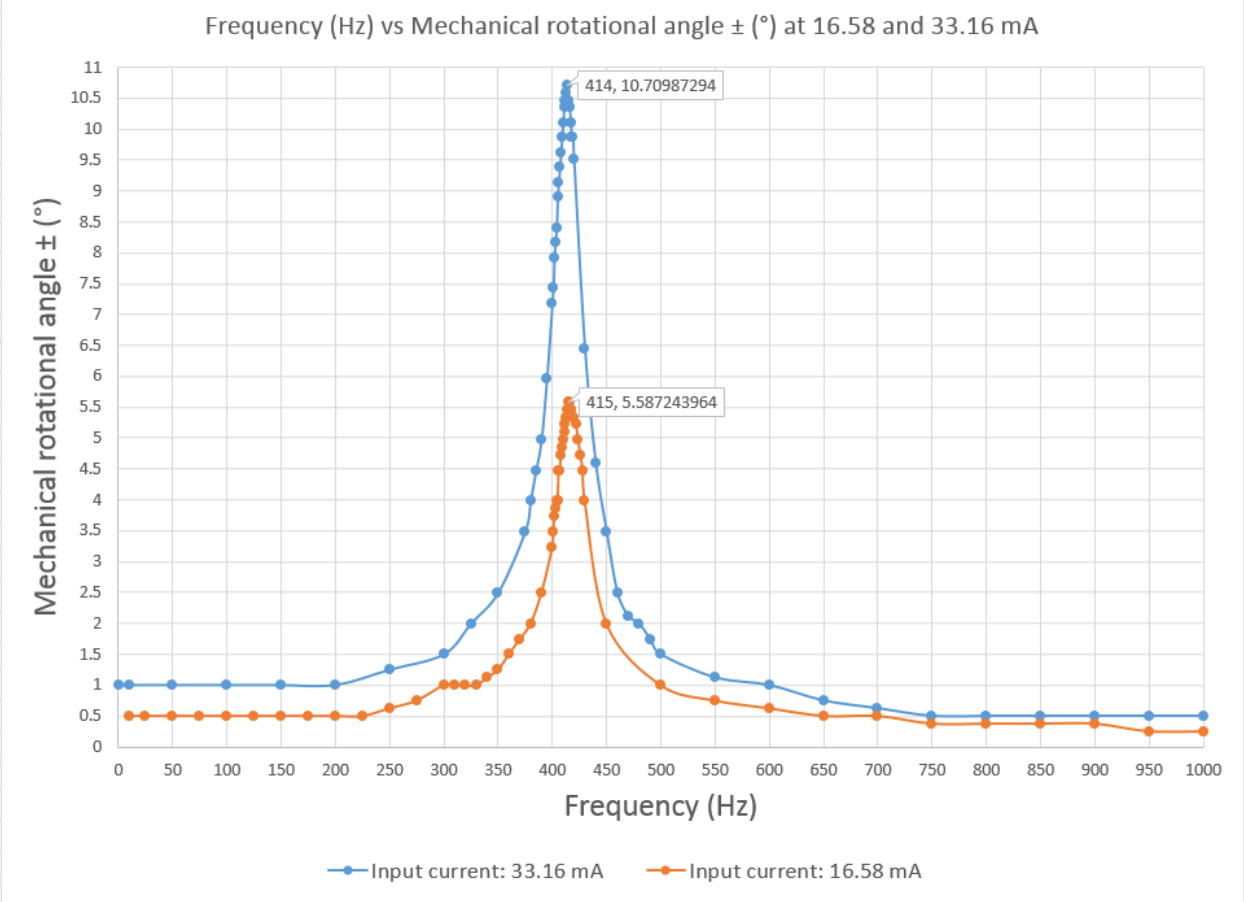

Figure 38. Frequency (Hz) vs Optical Rotational (°) at 16.58 and 33.16mA.

4.4.4 Response time test

Response time test is one of the crucial tests for designing the engraving/marking system as it determines the speed and stability of the micromirror. Further it determines the time taken by the mirror to rise from the rest position (rise time) to a new position for the applied current and the time taken to settle down due to the damping in the new position (settling time). This is useful to determine the speed of the engraving/marking, excluding the laser intensity. The experimental set up of the resonant frequency analysis is retained, but the function generator is switched back to RIO module and the grid screen is replaced with a Position Sensing Device (PSD). As the name suggests PSD is a photo sensor which senses the incoming light and its corresponding position on

the sensing screen. The signals are further amplified and processed to reduce noise using a position sensing amplifier (On-Tark OT-301). The data obtained from the amplifier as voltage signals are fed to an oscilloscope to visualize the performance of the mirror. The mirror response data are taken at ± 5% and to predict the real-time performance of the mirrors, the rise time, settling time and fall time of individual mirror is calculated for different current input for a wait time of 90ms or 11Hz as tabulated below in Table 12:

Table 12. Provides information about the rise time (ms) and settling time (ms) of the micromirrors at 11Hz.

Actuation type	Rise time (µs)	Settling time(ms)
Small jump (0 to 3 mA)	520	38.10
Medium jump (0 to 30 mA)	600	40.20
Large jump (0 to 81 mA)	640	41.40

The following Figure 39. shows the images of the settling time for different current input a) 0 to 3 mA and b) 0 to 81mA:

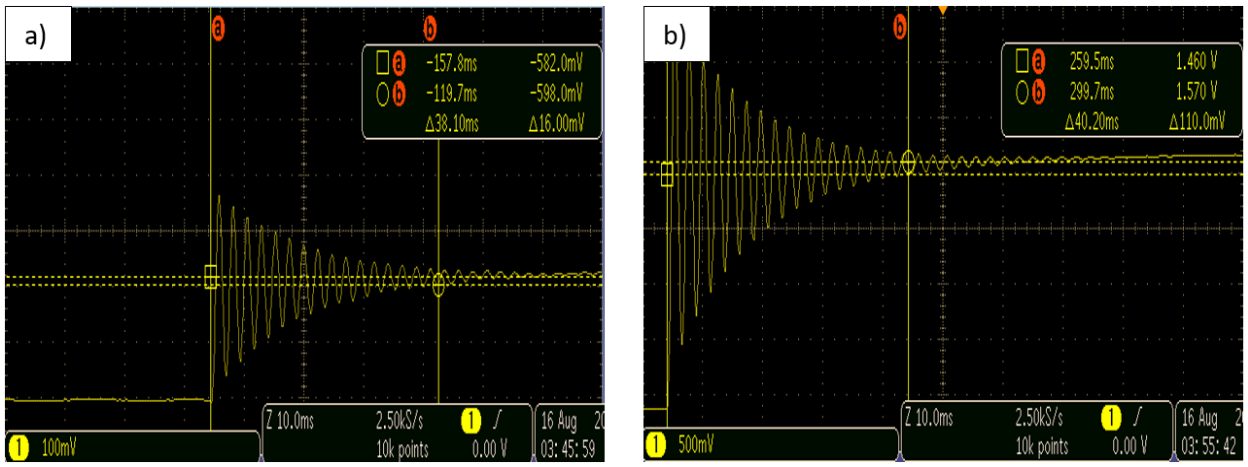

Figure 39. Settling time (ms) for different current input a) 0 to 3 mA and b) 0 to 81mA.

4.4.5 Observations regarding the experimental and simulation results

It is evident from the results that there are discrepancies between the simulated and experimental test results. The simulations results are less than the experimental results on an average of 17% and 2.345% in static and resonant frequency tests. This deviation in the static test is mainly attributed to the following reasons:

1) Material properties used in the simulation. The material is assumed to be transversely isotropic in nature for the simulation. But the commercial Polyimide film is anisotropic in nature for which (material properties) data is very limited.

2) The discrepancies are further associated with the manual bonding process as the process is not consistent and accurate. For mass production, dedicated processes and techniques can be introduced to achieve the consistency and perfection across all the models. More information regarding the discrepancies can be found in the referenced paper [43].

Since the simulated results are obtained based on approximation of polyimide material as transversely isotropic, to minimize the discrepancy in future the actuator has to be tested personally for its material properties which can be used in the simulation. Since its is an time-consuming process and due to the current time restriction, it will be added to the future development of the project. Though the performance of the laser scanner is good and suitable for the usage with engraving/marking system there is one major problem (drifting) as mentioned in previous section (section: Experimental testing conditions) which will be explained in depth in the following sections.

4.5 Drifting problem description

In addition to the numerous advantages associated with the FPCB based micromirrors there is one major hindrance, due to which the actuator starts to drift/move away from its fixed position over a period of time. Since the FPCB actuators are relatively novel there is no description of such problems in the available literature [43]. Based on the preliminary tests conducted it is concluded that the problem might be mostly associated with the material property (viscoelastic behaviour) of the polymide material which is used as the substrate or insulator film in the actuator [79] [80]. For the sake of simplicity this defect shall henceforth be addressed as drifting problem. The drifting problem exists irrespective of the magnitude of the current applied on the mirror. On further analysis, it was evident that the percentage of drifting is directly proportional to the magnitude of the current applied to mirrors. Due to this, the image or engravings made may not follow the calibration pattern and the design patterns which consists of multiple closely spaced lines may overlap each other after multiple loops. For example, when a complicate pattern such as jaguar logo is engraved the engraved lines overlap each other after second loop and thereby severely affect the quality of the engraved model. The following Figure 40. shows the misalignment of contour lines in an engraved jaguar image (wooden beam) due to the drifting problem:

Figure 40. The misaligned contour lines in a jaguar image due to drifting.

4.5.1 Problem analysis

By analyzing the drifting problem through various experimental test, the following conclusions were made. The problem is 1) time dependent, 2) accumulative and mostly associated with actuation force & the deflection produced on the connecting torsion beam.

4.5.1.1Time dependency

The drifting occurs as soon as the force is applied on the torsion beam and the rate of drifting is aggravated during initial few seconds after which it reduces with time. The following table 13 gives the quantitative description of the drifting problem for various input current values over a period of 60 seconds. The values provided are obtained using a low powered laser to exclude the effects of high powered laser:

Table 13. Percentage of drifting caused by the FPCB mirror for the applied current over 60 seconds.

Current (mA)	Mechanical Rotational angle before drifting (°)	Rotational angle due to drifting after 60 seconds (°)	Percentage of drifting
34	1.11	0.256	23.07%
68	2.38	0.56	23.6%
102	3.83	0.94	24.48%
136	5.18	1.58	30.40%

4.5.1.2 Accumulativeness

The drifting problem is accumulative in nature. Drifting might be very negligible, when actuators are positioned only for 40ms (response time of the mirror) for a data point, but when the time period (40ms) is repeated for a different voltage corresponding to different data points in the same quadrant, the drifting occurs within a short period of time (few milliseconds). Whereas, in the case of data points spread across all four quadrants, the drifting still occurs, but only after longer period (few hundred milliseconds). The following Figure 41. shows the data points used for calibration where the wait time for each data point used is 30ms (based on the assumption that the drifting does not occur before the settling time of the mirror). The lines 1 and 2 overlap each other which mainly attributes to drifting. Though the wait time is only (30ms) the accumulation of wait time on one actuator reaches around 600ms which induces drifting.

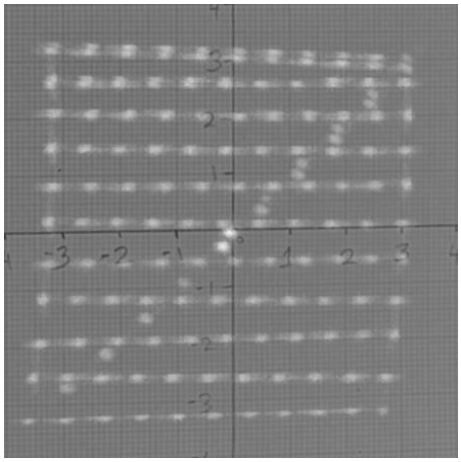

Figure 41. Drifting of the micromirrors due to accumulativeness.

The presence of the drifting issue would severely undermine the quality of the engraving and thus would make the entire concept worthless unless eliminated. To overcome this, the characteristics of drifting are studied and a possible solution is proposed in the forthcoming chapter.

Chapter 5. Implementation of new scanning methodology and test results

5.1 Possible solution to overcome drifting

Both the time dependency and accumulative characteristics of drifting are mainly associated with the force acting and the corresponding torsion of the polyimide based (FPCB) torsion beam. In both these conditions the time for which each mirror is kept in one quadrant is > 200ms. However, the minimum wait time for each data points must be greater than the response time (40ms) and in case of engraving/marking this wait time has to be long enough to ensure that the laser beam engraves/marks the target surface to obtain good quality finish. It is observed that the amount of drifting is higher for models in single quadrant compared to models in all four quadrants. This is because, when the model uses one quadrant the torsion beam twists only in one direction without any counteraction and after few seconds this may initiate drifting. Whereas, when the model involves four quadrants beam experiences twisting in both direction due to which the drifting might be lower than the one quadrant model. Though this problem can be rectified using closed loop control, but it makes the system more complicated and expensive. However, to provide a solution for the problem using only the open loop control, a new vector scanning methodology is used. It should be noted that when the time spent by each mirror in one quadrant is less than or equal to 100ms and the average current applied to each mirror after consecutive data points is equal to or close to zero, then the drifting would be negligible (< 5%) which is acceptable for some applications mentioned in the chapter 1.

5.2 Experimental verification of the proposed hypothesis

To verify the proposed hypothesis, a square wave was applied to the mirror at a frequency of 5Hz (200ms) using a function. The time period of 100ms for each data point was chosen as it would provide sufficient time for the mirror to settle down (50ms) and initiate the marking process (50ms). Three images were taken a) as soon as the process starts b) over a period of 5 minutes c) over a period of 10 minutes as shown in the following Figure 42.

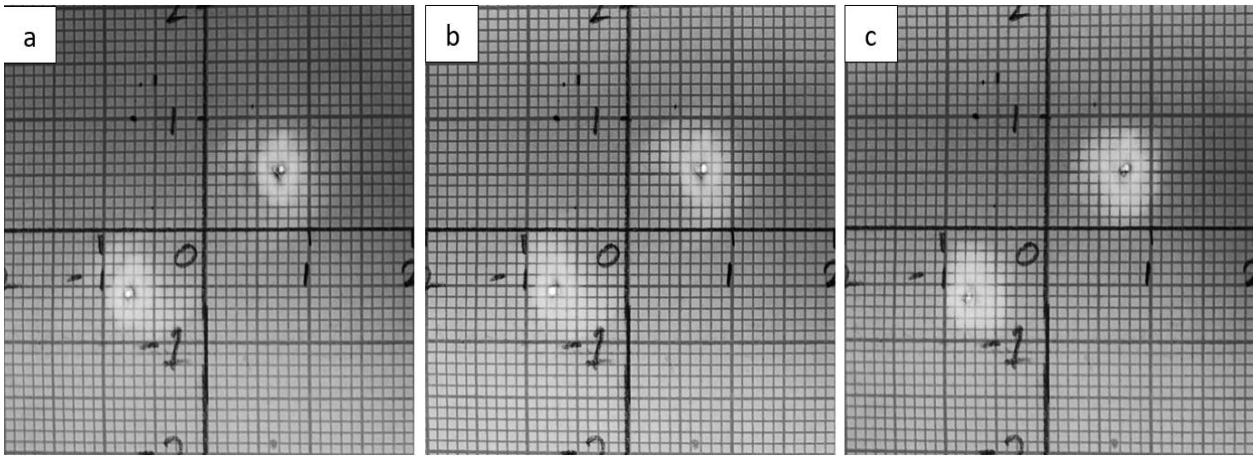

Figure 42. Verification of the hypothesis using square wave at 5 Hz a) Immediately after the process starts b) After 5 minutes c) After 10 minutes.

Since the laser is positioned to (0, 0) on the grid paper before the initiation of the test it would be easy to extract the two points from the images and compare them quantitively using the centroid plot method.

5.2.1 Centroid plot method

To ensure a quantitative comparison between the images, centroidal plot method is used. As the name suggests, the X and Y coordinates of each data points are obtained and the coordinates are easily extracted using a grid paper. Also, the Euclidean distance between each data point and the origin is calculated. Based on this data, a graph is plotted between the data point number and the

distance between the point and the origin. Similarly, the process can be repeated for a different image and by comparing the difference in the graphs, it is possible to quantitatively compare the three images. The following Figure 43. shows the graph of centroid plot for 2 points in each image of Figure 41. It should be noted that the difference in the error is less than 3% even after 5 minutes and less than 6% after a period of ten minutes whereas in reality the engraving time would be much lower than 5minutes.

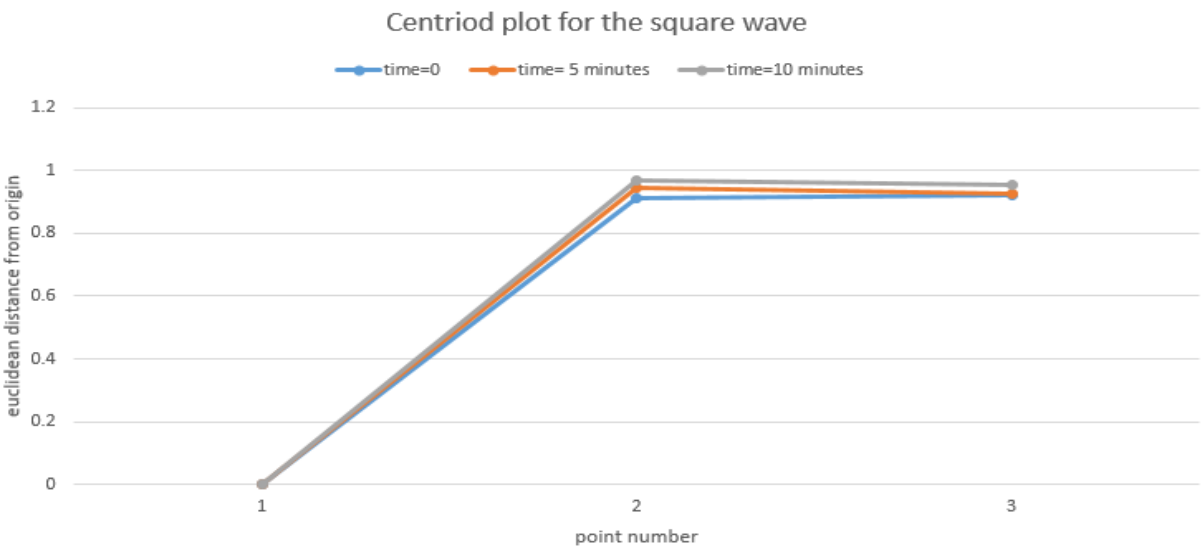

Figure 43. Centroid plot for the square wave at various time intervals.

Hence, it proves that this method may play a significant role in minimizing the drifting problem. Based on the above test, a new scanning method was created where each data point in any arbitrary shape is followed by a prime value, which is nothing but the negative of the previous data point. Hence by doing so, the torsion experienced by torsion beam for each data point is canceled by the prime point following it. In this method, the average voltage applied to the mirror can be maintained at zero. In addition, the time that each mirror spends in a quadrant before the counteractive force is applied is maintained at 100ms or less and thereby eliminating the

accumulative drifting. The laser is modulated accordingly in such a way that the prime points are no longer visible. The laser is turned ON only after 50ms for each data point after the mirror gets settled down.

- Data point – Voltage applied to the mirrors for each loop of the program.
- Prime point – Negative value of the previously applied data point.

The next step would be to apply the hypothesis for a complicated shape to test its effectiveness which is explained in the following sections.

5.3 Experimental verification

5.3.1 Calibration of data points

Before testing out the hypothesis, both the mirrors must be calibrated to identify the rotational angle for the corresponding input voltage/current. Though only current is used to drive the mirrors, the input values applied to labview software is in the form of voltages. The hypothesis can be tested by generating a matrix of 101 data point pairs representing the voltage range from -0.4 to 0.4V for each mirror in excel sheets and saved in .csv format. It is then fed to the program (LABVIEW) and their corresponding laser point movement on the grid paper starting from (0,0) is obtained using a long exposure camera. The exposure time for the camera is set based on the time taken to scan the 101 points at least twice which in this case is approximately 25 seconds. This image is preprocessed to enhance its quality using image editing software such as image j [81] and photo editor and then converted to a (8-bit image) greyscale image to enhance the visibility and its quality. Further, they are cropped exactly to 4X4 cm with help of the grid scale in the image. A square of 4X4 cm is created in Autocad with its centre at (0,0). The cropped image is then fitted into this square and manually aligned in such a way that their origins coincide. Since

the calibration is done using prime method the drifting is very negligible. The image of calibration points are taken consecutively for three whole loops and the centre of each data point is more illuminated than its surroundings, making it easy to find them manually. Later the coordinate points of each calibrated point is transferred to an excel sheet from Autocad using an application known as “Click2xls” [82]. The X and Y coordinates along with the voltage of one mirror are imported to Matlab and the interpolation is carried out using the curve fitting tool. Biharmonic v4 interpolation method is used while treating the entire model to be a surface as it better suits our requirement [83]. The X and Y data acts as X & Y coordinates and the corresponding voltage on one of the mirror (X axis scanning mirror) acts as the Z-coordinate. Based on these data a .sift file is generated and saved as voltage 1. Similarly, another file with voltage of Y axis scanning mirror is generated and saved as voltage 2. Using the two sfit files, for any data point (x,y) input, the corresponding (v1,v2) voltages of the micromirrors within the calibrated space can be obtained. The following Figure 44. shows the voltage2 sfit file in curve fitting tool using biharmonic v4 interpolation:

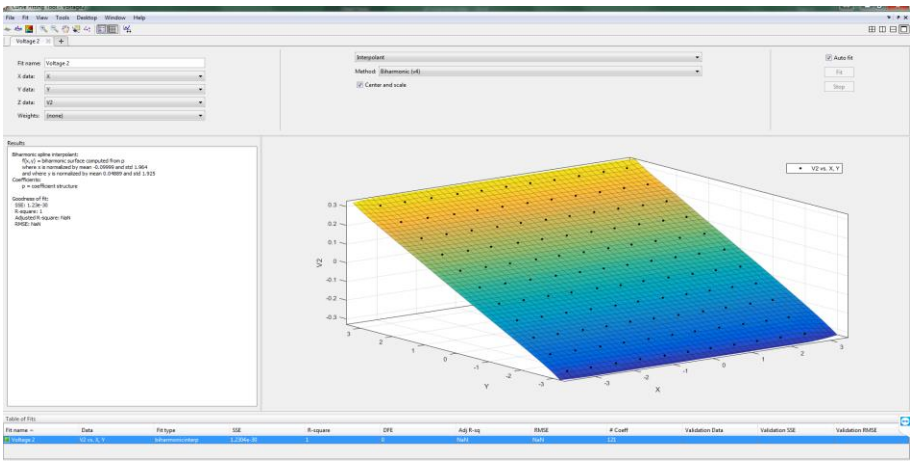

Figure 44. Matlab Surface fitting datafile for the Y axis scanning mirror.

The following Figure 45. shows the difference in calibration with and without prime method at a working distance of 300 mm only for better visualization. But, in actual case the working distance is only 115 mm hence the calibrated image may appear very close. All the results are obtained using the latter calibration (with prime). It should be noted that the points do not overlap after the implementation of the new scanning method and thus would give better results.

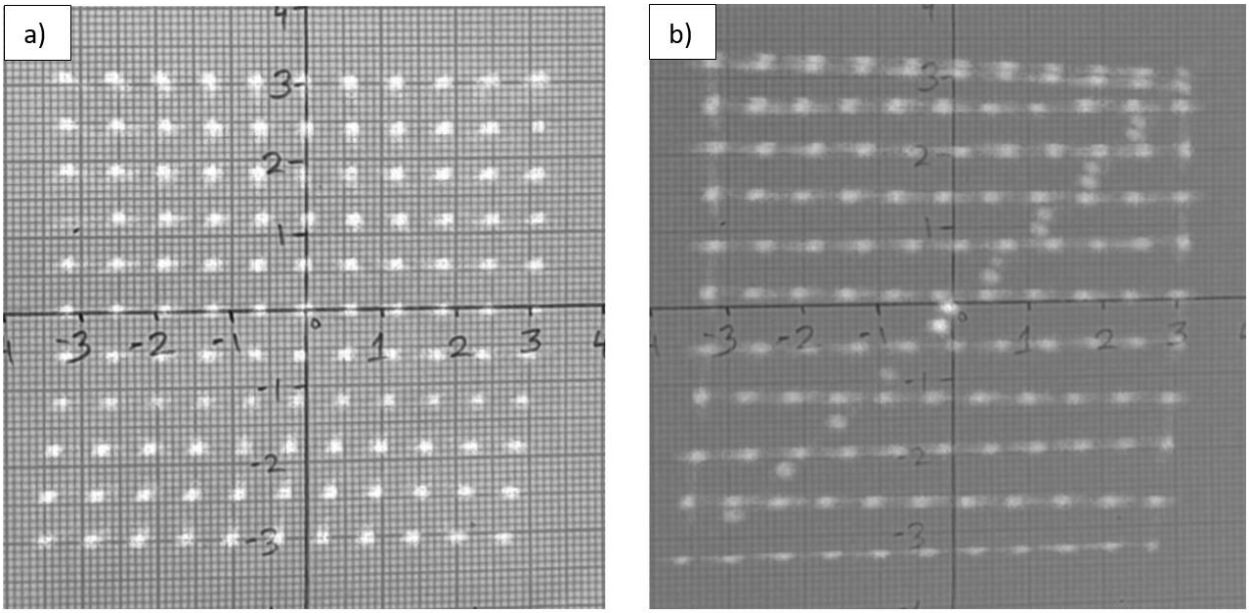

Figure 45. Calibration table a) using prime method b) without using prime method.

5.3.2 Engraving a vector image pattern

Based on the calibration data, any image can be engraved/marked. To do so, a vector pattern of the image is extracted using Inkscape software. Then the contour of the image is transferred to AutoCAD where they are readjusted to fit into calibrated space having a working area of 20 X 20 mm. The contour lines are then divided into equal number of data points. More the number of points, sharper the engraving would be but at the expense of increased engraving/marking time. The position of the data points is extracted into excel sheets. These position data are fed into Matlab

to obtain the corresponding voltages to move the micromirrors along the image contour using the calibrated sfit files (voltage 1 and 2) and stored in individual excel sheets. Further the voltage data are preprocessed to include the corresponding prime values which are nothing but the negative of preceding value in Microsoft excel and stored as individual X and Y voltage files (.csv). Similarly, the corresponding modulation voltages (for simple images it can be either ON or OFF represented as 1 or 0. Whereas for complicated grey scale images it can be any number based on the required laser intensity) are generated and saved as separate (.csv) file. Though FPGA module 7854R is currently used to send out the control signals, the actual system uses single board microcontrollers such as Arduino boards [84] which would be used to keep the overall form factor small.

Based on these steps, the outline of the jaguar logo with 49 points is created to test the effectiveness of the prime method using a low powered laser. The images are captured using long exposure camera set to capture the one complete loop. The following Figure 46. shows 49 points along the outer contour of jaguar logo with a wait time of 90 ms. a) using prime method b) reference image c) without using prime method.

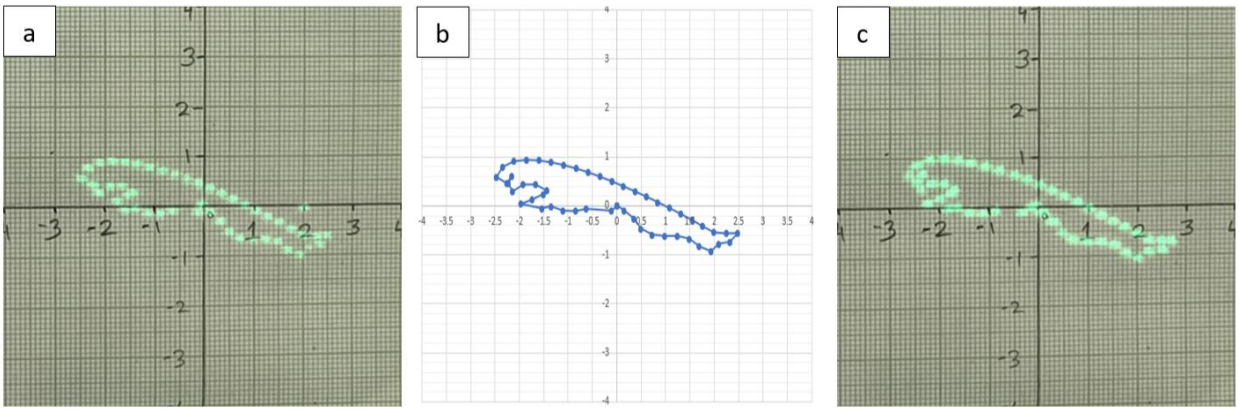

Figure 46.Verification of the prime scanning method using 49 points on the contour of jaguar logo.

The images obtained above are preprocessed using the same method of calibration and the corresponding X and Y coordinates of the laser points on the contour are obtained. Based on the X and Y coordinates of the data points the Euclidean distance of the corresponding points from the origin is obtained and used in the centroid plot to compare them quantitatively. The following Figure 47. compares the centroid plot of a) reference square b) using prime method c) without using prime method:

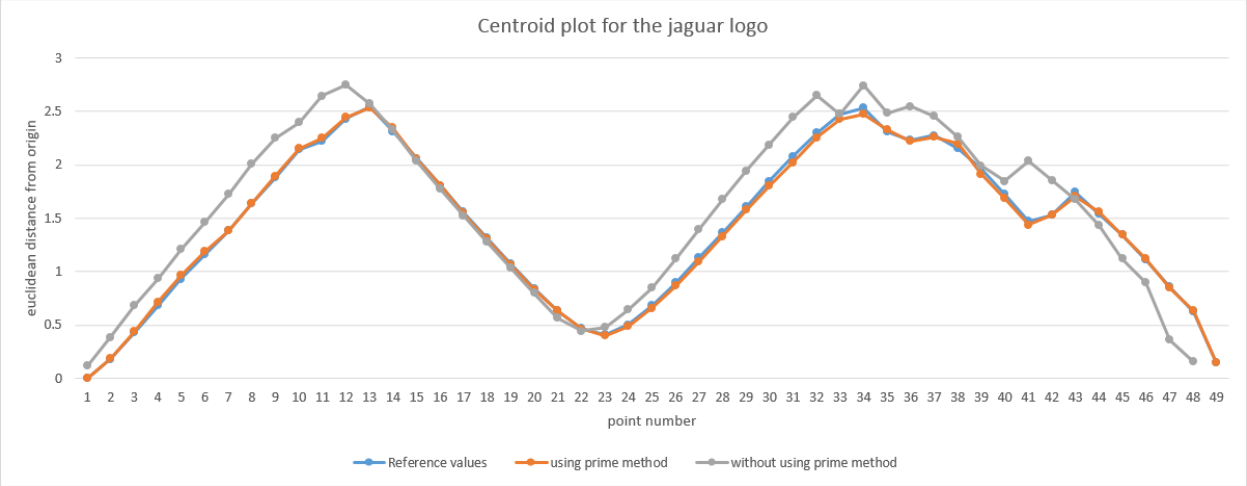

Figure 47. Centroid plot for the jaguar logo.

It could be noted that the prime method significantly reduces the error percentage from 10% (average) to 1.5 % (average). It is evident from these data that the prime method is capable of significantly reducing the drifting phenomenon in low powered lasers.

In case of high powered lasers (>0.6 watts) due to the uneven transfer of heat to the polyimide actuators there is a warping of the actuators which in turn leads to secondary drifting. The secondary drifting is attributed to the following factors:

1) Surface Quality of new batch mirrors
2) Intense heat generated by the incident laser beam may heat the surrounding air
3) Thermal properties of the polyimide material used in FPCB structure

To completely understand the secondary drifting, more research needs to be done into the material properties (viscoelastic behaviour) of the polyimide which are to be done in future. Due to time restrictions and intense heat generated by the laser, the laser power is capped to 0.5watts for the current prototype as the drifting is eliminated/negligible at such low power. Since the laser power is capped to 0.5watts in the current setup there is a limitation of the target materials that can be engraved/marked. However, the system can still engrave/mark materials which were set as the thesis objective such as leather and silicone smartphone cases. The marking process was carried out on a leather strip (50 points on the jaguar logo) with and without prime method and for both the cases the wait time was kept constant at 90ms for each data point. Out of the 90 ms the laser is modulated in such a way that it turns on only for 25 ms providing 65 ms for the laser beam to settle down the (prime method). It is evident from the Figure 48. a) without using prime b) using prime method that, by using prime method there is significant reduction in the drifting qualitatively.

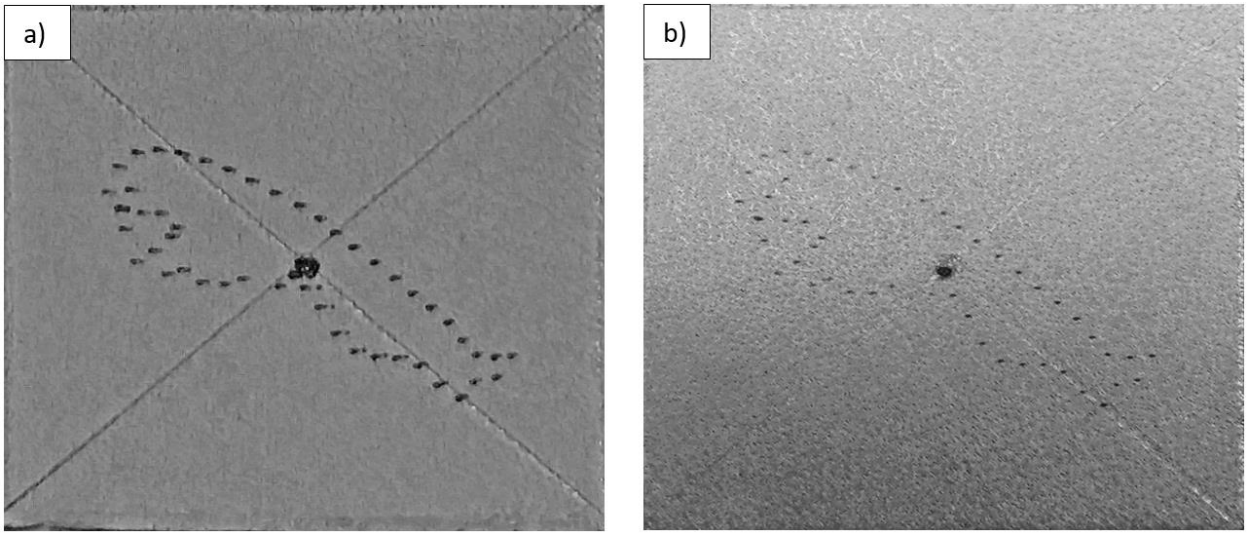

Figure 48. Marked Jaguar logo (50 points) a) Without prime b) With prime method.

The image a) in Figure 48. is darker than its counterpart but the points are not precise instead there is a indication of drifting which is visible from individual marked points.

To ensure a proper quantitative comparison between the images marked with and without prime method, the centroid plot is created for both the images and compared with each other and the reference image (created as input). The following Figure 49. shows the centroid plot developed for the marking of the jaguar logo (50 points) with &without prime method and the reference image.

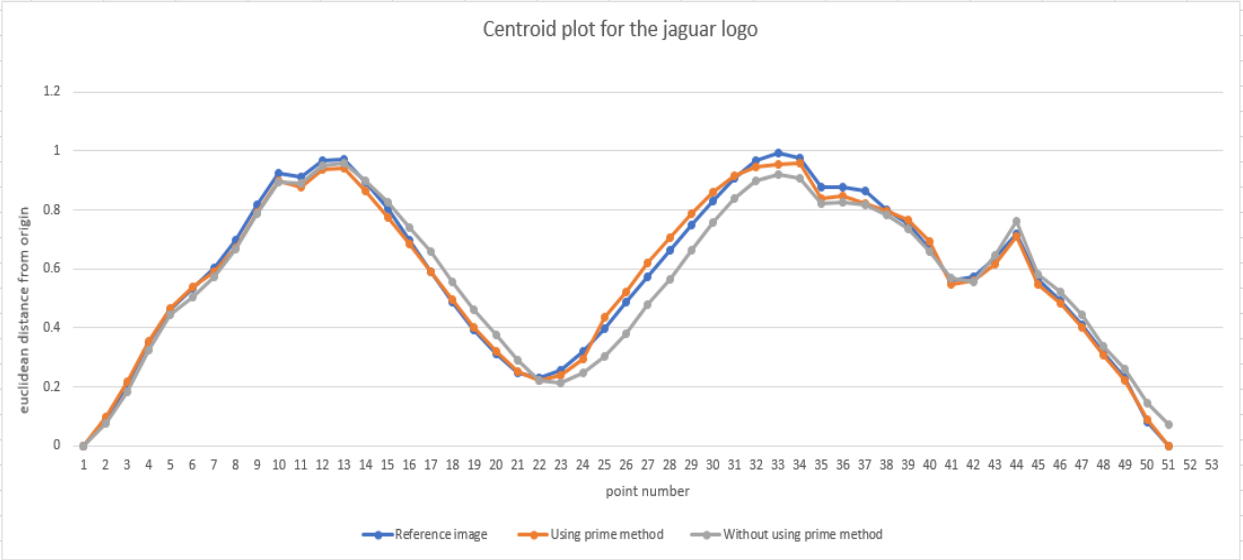

Figure 49.Centroid plot developed for the marking of the jaguar logo (50 points) with and without prime method.

Using the prime method has significantly reduced the error percentage from 9% (average) to 3 % (average). In both the cases 1) using low powered laser 2) using high powered laser, the prime method has played crucial role in keeping the drifting value overall <5%. (average). Based on the Figure 48 and 49. It should be noted that marking is done with multiple pass of the laser beam over the target area (minimum three passes for the image marked without using prime method and ten loops for the image marked using prime method. Unlike the normal vector scanning, even after multiple pass, the points appear to be sharp and distinct in the modified vector scanning. As the new method provides promising solution to over come the drifting problem for low powered laser engraving/marking, it has been used to mark materials such as leather (leather strips) and

silicon/TPU rubber smartphone cases. The following Figure 50. shows the various sample images engraved/marked using with and without prime method after two passes. A) jaguar logo B) Toronto logo C) batman logo D) wordings = Ryerson E) jaguar logo on a TPU rubber smartphone case.

A i) without prime and wait time 90ms, A ii) without prime and wait time 40ms A iii) with prime and wait time 90ms.

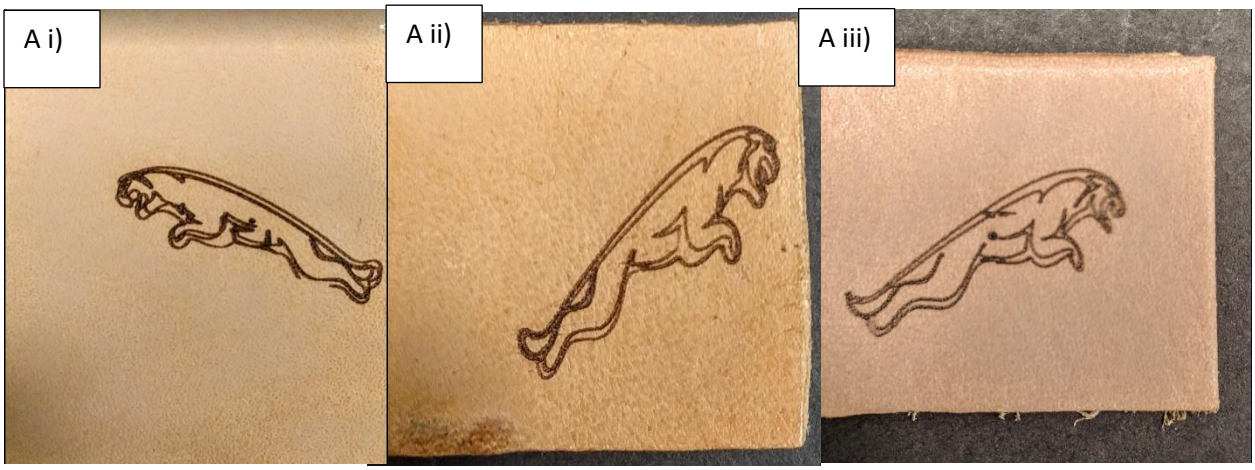

B i) Toronto logo without prime B ii) Toronto logo with prime.

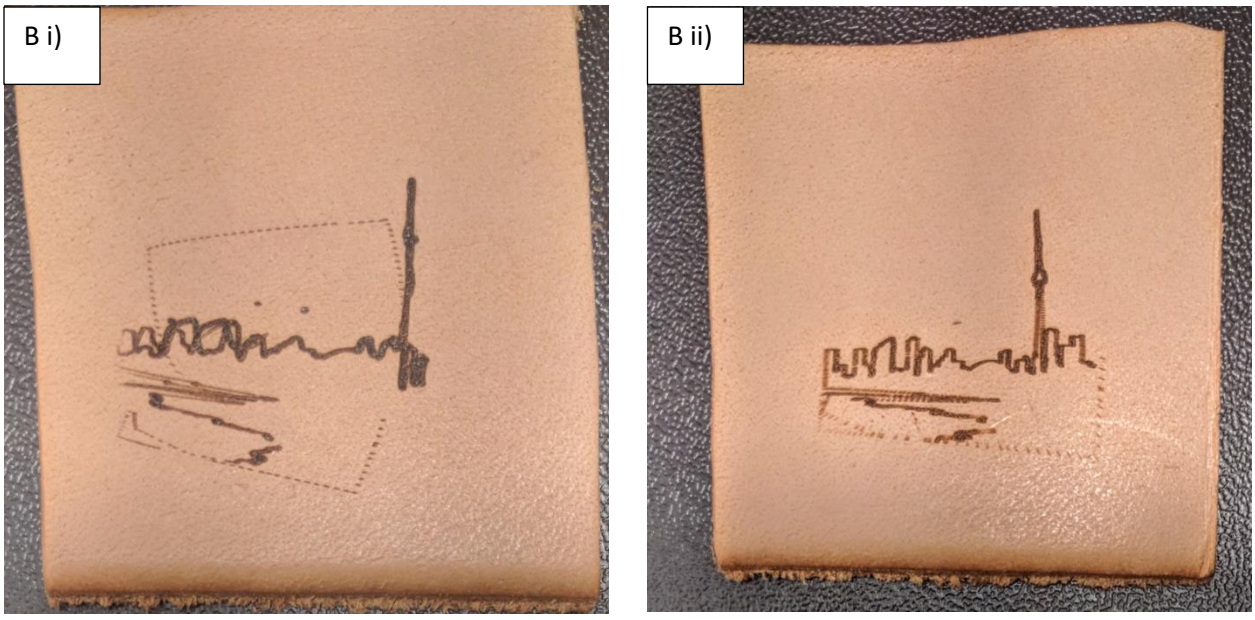

C i) Batman logo without prime C ii) Batman logo with prime.

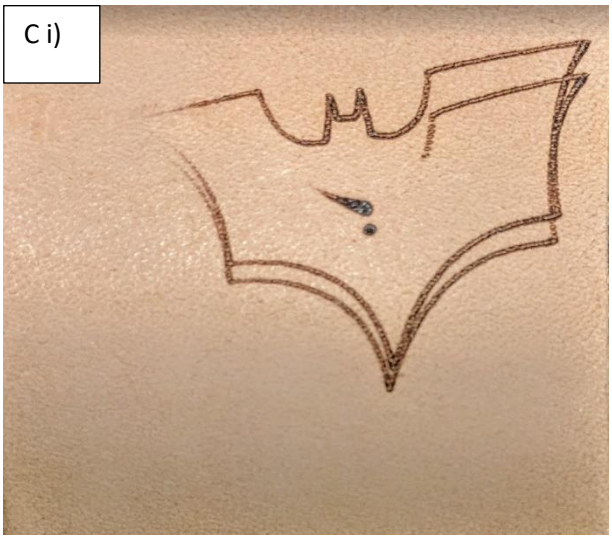

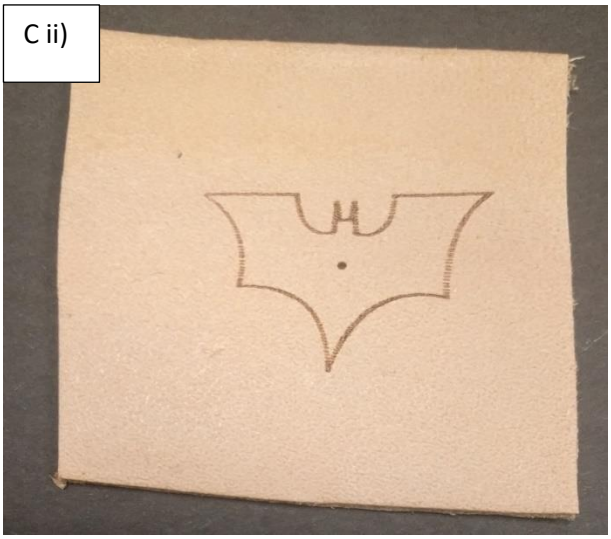

D i) Wordings marking: Ryerson without prime D ii) Wordings marking: Ryerson with prime

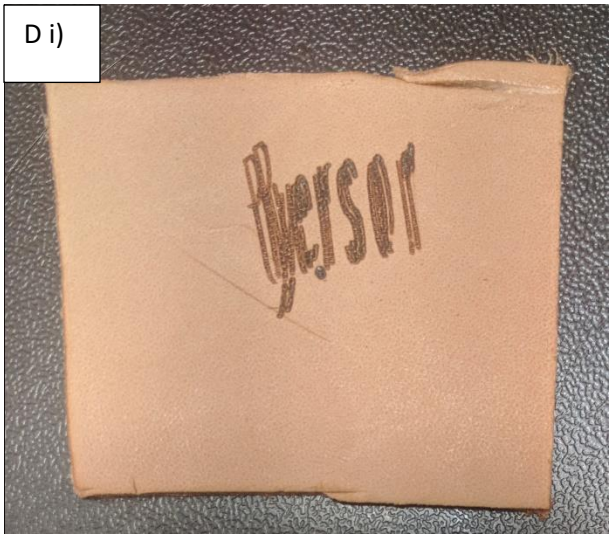

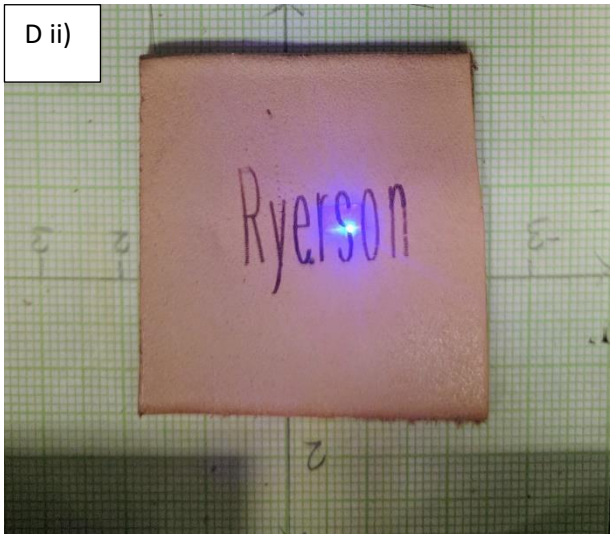

E) jaguar logo on a TPU rubber smartphone case.

Figure 50. Sample images of engraving with and without using prime method.

All the images taken, have a wait time of 90ms for each datapoint. These images are mainly intended for visualizing drifting problem in real time marking after the second pass of the laser. Since, these data points are not calibrated to the mirrors, the size and alignment of the images may not be perfect as the intended image but in reality, all the images will be calibrated to the micromirrors hence the shape and the size of the original image are retained. it is clearly evident that markings done using the prime method significantly minimize or eliminate the drifting problem. Thus, making the current FPCB based micromirrors more suitable for the low cost and compact laser scanners.

Chapter 6. Conclusion

The objectives set out initially were accomplished and summarized as follows:

1) Developed a novel, high surface quality micromirror using a new material known as flexible printed circuit board (FPCB) which could cost as low as few USD (< 5 USD) even for the customized models, that is mainly suitable for the applications involving laser marking/engraving.

   The developed mirrors can achieve a maximum optical rotational angle of ± 7° at quasi static mode and ± 10 ° at resonant mode (30 mA) respectively. However, the resonant performance of the mirror is restricted to ± 10° only due to the limitation of the current mechanical structures and not the mirrors capability. The rotational angle can be increased up to ± 50° with the increase in the input current (up to 150 mA).

2) Developed a laser scanning system based on the FPCB micromirrors by placing two individual X and Y axis scanner orthogonal to each other. The developed scanner can operate at both raster and vector scanning modes. The scanning system caters to the applications involving low powered laser, low scanning system and small working area. By using the developed scanning system, it is possible to reduce the overall size and cost of a laser engraving/marking system with the above-mentioned' requirements.

3) Developed a complete laser engraving/marking system with an working area of 20 x20 mm at a working height of 115mm. It is capable of engraving materials such as leather, TPU rubber in the current configuration. The development process includes both hardware and software of the engraving/marking system. The current control software was developed in labview FPGA environment and can operate the marking/engraving system in vector scanning mode.

4) Since the quasi static FPCB actuators are a relatively a new concept, A new problem associated in using them was identified. The problem such as drifting, posses a major hindrance in using FPCB materials as actuators. To overcome that using open loop control, a novel scanning methodology was adopted which offers significant reduction (<5%) of the drifting and thereby enhancing the final product quality. The novel scanning methodology is based on the vector scanning method with prime values. Hence the mirror scans an image as both positive (original data points) and negative image (prime points) alternatively while the high-powered laser modulated to operate only at positive section (original data point) of the scanned image.

6.1 Future scope and recommendations:

The development of a cost effective compact laser engraving system has already been well received by the consumer market. A Taiwanese start-up company known as “CUBIIO” working on one such machine has already received $1,062,909 USD in funding from a kickstarter program [23]. Hence there is a huge market and potential for compact laser engraving/marking machines in the forthcoming future. But due to time restrictions, the laser engraving/marking model proposed and developed in this work can be considered as a proof of concept model or prototype which can be improved in several ways. For all the improvements that can be made in the future, the current project would serve as a good base structure.

1) Most of the limitations regarding the small engraving area associated with the current prototype is due to the scanning system used. By replacing the current 2 unidirectional scanners with one 2 directional scanners, significant improvements can be made such as.

1) The problem associated with laser overshoot from the second mirror can be eliminated.
2) The loss of laser power due to the second mirror can be eliminated.
3) Implementation of feedback sensors to establish a closed loop control, which can increase the speed and stability of the system of the system while eliminating the problems caused by drifting issue.
4) It is possible to increase mirror aperture without increasing the size factor of the scanning system. Due to the lager mirror aperture, the scanner can handle higher laser power.
5) The scanner can be made more compact by providing additional space to include the control unit within the system itself.

2) Analyze the anisotropic material property of the polyimide material by testing them in our lab in order to minimize the discrepancy between the experimental and simulated results.
3) Though the bonded MEMS mirrors have lot of advantages over the regular MEMS mirrors, there are discrepancies in the performance of each mirrors which is mainly attributed to the manual bonding process that involves the bonding of the actuators to the base plate and the mirrors to the actuator, as the process is not consistent and accurate. So, a suitable bonding technique should be developed to ensure the consistency and perfection across all the models in the future.
4) The laser source should be replaced with a newer small model to make the entire system compact and more suitable for point and shoot operations.

References

[1] P. J. Ogrodnik, C. I. Moorcroft, and P. Wardle, “The Effects of Laser Marking and Symbol Etching on the Fatigue Life of Medical Devices,” *J. Med. Eng.*, vol. 2013, pp. 1–6, Apr. 2013.

[2] Faycal Benayad-Cherif, “Feature Story: Laser Marking « MPMA – Precision Manufacturing Journal.” [Online]. Available: http://pm-mn.com/2017/07/feature-story-laser-marking/. [Accessed: 05-Aug-2017].

[3] “Difference between various laser process (marking and engraving) -service provider website data.” [Online]. Available: http://www.lumicision.com/2015/02/difference-between-laser-marking-and-engraving/. [Accessed: 03-Aug-2017].

[4] “Difference between various laser process (marking and engraving)-manufacturer website data.” [Online]. Available: http://www.permanentmarking.com/what-are-the-differences-between-laser-marking-laser-engraving-and-laser-etching/. [Accessed: 03-Aug-2017].

[5] “Laser machines used for cutting,engraving and marking purposes- manufacturer website data.” [Online]. Available: https://www.troteclaser.com/en-ca/laser-machines/. [Accessed: 03-Aug-2017].

[6] F. J. C. I. Eur. Ing., Ceng, Laser Processing of Engineering Materials: Principles, Procedure and Industrial Application, 1st ed. Elsevier Butterworth Heinemann, 2005.

[7] “Laser marking/engraving appliations in various industries-manufactuer website data.” [Online]. Available: https://www.troteclaser.com/en-ca/applications/. [Accessed: 05-Aug-2017].

[8] “Epilog Laser Engraving Photo Gallery-manufacturer website data.” [Online]. Available: https://www.epiloglaser.ca/how-it-works/anodized.htm. [Accessed: 06-Aug-2017].

[9] “Advantages of Laser Marking and Engraving- manufacturer website data.” [Online]. Available: http://info.laserstar.net/blog/advantages-of-laser-marking-and-engraving. [Accessed: 06-Aug-2017].

[10] “Advantages of Laser Marking | SHT GmbH-service provider website data.” [Online]. Available: http://www.sht-gmbh.de/webeng/laser-general/advantages/. [Accessed: 06-Aug-2017].

[11] Lydia Sobotova1 And Peter Demec, “Laser Marking Of Metal Materials,” *MM Sci. Journal-carbon*, vol. 26, no. 8, pp. 808–812, 2015.

[12] “Comparison of different Laser Types - CO2, Fiber Laser, Vanadat, Yag U-Manufacturer website data.” [Online]. Available: https://www.troteclaser.com/en-us/knowledge/faqs/laser-types/. [Accessed: 06-Aug-2017].

[13] “Laser Modules for Cutting/Engraving (CNC) - manufacturer website data.” [Online]. Available: http://odicforce.com/epages/05c54fb6-7778-4d36-adc0-0098b2af7c4e.sf/en_GB/?ObjectPath=/Shops/05c54fb6-7778-4d36-adc0-0098b2af7c4e/Categories/Background_and_Projects/Laser_Diode_Cutting_and_Engraving. [Accessed: 06-Aug-2017].

[14] “Wavelength Types used for Laser Marking- manufacturer website data.” [Online]. Available:http://www.keyence.com/ss/products/marking/marking_central/select/wavelength.jsp. [Accessed: 07-Aug-2017].

[15] “Laser Engraving Training | Industrial Cutting Training -manufacturer website data.” [Online]. Available: http://www.vy-tek.com/Help/help-gantry.html. [Accessed: 07-Aug-2017].

[16] G. Ghiani and G. Improta, “The Laser-Plotter Beam Routing Problem,” *The Journal of the Operational Research Society*, vol. 52. Palgrave Macmillan JournalsOperational Research Society, pp. 945–951.

[17] “Darkly Labs (laser plotter) -manufacturer website data.” [Online]. Available: https://darklylabs.com/. [Accessed: 09-Aug-2017].

[18] T. Hegna, H. Pettersson, and K. Grujic, “Inexpensive 3-D Laser Scanner System Based On A Galvanometer Scan Head,” *Int. Arch. Photogramm. Remote Sens. Spat. Inf. Sci.*, 2010.

[19] “Product Focus: Galvanometer Scanners: What you need to know to buy a galvo-positioner (Laser Focus World) - OEM supplier website data.” [Online]. Available: http://www.laserfocusworld.com/articles/2010/09/product-focus-galvanometer.html. [Accessed: 09-Aug-2017].

[20] “Small Beam Diameter Scanning Galvo Mirror Systems-manufacturer website data.” [Online].Available:Https://www.thorlabs.com/newgrouppage9.cfm?objectgroup_id=3770&pn=GVS002. [Accessed: 09-Aug-2017].

[21] “Dual Axis Galvanometer Optical Scanners (Edmund Optics)-manufacturer website data.” [Online]. Available: https://www.edmundoptics.com/lasers/laser-mechanics/dual-axis-galvanometer-optical-scanners/. [Accessed: 09-Aug-2017].

[22] “Digital Laser Scanner System | GM Series | Canon USA-manufacturer website data.” [Online]. Available: https://www.usa.canon.com/internet/portal/us/home/products/details/optoelectronic-products/digital-laser-scanner-system/gm-series/. [Accessed: 09-Aug-2017].

[23] “1000mw High Speed Laser Engraver Carver Automatic DIY Print U3y8 | eBay-supplier website data.” [Online]. Available: https://www.ebay.com/p/Neje-Dk-8-kz-1000mw-High-Speed-Laser-Engraver-Carver-Automatic-DIY-Print-U3y8/20004018610?iid=222559427180. [Accessed: 09-Aug-2017].

[24] “Cubiio: The Most Compact Laser Engraver by Muherz -a startup company.” [Online]. Available: https://www.kickstarter.com/projects/880456201/cubiio-the-most-compact-laser-engraver. [Accessed: 09-Aug-2017].

[25] “Low power laser modules (J Tech Photonics, Inc.)- Supplier website data.” [Online]. Available: https://jtechphotonics.com/?post_type=product. [Accessed: 09-Aug-2017].

[26] “Low powered laser modules specifications-supplier website data.” [Online]. Available: http://odicforce.com/epages/05c54fb6-7778-4d36-adc0-0098b2af7c4e.sf/en_GB/?ObjectPath=/Shops/05c54fb6-7778-4d36-adc0-0098b2af7c4e/Categories/23. [Accessed: 09-Aug-2017].

[27] J. Sun and H. Xie, “MEMS-Based Endoscopic Optical Coherence Tomography,” *Int. J. Opt.*, vol. 2011, pp. 1–12, Jun. 2011.

[28] C.-D. Liao and J.-C. Tsai, “The Evolution of MEMS Displays,” *IEEE Trans. Ind. Electron.*, vol. 56, no. 4, 2009.

[29] J. Chong, S. He, and R. Ben Mrad, “Development of a Vector Display System Based on a Surface-Micromachined Micromirror,” *IEEE Trans. Ind. Electron.*, vol. 59, no. 12, pp. 4863–4870, Dec. 2012.

[30] U. Hofmann and J. Janes, “MEMS Mirror for Low Cost Laser Scanners,” in *Advanced Microsystems for Automotive Applications 2011*, Berlin, Heidelberg: Springer Berlin Heidelberg, 2011, pp. 159–165.

[31] R. Moss *et al.*, “Low-cost compact MEMS scanning ladar system for robotic applications,” 2012, p. 837903.

[32] P.-A. Blanche, L. LaComb, Y. Wang, and M. Wu, “Diffraction-Based Optical Switching with MEMS,” *Appl. Sci.*, vol. 7, no. 4, p. 411, Apr. 2017.

[33] G.-D. J. Su, H. Toshiyoshi, and M. C. Wu, “Surface-micromachined 2-D optical scanners with high-performance single-crystalline silicon micromirrors,” *IEEE Photonics Technol. Lett.*, vol. 13, no. 6, pp. 606–608, Jun. 2001.

[34] V. Milanovic, “Multilevel Beam SOI-MEMS Fabrication and Applications,” *J. Microelectromechanical Syst.*, vol. 13, no. 1, pp. 19–30, Feb. 2004.

[35] H. Zuo and S. He, “FPCB Micromirror-Based Laser Projection Availability Indicator,” *IEEE Trans. Ind. Electron.*, vol. 63, no. 5, pp. 3009–3018, May 2016.

[36] “Mirrorcle Technologies MEMS Mirrors Technical Overview-manufacturer website data.” [Online]. Available: http://mirrorcletech.com/pdf/Mirrorcle Technologies MEMS Mirrors - Technical Overview.pdf. [Accessed: 10-Aug-2017].

[37] “Nexgen Portable Laser Marker- Laser Marking/Engraver-Manufacturer website data.”

[Online]. Available: http://www.nexgenlasermarker.com/about. [Accessed: 11-Aug-2017].

[38] "MEMS mirror price list- manufacturer website data." [Online]. Available: http://mirrorcletech.com/pdf/MirrorcleTech_Device_Prices.pdf. [Accessed: 11-Aug-2017].

[39] "NLL 10 label laser by NanoSec Technology GmbH - Product data sheet." [Online]. Available: http://www.nanosec.eu/download/NLL_10_datasheet.pdf. [Accessed: 11-Aug-2017].

[40] V. Milanovic, "Linearized Gimbal-Less Two-Axis MEMS Mirrors," in *Optical Fiber Communication Conference and National Fiber Optic Engineers Conference*, 2009, p. JThA19.

[41] "Gimbal-less Two Axis (Tip-Tilt) MEMS Mirrors by Mirrorcle Technologies INC - manufacturer website data." [Online]. Available: http://mirrorcletech.com/devices.html. [Accessed: 11-Aug-2017].

[42] "Mirrorcle mirror specifications- manufacturer website data." [Online]. Available: http://mirrorcletech.com/support.php. [Accessed: 12-Aug-2017].

[43] H. Zuo and S. He, "Fpcb Actuator Driven Micromirror Based Availability Indicator And Laser Pattern Pointer." Ryerson university, 2015.

[44] "Flexible Printed Circuit Description | What is a flexible printed circuit | All Flex Inc.- manufacturer website data." [Online]. Available: http://www.allflexinc.com/flexible-printed-circuits/. [Accessed: 14-Aug-2017].

[45] "Flexible Printed Circuit Board Manufacturing | Assembly - manufacturer website data."

[Online]. Available: https://www.pcbcart.com/pcb-fab/flexible-pcb.html. [Accessed: 14-Aug-2017].

[46] "Flex Circuits Design Guide (Minco)- manufacturer design guide." [Online]. Available: http://webcache.googleusercontent.com/search?q=cache:GKBYzEFXDKUJ:www.minco.com/~/media/files/minco/productguides/flex/minco%2520flex%2520circuit%2520design%2520guide%25202015.ashx+&cd=3&hl=en&ct=clnk&gl=ca. [Accessed: 15-Aug-2017].

[47] W. C. Wilson and G. M. Atkinson, "Review of Polyimides Used in the Manufacturing of Micro Systems," 2007.

[48] S. Xiao, L. Che, X. Li, and Y. Wang, "A cost-effective flexible MEMS technique for temperature sensing," *Microelectronics J.*, vol. 38, no. 3, pp. 360–364, Mar. 2007.

[49] S. Y. Xiao, L. F. Che, X. X. Li, and Y. L. Wang, "A novel fabrication process of MEMS devices on polyimide flexible substrates," *Microelectron. Eng.*, vol. 85, no. 2, pp. 452–457, Feb. 2008.

[50] J. Y. Kim, K. E. Lee, and S. Han, "Developmemnt Of Flexible Thermoelectric Generator Using Fpcb."

[51] A. Samanta, M. Shahrukh, "Flexible Printed Circuit Board (Its Theory and Real Time Survey)," *Int. J. Innov. Res. Sci. Eng. Technol. (An ISO Certif. Organ.*, vol. 3297, no. 7, 2007.

[52] "A video on flexible printed circuit manufacturing procedure - YouTube." [Online]. Available: https://www.youtube.com/watch?v=SaGVOnSltHo. [Accessed: 16-Aug-2017].

[53] A. Kheyraddini Mousavi *et al.*, "Basic MEMS Actuators," in *Encyclopedia of*

Nanotechnology, Dordrecht: Springer Netherlands, 2012, pp. 173–185.

[54] S. He and R. BenMrad, "Large-Stroke Microelectrostatic Actuators for Vertical Translation of Micromirrors Used in Adaptive Optics," *IEEE Trans. Ind. Electron.*, vol. 52, no. 4, pp. 974–983, Aug. 2005.

[55] M.-H. Jun, S. Moon, B. H. Lee, and J.-H. Lee, "A gimbal-less two-axis electrostatic scanner with tilted stationary vertical combs and serially connected springs via a microassembly process," *J. Micromechanics Microengineering*, vol. 24, no. 9, p. 95008, Sep. 2014.

[56] S. He, R. Ben Mrad, and J. Chong, "Repulsive-force out-of-plane large stroke translation micro electrostatic actuator," *J. Micromechanics Microengineering*, vol. 21, no. 7, p. 75002, Jul. 2011.

[57] B. K. Gale (university of Utah, "A lecture session on fundamental of mechanical MEMS mechanical actuators and electrostatic actuator."[Online].Available:http://www.eng.utah.edu/~gale/mems/Lecture%2022%20Mechanical%20Microsystems.pdf. [Accessed: 16-Aug-2017].

[58] W. Liao, W. Liu, Y. Zhu, Y. Tang, B. Wang, and H. Xie, "A Tip-Tilt-Piston Micromirror With Symmetrical Lateral-Shift-Free Piezoelectric Actuators," *IEEE Sens. J.*, vol. 13, no. 8, pp. 2873–2881, Aug. 2013.

[59] J. Sam, J. Kumar, E. A. Tetteh, and E. P. Braineard, "A Study Of Why Electrostatic Actuation Is Preferred And A Simulation Of An Electrostatically Actuated Cantilever Beam For Mems Applications," *Int. J. Eng. Sci. Emerg. Technol.*, vol. 6, no. 5, pp. 441–446, 2014.

[60] C. Livermore, “Design choices: MEMS actuators Motivation.” [Online]. Available: https://ocw.mit.edu/courses/electrical-engineering-and-computer-science/6-777j-design-and-fabrication-of-microelectromechanical-devices-spring-2007/lecture-notes/07lecture21.pdf. [Accessed: 22-Aug-2017].

[61] M. Kabla, E. Ben-David, and D. Shilo, “A novel shape memory alloy microactuator for large in-plane strokes and forces,” *Smart Mater. Struct.*, vol. 25, no. 7, p. 75020, Jul. 2016.

[62] I.-J. Cho, “A low-voltage three-axis electromagnetically actuated micromirror for fine alignment among optical devices,” *J. Micromechanics Microengineering*, vol. 19, no. 8, Aug. 2009.

[63] Y. Xue and Siyuan He, “A translation micromirror with large quasi-static displacement and high surface quality,” *J. Micromechanics Microengineering*, vol. 27, no. 1, Jan. 2017.

[64] “Understanding Forces on Current-Carrying Wires in Magnetic Fields | Study.com.” [Online]. Available: http://study.com/academy/lesson/understanding-forces-on-current-carrying-wires-in-magnetic-fields.html. [Accessed: 18-Aug-2017].

[65] “Laser beam divergence and spot size (Theory) : Laser Optics Virtual Lab : Physical Sciences : Amrita Vishwa Vidyapeetham University Virtual Lab.” [Online]. Available: http://vlab.amrita.edu/?sub=1&brch=189&sim=342&cnt=1. [Accessed: 18-Aug-2017].

[66] “F-Theta Scan Lenses database (Thor Labs) -manufacturer website data.” [Online]. Available: https://www.thorlabs.com/newgrouppage9.cfm?objectgroup_id=6430. [Accessed: 18-Aug-2017].

[67] “F-Theta Scanning Lenses database (Edmund Optics)-manufacturer website data.” [Online]. Available: https://www.edmundoptics.com/optics/laser-optics/laser-optical-assemblies/F-Theta-Scanning-Lenses/. [Accessed: 18-Aug-2017].

[68] “3 element / G2 / G7 / Laser focus Lenses (Sanwu Lasers)-manufacturer website data.” [Online]. Available: https://www.sanwulasers.org/product/lenses. [Accessed: 18-Aug-2017].

[69] “Nanofabrication: Principles, Capabilities and Limits - Zheng Cui section (3.3.3),” .

[70] S. Franssila, *Introduction to microfabrication (section 8)*. Wiley, 2013.

[71] K. C. Sheth, “Stress,Mechanical and Thermal Characterization of Anisotropic Polymide thin Films and Coatings,” University of Massachusetts,Amherst, 1996.

[72] “Hot Rolled and Annealed (O25) C10400 Copper (makeitform.com)-material property database.” [Online]. Available: http://www.makeitfrom.com/material-properties/Hot-Rolled-and-Annealed-O25-C10400-Copper. [Accessed: 19-Aug-2017].

[73] “Reflectance - Wikipedia webpage.” [Online].Available:https://en.wikipedia.org/wiki/Reflectance. [Accessed: 20-Aug-2017].

[74] “Laser source (Opt Lasers)- manufacturer website data.” [Online]. Available: https://optlasers.com/en/. [Accessed: 20-Aug-2017].

[75] “Cube magnets B444-N52 (K&J Magnetics)-manufacturer website data.” [Online]. Available: https://www.kjmagnetics.com/proddetail.asp?prod=B444-N52. [Accessed: 20-Aug-2017].

[76] “Learn LabVIEW (National Instruments)- Software tutorial.” [Online]. Available: http://www.ni.com/academic/students/learn-labview/. [Accessed: 22-Aug-2017].

[77] “Getting Started With LabVIEW FPGA (National Instruments)- software tutorial.” [Online]. Available: http://www.ni.com/tutorial/14532/en/. [Accessed: 22-Aug-2017].

[78] “Representing Data Types on FPGA Targets (Simulation Interface Toolkit) - LabVIEW 2010 Simulation Interface Toolkit Help - National Instruments.” [Online]. Available: http://zone.ni.com/reference/en-XX/help/371504F-01/lvsitconcepts/sit_c_fpgadatatypes/. [Accessed: 22-Aug-2017].

[79] S. Zhang, S. Mori, M. Sakane, T. Nagasawa, and K. Kobayashi, “Tensile Properties and Viscoelastic Model of a Polyimide Film,” *J. Solid Mech. Mater. Eng.*, vol. 6, no. 6, 2012.

[80] L. Arruda, R. Bonadiman, C. Josineto, and G. Freitas, “Experimental and numerical analyses of flexible PCBs under various loading conditions,” in *EuroSimE 2009 - 10th International Conference on Thermal, Mechanical and Multi-Physics Simulation and Experiments in Microelectronics and Microsystems*, 2009, pp. 1–10.

[81] “ImageJ - image processing software webpage.” [Online]. Available: https://imagej.nih.gov/ij/. [Accessed: 22-Aug-2017].

[82] “Autocad application- click2xls; (CAD Forum).”

[83] “Selecting an Interpolant Fit - MATLAB & Simulink.” [Online]. Available: https://www.mathworks.com/help/curvefit/selecting-an-interpolant-fit.html. [Accessed: 22-Aug-2017].

[84] “Arduino - Home (microcontrollers).” [Online]. Available: https://www.arduino.cc/.

Appendix A

Design sketches of individual mechanical parts sent out for fabrication:

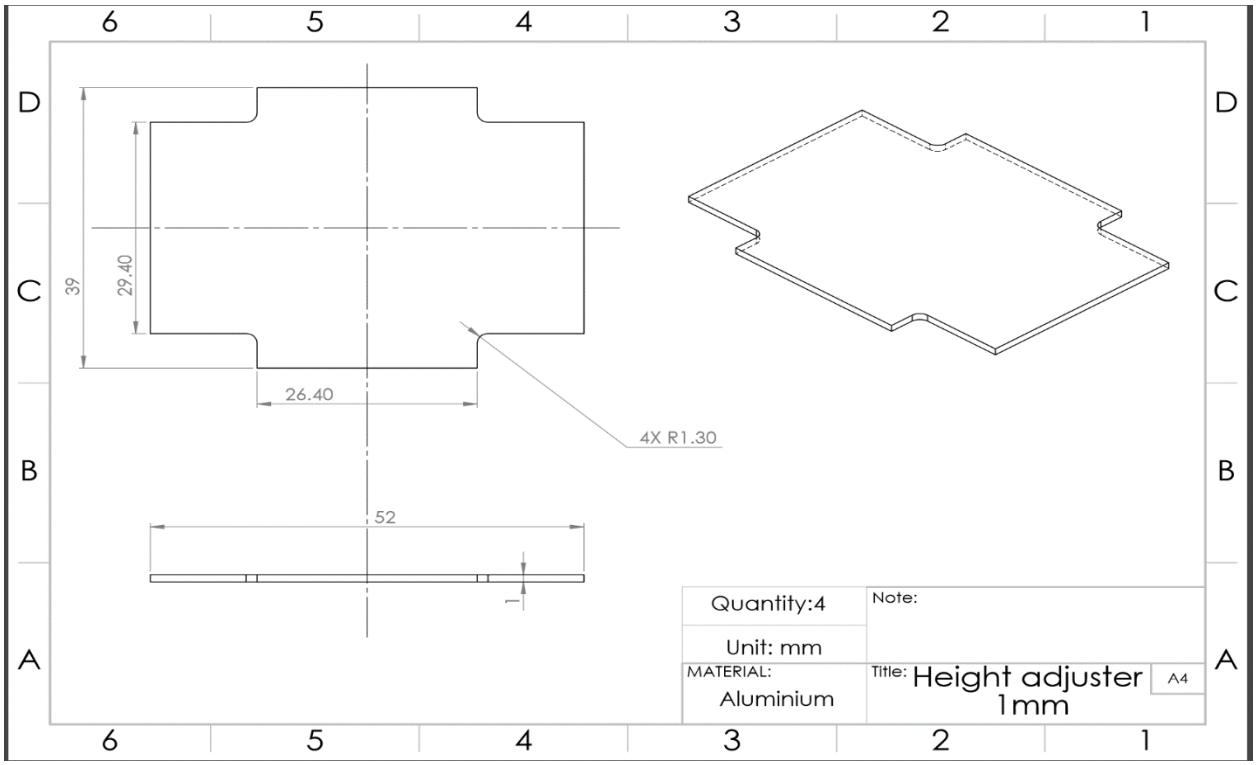

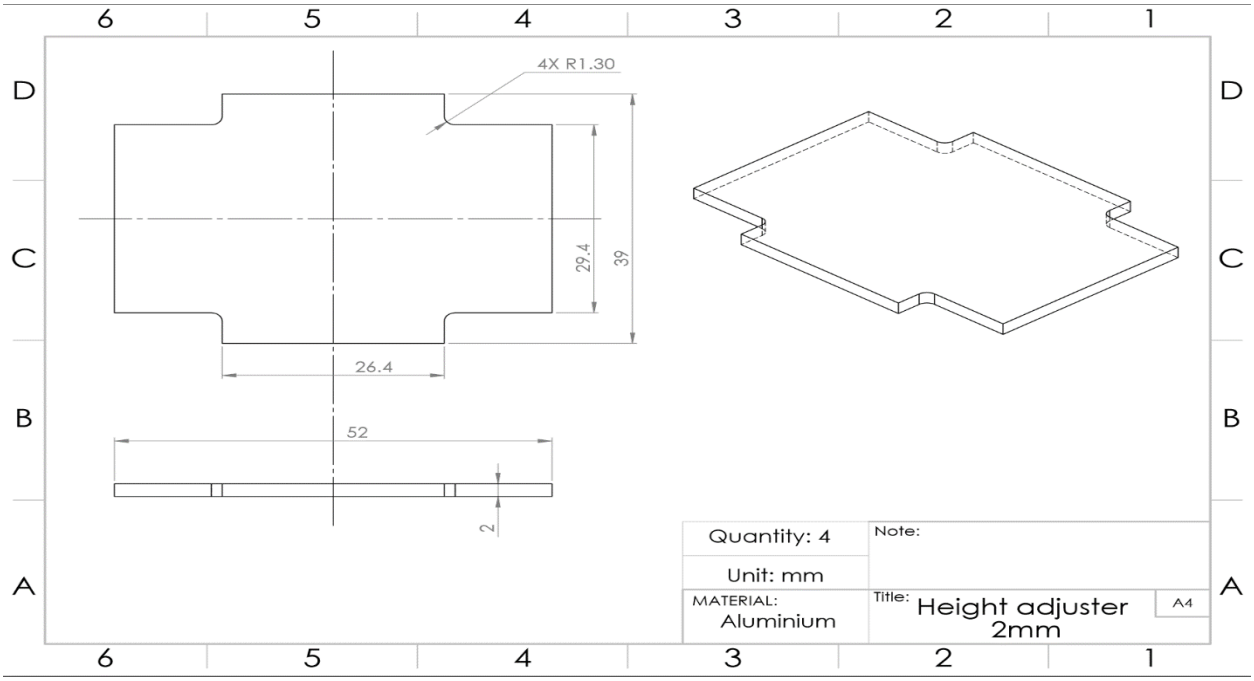

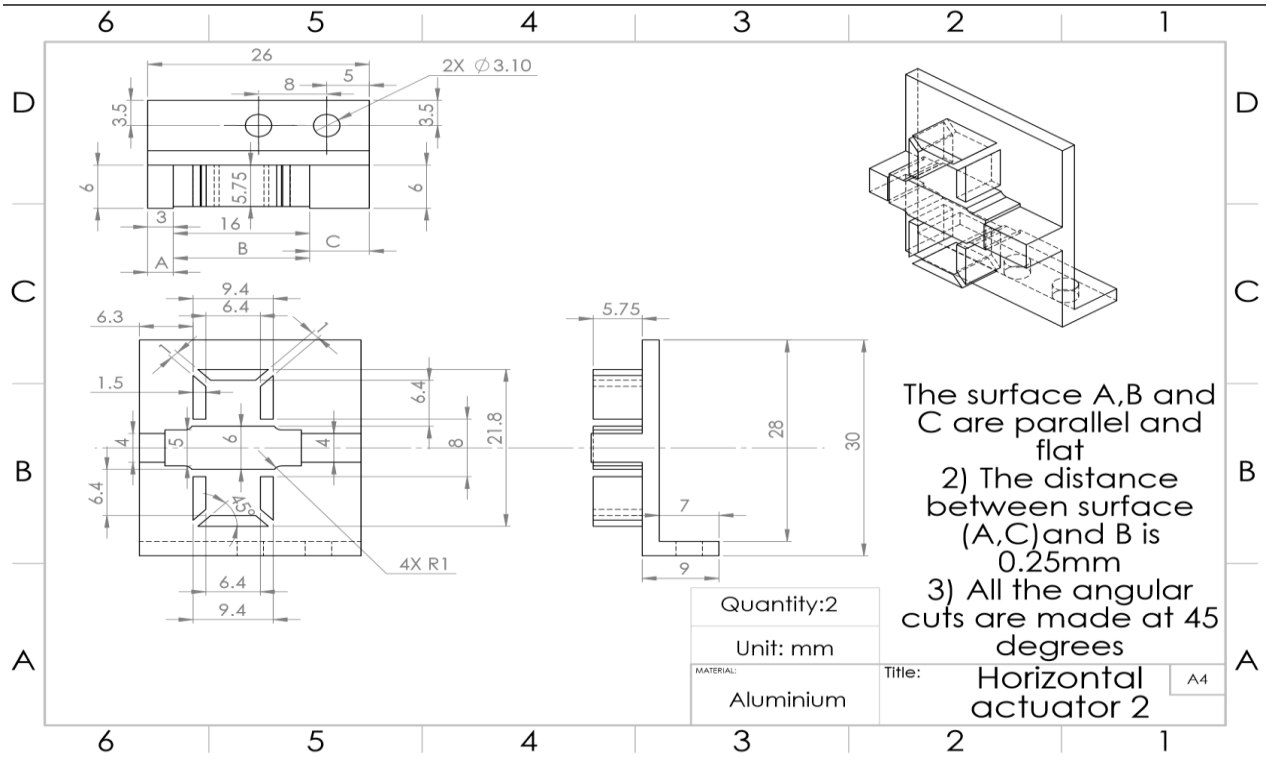
26
8
5
2X ∅3.10
3.5
3.5
6
6
5.75
3
16
B
C
A
9.4
6.4
6.3
1.5
6.4
21.8
8
4
5
6
4
6.4
45°
4X R1
6.4
9.4
5.75
28
30
7
9
Quantity:2
Unit: mm
MATERIAL:
Aluminium
Title:
Horizontal actuator 2
A4
The surface A,B and C are parallel and flat
2) The distance between surface (A,C)and B is 0.25mm
3) All the angular cuts are made at 45 degrees

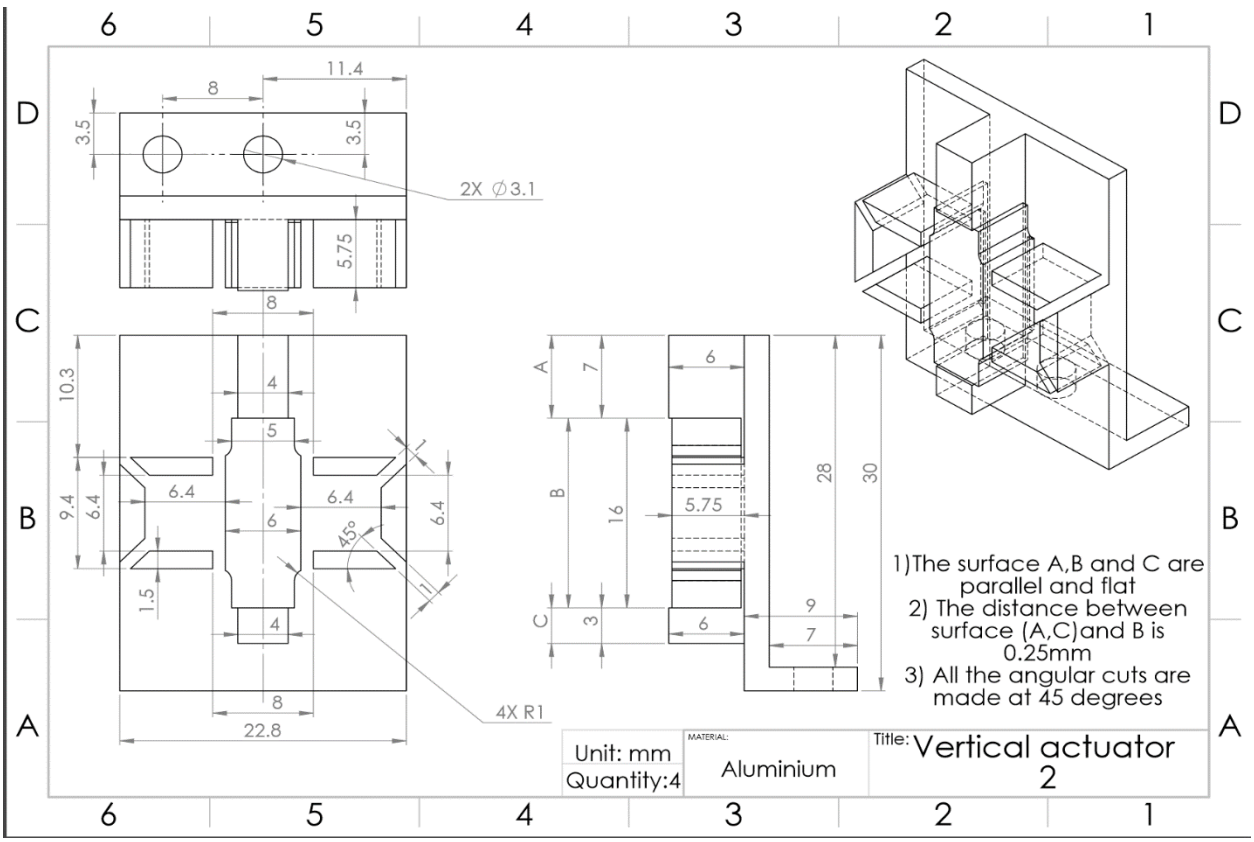
11.4
8
3.5
3.5
2X ∅3.1
5.75
8
10.3
4
5
1
6.4
6.4
9.4
6.4
6
6.4
45°
1.5
4
8
22.8
4X R1
A
7
6
B
16
5.75
28
30
C
3
6
9
7
Unit: mm
Quantity:4
MATERIAL:
Aluminium
Title:
Vertical actuator 2
1)The surface A,B and C are parallel and flat
2) The distance between surface (A,C)and B is 0.25mm
3) All the angular cuts are made at 45 degrees

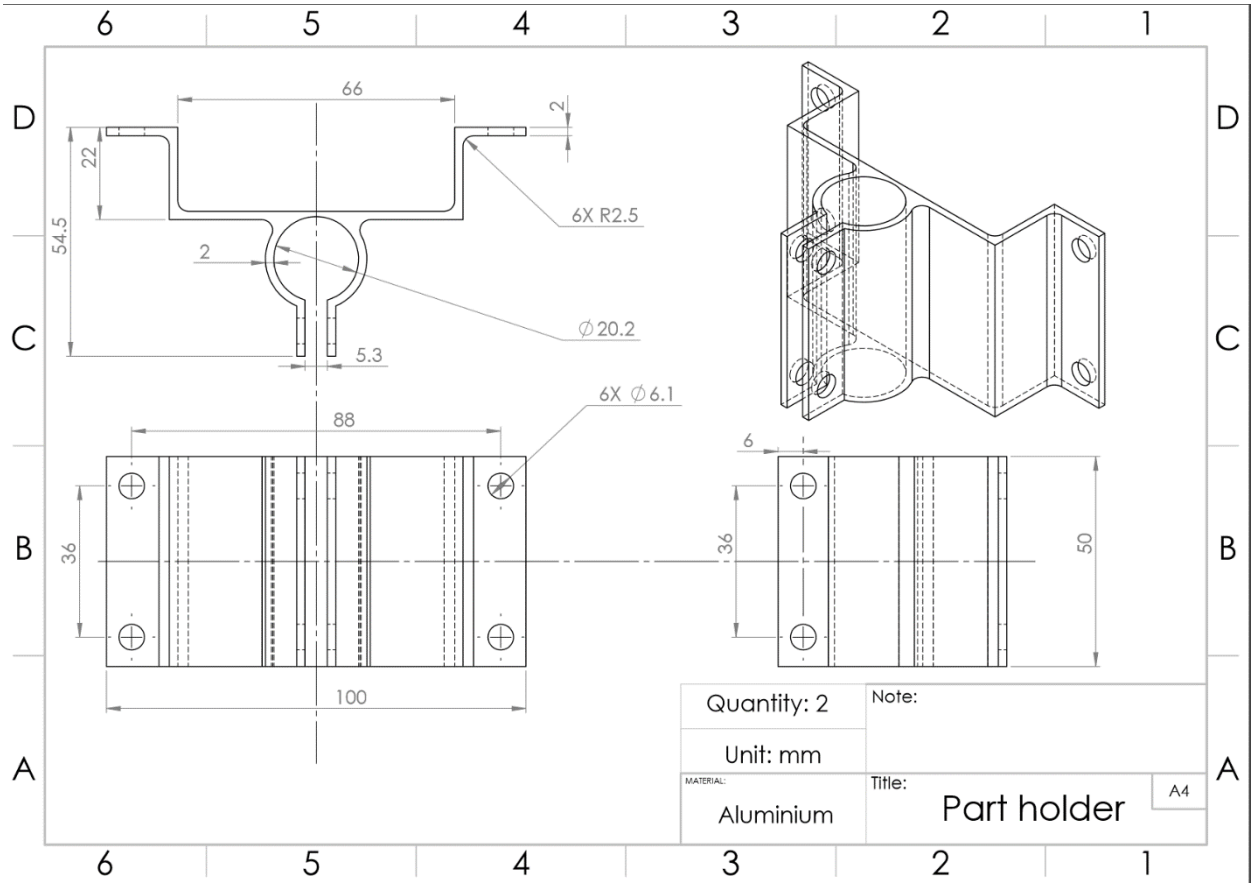
66
2
22
54.5
6X R2.5
2
∅20.2
5.3
6X ∅6.1
88
36
100
6
36
50
Quantity: 2
Note:
Unit: mm
MATERIAL:
Aluminium
Title:
Part holder
A4

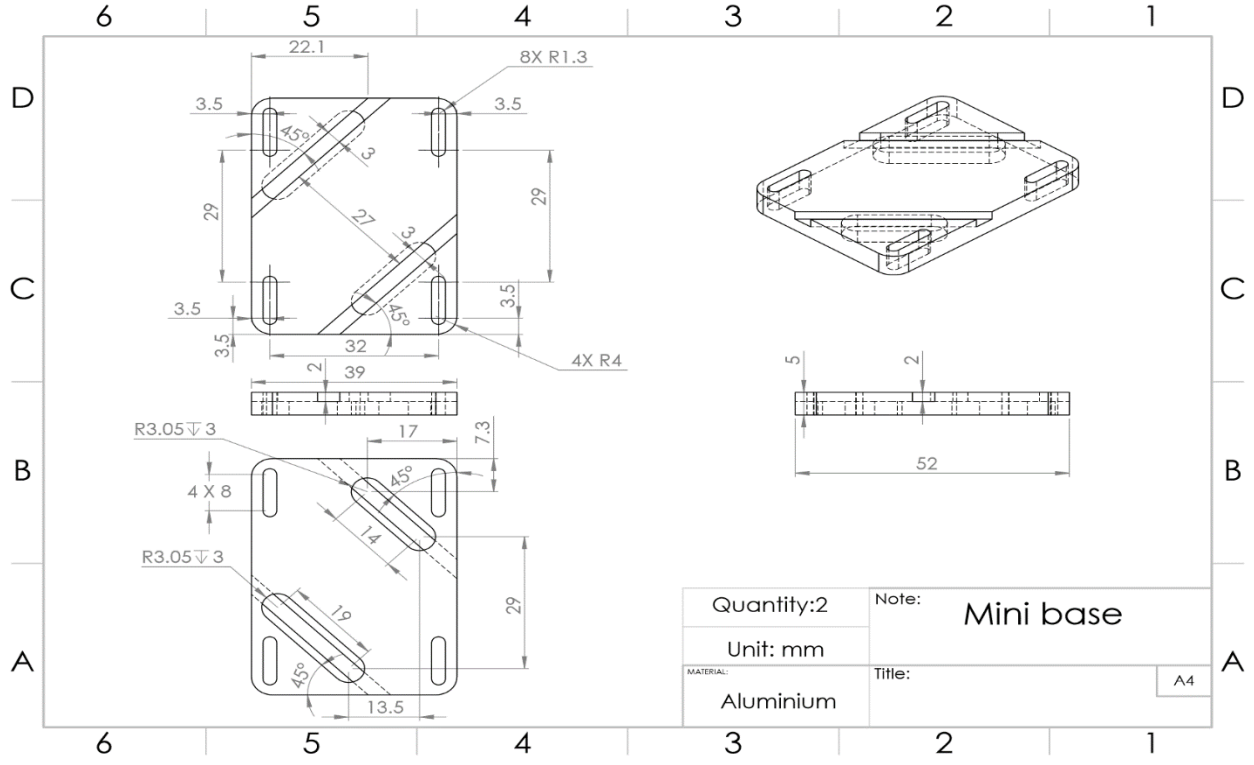
22.1
8X R1.3
3.5
3.5
45°
3
29
29
27
3
3.5
3.5
45°
3.5
32
4X R4
2
39
R3.05↧3
17
7.3
45°
4 X 8
14
R3.05↧3
19
29
45°
13.5
5
2
52
Quantity:2
Note:
Mini base
Unit: mm
MATERIAL:
Aluminium
Title:
A4

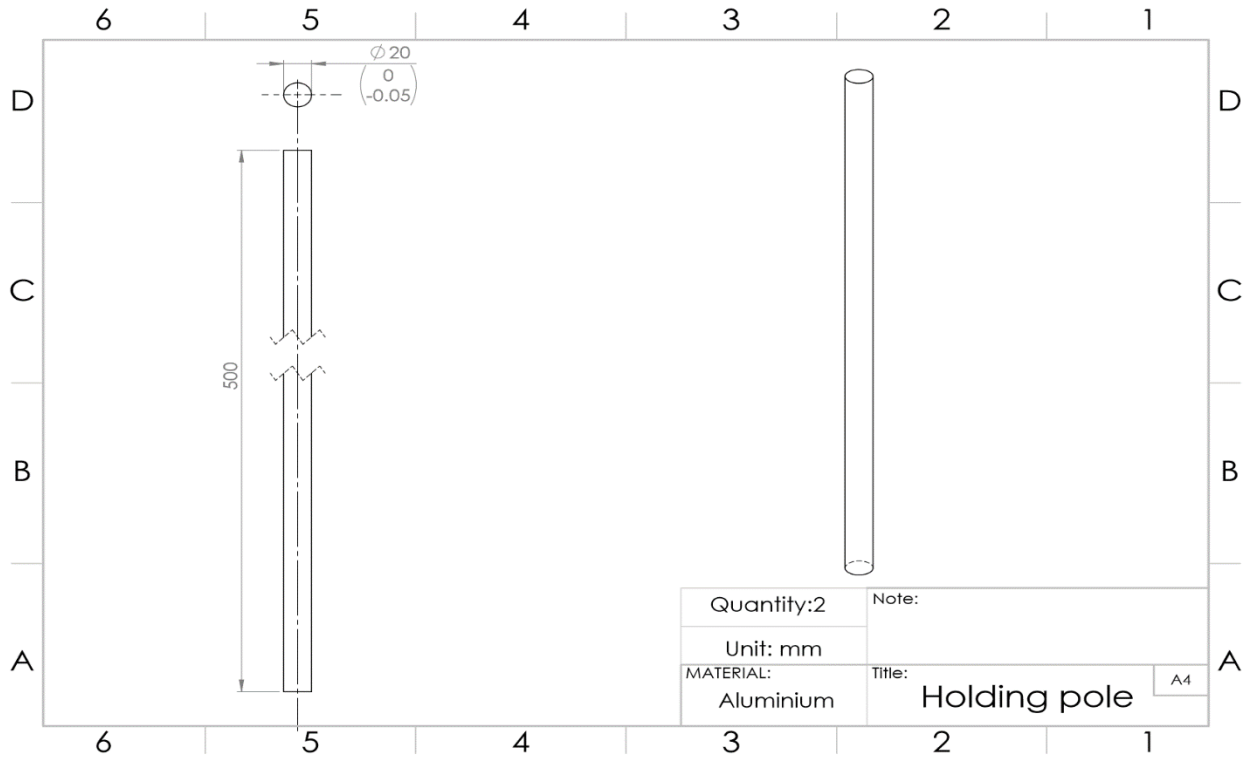
6 5 4 3 2 1
D C B A
∅20 0 -0.05
500
Quantity:2
Note:
Unit: mm
MATERIAL:
Aluminium
Title:
Holding pole
A4

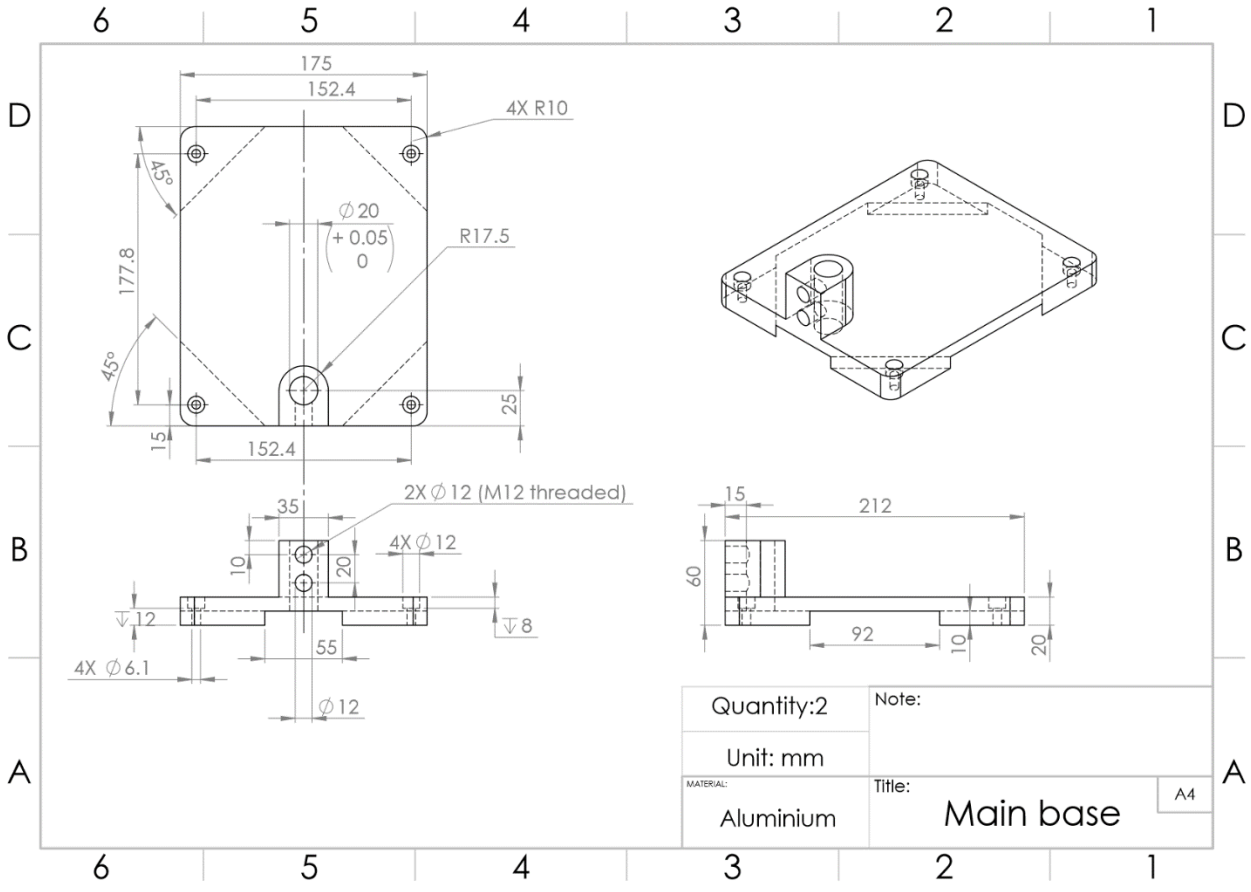
6 5 4 3 2 1
D C B A
175
152.4
4X R10
45°
∅20 + 0.05 0
R17.5
177.8
45°
25
15
152.4
2X∅12 (M12 threaded)
35
4X∅12
10
20
12
8
55
4X ∅6.1
∅12
15
212
60
92
10
20
Quantity:2
Note:
Unit: mm
MATERIAL:
Aluminium
Title:
Main base
A4

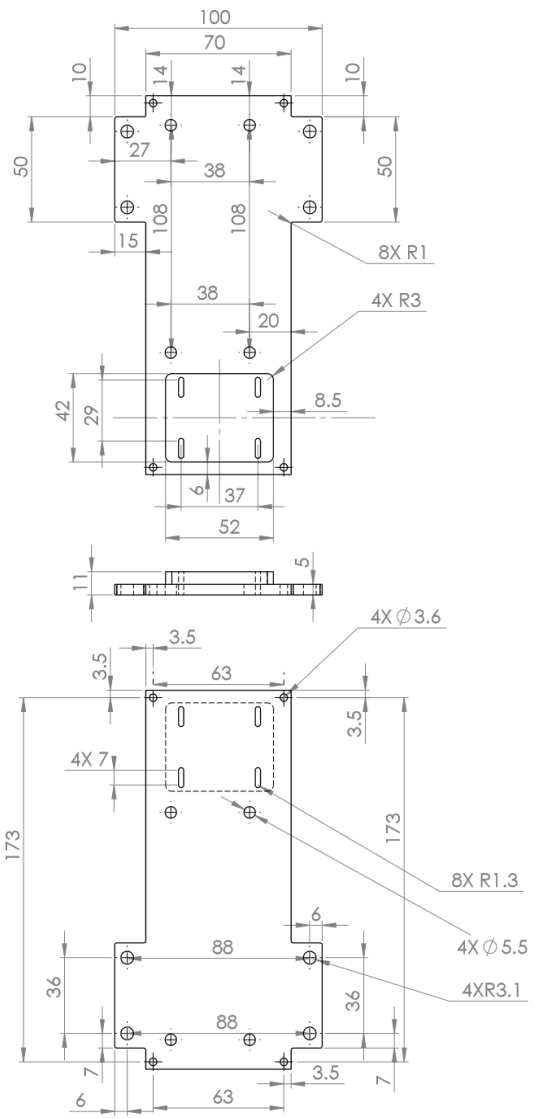

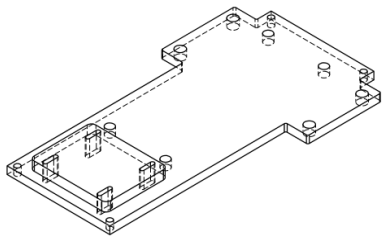

UNLESS OTHERWISE SPECIFIED: DIMENSIONS ARE IN MILLIMETERS SURFACE FINISH: TOLERANCES: LINEAR: ANGULAR:			FINISH: Quantity:2		DEBURR AND BREAK SHARP EDGES	DO NOT SCALE DRAWING	REVISION
						Unit:mm	
	NAME	SIGNATURE	DATE			TITLE: Compiler	
DRAWN							
CHK'D							
APPV'D							
MFG							
Q.A				MATERIAL: Aluminium		DWG NO.	A3
				WEIGHT:		SCALE:1:2	SHEET 1 OF 1

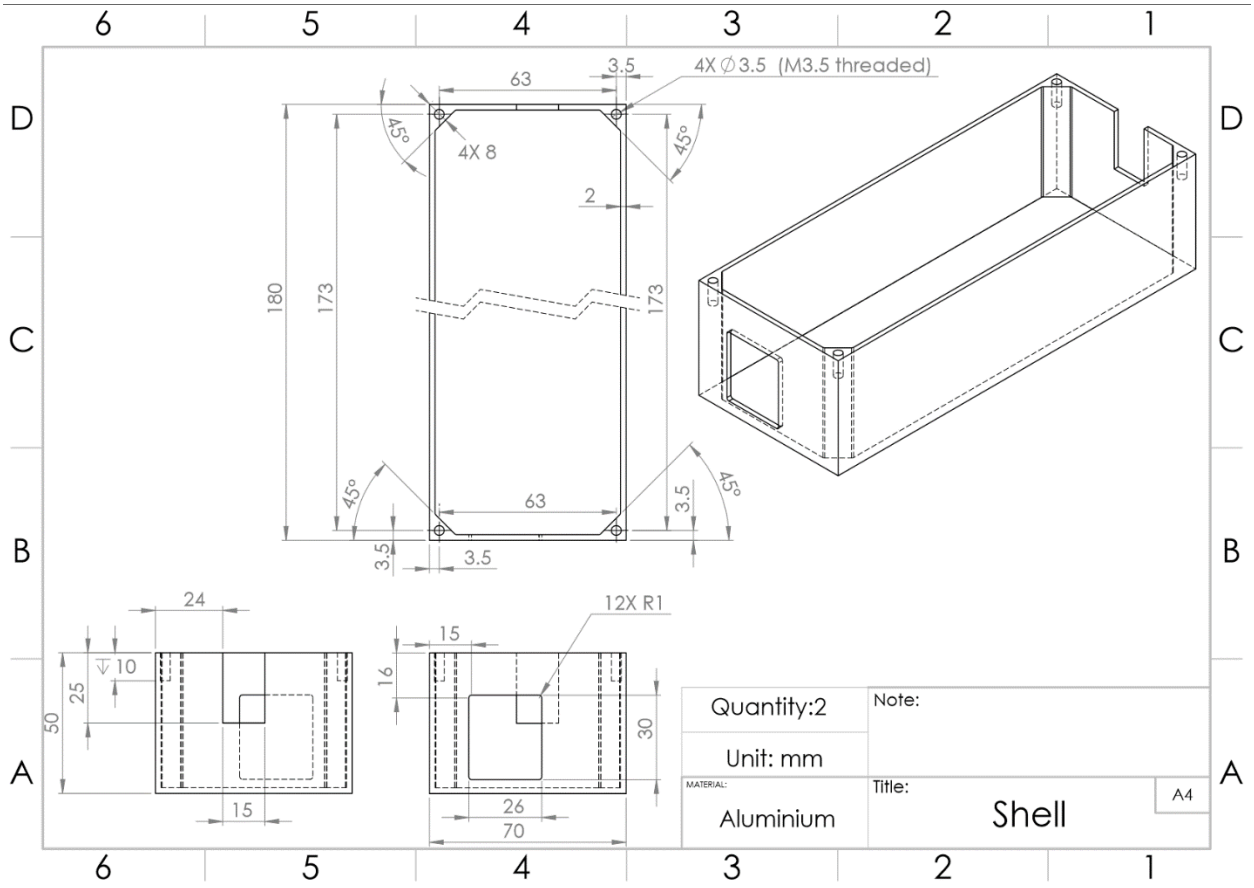
6
5
4
3
2
1
D
C
B
A
63
3.5
4X ∅3.5 (M3.5 threaded)
4X 8
45°
2
180
173
63
3.5
3.5
24
10
25
50
15
12X R1
15
16
30
26
70
Quantity:2
Note:
Unit: mm
MATERIAL:
Aluminium
Title:
Shell
A4